

**ALMA MATER STUDIORUM - UNIVERSITÀ DI BOLOGNA**

---

**SCHOOL OF ENGINEERING AND ARCHITECTURE**

Department of Civil, Chemical, Environmental and Materials Engineering

Master's degree course in

**CHEMICAL AND PROCESS ENGINEERING**

Sustainable Technologies and biotechnologies for Energy and Materials

**A RHEOLOGICAL STUDY OF THE CAVITATION  
MECHANISM OF RUBBER PARTICLES IN ABS  
COPOLYMERS**

CANDIDATE

Ilenia Marino

SUPERVISOR

Prof. Dr. Ferruccio Doghieri

CO-SUPERVISOR

Dr. Dino Ferri

Academic Year 2021/22

Session III



## ***Abstract***

This thesis is the result of a work carried out in the rheology and processability characterization laboratory of the industrial site of Versalis S.p.a in Mantua.

Cavitation of rubber particles in acrylonitrile-butadiene-styrene (ABS) copolymers can be both mechanically and thermally induced. In the latter case cavitation is due to a volume strain generated, on cooling below room temperature, by the mismatch of the values of the thermal expansion coefficients of the glassy matrix and the polybutadiene dispersed rubber. The resulting strong hydrostatic negative stress can also decrease the glass transition temperature value of the rubber particles by several degrees.

An energy balance model has been proposed to study this phenomenon, considering a homogeneous spherical rubber particle embedded in a shell of thermoplastic matrix, in which the cavity is supposed to grow at the center of the particle. When the volume strain to which rubber particles are subjected is sufficiently high, the energy balance predicts a small maximum, followed by a more pronounced minimum.

Data in the literature suggest that rubber particles are more resistant to cavitation than predicted by the energy minimum. It was proposed that the reason for this is the energy barrier maximum which plays the role of an activation energy for void nucleation. In this work a method based on the detection of isothermal cavitation kinetics is proposed to investigate whether an activation step governs the formation of the voids. The activation energy barrier was measured and discussed at different temperatures for three emulsion-like ABS copolymers with different particle size distribution.

# *Index*

<b>LIST OF FIGURES .....</b>	<b>IV</b>
<b>INTRODUCTION .....</b>	<b>XI</b>
<b>DEFORMATION MECHANISM IN HOMOGENOUS POLYMERIC MATERIALS.....</b>	<b>1</b>
<b>1.1 ELASTIC DEFORMATION .....</b>	<b>2</b>
<b>1.2 PLASTIC DEFORMATION.....</b>	<b>3</b>
<b>1.3 VISCOELASTICITY .....</b>	<b>4</b>
<b>1.4 SHEAR YIELDING .....</b>	<b>8</b>
<b>1.5 EYRING’S MODEL .....</b>	<b>10</b>
<b>1.6 CRAZING.....</b>	<b>12</b>
<b>1.7 INTERACTION BETWEEN SHEAR BANDS AND CRAZES.....</b>	<b>14</b>
<b>RUBBER TOUGHENED POLYMERS.....</b>	<b>17</b>
<b>2.1 ABS ACRYLONITRILE-BUTADIENE-STYRENE.....</b>	<b>17</b>
<b>2.2 PRODUCTION OF ABS .....</b>	<b>18</b>
<b>2.3 TOUGHENING MECHANISM IN RUBBER REINFORCED POLYMERS .....</b>	<b>19</b>
<b>2.4 EFFECT OF RUBBER PARTICLES ON STRESS FIELD .....</b>	<b>21</b>
<b>2.5 MULTIPLE CRAZING AND SHEAR YIELDING.....</b>	<b>22</b>
<b>2.6 INTRODUCTION ABOUT CAVITATION OF RUBBER PARTICLES.....</b>	<b>24</b>
<b>CAVITATION OF RUBBER PARTICLES IN RUBBER TOUGHENED POLYMERS.....</b>	<b>26</b>
<b>3.1 A MODEL FOR PARTICLE CAVITATION .....</b>	<b>26</b>
<b>3.2 CRITERIA FOR CAVITATION.....</b>	<b>34</b>
<b>3.3 PARAMETERS INFLUENCING CAVITATION PHENOMENON .....</b>	<b>37</b>
<i>Rubber characteristics and content .....</i>	<i>37</i>
<i>Rubber particles size.....</i>	<i>38</i>
<i>Particle morphology .....</i>	<i>39</i>
<i>Strain rate and temperature.....</i>	<i>40</i>
<b>3.4 EFFECT OF CAVITATION PHENOMENON ON YIELDING BEHAVIOUR.....</b>	<b>41</b>
<b>3.5 IMPORTANCE OF CAVITATION ON IMPACT TOUGHNESS .....</b>	<b>46</b>

<b>HOW CAN CAVITATION PHENOMENON BE STUDIED ? .....</b>	<b>48</b>
<b>4.1 DILATOMETRIC TECHNIQUE .....</b>	<b>49</b>
<b>4.2 DYNAMIC MECHANICAL THERMAL ANALYSIS (DMTA) .....</b>	<b>54</b>
<b>4.3 TRANSMISSION ELECTRON MICROSCOPE (TEM) .....</b>	<b>59</b>
<b>4.4 DIFFERENTIAL SCANNING CALORIMETER (DSC) .....</b>	<b>61</b>
<b>4.5 SMALL-ANGLE X-RAY SCATTERING (SAXS) .....</b>	<b>63</b>
<b>MATERIALS AND INSTRUMENTS .....</b>	<b>65</b>
<b>5.1 SAMPLES .....</b>	<b>65</b>
<i>Sample A .....</i>	<i>65</i>
<i>Sample B .....</i>	<i>66</i>
<i>Sample C .....</i>	<i>67</i>
<i>Samples' distribution of particles dimensions .....</i>	<i>68</i>
<b>5.2 RSA-G2 AND ACCESSORIES .....</b>	<b>69</b>
<b>5.3 RHEOMETRICS MECHANICAL SPECTROMETER MODEL 800 (RMS-800) .....</b>	<b>72</b>
<b>5.4 OTHER INSTRUMENTS (DSC, TEM, NMR).....</b>	<b>74</b>
<b>EXPERIMENTAL WORK AND RESULTS.....</b>	<b>76</b>
<b>6.1 OPTIMIZATION OF TESTS CONDITIONS .....</b>	<b>76</b>
<b>6.2 SPECIMEN PREPARATION .....</b>	<b>80</b>
<b>6.3 DYNAMIC TEMPERATURE RAMP RESULTS .....</b>	<b>80</b>
<b>6.4 PARAMETERS AFFECTING <math>T_g</math> .....</b>	<b>84</b>
<i>Molecular Weight .....</i>	<i>85</i>
<i>Isomeric composition of the rubber .....</i>	<i>86</i>
<i>Degree of crosslinking .....</i>	<i>88</i>
<i>Hydrostatic tension in rubber particles .....</i>	<i>91</i>
<i>Sample B and C: Quantitative analysis of the position of <math>T_g</math> .....</i>	<i>94</i>
<i>Sample A: Quantitative analysis of the position of <math>T_g</math> .....</i>	<i>96</i>
<i>The problematic nature of the rubber bulk modulus .....</i>	<i>98</i>
<b>6.5 DILATOMETRIC CURVES .....</b>	<b>99</b>
<b>6.6 ISOTHERMAL CAVITATION.....</b>	<b>104</b>

<b>6.7 DOUBLE ISOTHERMAL CURVES.....</b>	<b>110</b>
<b>ANALYSIS OF THE KINETIC BARRIER .....</b>	<b>113</b>
<b>7.1 CRITICAL VOLUME STRAIN .....</b>	<b>113</b>
<b>7.2 ANALYTICAL EXPRESSIONS OF MAXIMUM AND MINIMUM.....</b>	<b>116</b>
<b>7.3 CAVITATION KINETICS .....</b>	<b>119</b>
<i>Arrhenius equation .....</i>	<i>119</i>
<i>Eyring equation.....</i>	<i>123</i>
<b>CONCLUSIONS.....</b>	<b>126</b>
<b>APPENDIX.....</b>	<b>129</b>
<i>Derivation of the formula for the volume strain .....</i>	<i>129</i>
<b>BIBLIOGRAPHY.....</b>	<b>132</b>

## *List of Figures*

### *CHAPTER 1*

Figure 1. 1 Stress-strain curves for PS and HIPS <sup>2</sup> .....	1
Figure 1. 2 Stress-strain behavior of polymers <sup>29</sup> .....	3
Figure 1. 3 Elastic and Viscous behaviour <sup>30</sup> .....	5
Figure 1. 4 Viscoelastic Behaviour <sup>30</sup> .....	6
Figure 1. 5 Geometrical approach to complex modulus <sup>30</sup> .....	7
Figure 1. 6 Schematic representation of a shear band <sup>31</sup> .....	8
Figure 1. 7 The nine components of the stress tensor <sup>2</sup> .....	9
Figure 1. 8 Evolution of crazes in Polystyrene.....	12
Figure 1. 9 Failure envelope under biaxial stress <sup>2</sup> .....	15

### *CHAPTER 2*

Figure 2. 1 Contour map showing stress concentration <sup>2</sup> .....	21
Figure 2. 2 Crack toughening mechanism in rubber reinforced polymers <sup>31</sup> .....	25

### *CHAPTER 3*

Figure 3. 1 Composite spherical element used in the model .....	27
Figure 3. 2 Composite spherical element used in the model, after cavitation (formation of the void).....	28
Figure 3. 3 Normalized energy of a cavitated particle as function of $r/R$ , keeping the volume strain constant at 0.004 <sup>25</sup> .....	32
Figure 3. 4 Normalized energy of a rubber particle as function of $r/R$ , keeping a series of volume strain constant during cavitation <sup>25</sup> .....	33

Figure 3. 5 Contributions from volume strain energy and cavity formation energy to the total energy of a rubber particle at -20 and +20 °C, for calculations made with $\Gamma_r = 20 \text{ mJ m}^{-2}$ , $R=100 \text{ nm}$ , $G_r = 0.5 \text{ MPa}$ , $K_r = 2 \text{ GPa}$ , $K_m = 4 \text{ GPa}$ , $G_m = 1.2 \text{ GPa}$ and $\phi_r = 0.16$ <sup>27</sup> .....	35
Figure 3. 6 Initial sections of calculated energy void size curves based on Figure 3.5, comparing energy maxima at (a) +20 °C and (b) -20 °C <sup>27</sup> .....	36
Figure 3. 7 Schematic diagram showing typical morphologies of rubber particles: (a) soft core-hard shell, (b) hard core-soft shell-hard shell, (c) onion morphology, (d) salami particle, (e) can of worms morphology <sup>3</sup> .....	40
Figure 3. 8 Element of ductile polymer with a large number of micro voids <sup>7</sup> .....	42
Figure 3. 9 Pressure modified von Mises yield surface of a non cavitating polymer <sup>7</sup> .....	44
Figure 3. 10 Effect of void volume fraction on the yield locus of pressure dependent material. (a)Uniaxial tension (b) crack tip plane strain tension <sup>7</sup> .....	45
Figure 3. 11 Effect of void volume fraction on the (a) adimensional tensile yield stress and (b)adimensional effective stress at yield according to the modified Gurson model <sup>7</sup> .....	46
 <i>CHAPTER 4</i>	
Figure 4. 1 Thermal expansion scheme of a sample <sup>32</sup> .....	49
Figure 4. 2 Thermal contraction behaviour of three fresh specimens of ABS with 16% of rubber particles, data are normalized with respect to the initial length at 0°C .....	52
Figure 4. 3 Experimental expansion-contraction curve for PSAN (0% of rubber) compared with calculated curve for ABS containing different rubber content using Equation 4.4.....	53
Figure 4. 4 Thermal contraction and expansion behavior of an ABS specimen, cooling represented with black squares and heating with white squares. Reference length taken as the initial length at 100°C .....	53
Figure 4. 5 Temperature Ramp on a Polycarbonate specimen <sup>30</sup> .....	56
Figure 4. 6 Schematic representation of a Temperature Ramp conducted on a RT-plastic <sup>9</sup> ....	57

Figure 4. 7 Temperature Ramp on a specimen showing partial cavitation with splitting of damping peak.....	57
Figure 4. 8 Temperature Ramp on a specimen showing partial cavitation, with small shoulder on the righten side of the peak.....	58
Figure 4. 9 TEM viewing of an ABS with voids in rubber particles.....	59
Figure 4. 10 TEM image of an ABS.....	60
Figure 4. 11 Example of DSC thermogram, highlighting endothermic events .....	62
Figure 4. 12 DSC thermogram of an ABS showing partial cavitation .....	63

## *CHAPTER 5*

Figure 5. 1 TEM image of Sample A .....	65
Figure 5. 2 Table of properties of Sample A .....	66
Figure 5. 3 TEM image of Sample B .....	66
Figure 5. 4 Table of properties of Sample B .....	67
Figure 5. 5 TEM image of Sample C .....	67
Figure 5. 6 Table of properties for Sample C .....	68
Figure 5. 7 Distribution of particles dimensions .....	68
Figure 5. 8 Fit of particles dimensions distribution.....	69
Figure 5. 9 RSA-G2 instrument <sup>30</sup> .....	70
Figure 5. 10 Schematic representation of a specimen deformation <sup>30</sup> .....	71
Figure 5. 11 RSA-G2 geometries <sup>30</sup> .....	72
Figure 5. 12 Scheme of torsional geometry in the RMS-800.....	73

## CHAPTER 6

Figure 6. 1 Dynamic Temperature Ramp on ABS samples, cooling and heating scans measured at 1°C/min .....	77
Figure 6. 2 Dynamic Temperature Ramp on ABS samples, cooling and heating scans measured at 2°C/min and 5°C/min .....	78
Figure 6. 3 Variation of $\Delta T_g$ with respect to the cooling or heating rate .....	79
Figure 6. 4 Shape and dimensions of the specimens used.....	80
Figure 6. 5 Loss and damping peaks for Sample A, registered during the heating scan in RMS800.....	81
Figure 6. 6 Multi peaks Gaussian fit for loss modulus of Sample A.....	82
Figure 6. 7 Damping curve of Sample A-B-C measured with three-points bending geometry in RSA-G2 .....	83
Figure 6. 8 Glass transition Temperature vs number average molecular weight <sup>34</sup> .....	85
Figure 6. 9 Tg of the homopolymers of polybutadiene .....	86
Figure 6. 10 Glass transition temperature versus vinyl percentage.....	86
Figure 6. 11 Weight percentage distribution for Sample B and C .....	87
Figure 6. 12 Percentage of 1,2 Vinyl for Sample B and C .....	87
Figure 6. 13 Swelling index of Sample B and C .....	89
Figure 6. 14 TEM image of Sample D .....	89
Figure 6. 15 Tg of Sample D versus Swelling index. Position of Sample B and C are also reported.....	90
Figure 6. 16 Variation of Tg with respect to pressure, shown as function of 1,2 vinyl .....	93
Figure 6. 17 Tg and shear modulus of anionic rubber 75 KDa .....	94
Figure 6. 18 Loss modulus of Sample B and C compared with the value of glass transition temperature of the rubber reported by the dashed line .....	94

Figure 6. 19 Table of properties for Sample B with calculation of volume strain and $\Delta T_g$ .....	95
Figure 6. 20 Table of properties for Sample A along with volume strain and experimental and calculated difference in glass transition.....	97
Figure 6. 21 Bulk modulus of a rubber with 0.3 MPa of shear modulus as function of the Poisson's ratio .....	98
Figure 6. 22 Table of properties for Sample B, $K_r$ changed according to the difference in glass transition temperature .....	99
Figure 6. 23 Dilatometric curves obtained at 2°C/min .....	100
Figure 6. 24 Parametric curves shown separately for each sample .....	101
Figure 6. 25 Schematic representation of the approach used to calculate the percentage of cavitation. ....	102
Figure 6. 26 Amount of cavitated particles versus Temperature for Sample A, B and C .....	103
Figure 6. 27 Evidence of cavitation kinetics in Sample A .....	105
Figure 6. 28 Scheme representing how the cavitation will be monitored .....	106
Figure 6. 29 Best fit of the amount of cavitated particles versus time at $T_{iso}=-42.5^\circ\text{C}$ .....	107
Figure 6. 30 Percentage of cavitation shifted of $t_0$ .....	107
Figure 6. 31 Isothermal curves fitted. Percentage of cavitation and time to reach a plateau shown.....	108
Figure 6. 32 Amount of cavitated particles during cooling and isothermal curve for Sample A .....	108
Figure 6. 33 Isothermal curves and percentage of cavitation during cooling and isothermal curves for Sample B and C .....	109
Figure 6. 34 Time, percentage of cavitation and temperature of the isothermal curves for Sample A, B and C .....	110

Figure 6. 35 Double isothermal curve conducted on Sample A, first at -50 and then at -57 °C .....	111
Figure 6. 36 Percentage of cavitated particles for Sample A for all the isothermal curves ...	111

*CHAPTER 7*

Figure 7. 1 Normalized energy density as function of the void diameter. Values calculated using $\Gamma = 0.03\text{Jm}^2$ , $G_r = 0.4 \text{ MPa}$ , $K_r = 2000 \text{ MPa}$ , $F(\lambda f = 1$ .....	115
Figure 7. 2 Value of diameter of the void $d$ at which the energy becomes maximum, solution of Wolfram Alpha.....	116
Figure 7. 3 Expression of the void diameter $d$ at which the energy density is minimum, solution from Wolfram Alpha .....	117
Figure 7. 4 Normalized energy density as function of the void diameter at different volume strain. Continuous lines parallel to the y-axis represent the value of void diameter at which the density energy is maximum. Values calculated using $\Gamma = 0.03\text{Jm}^2$ , $G_r = 0.4 \text{ MPa}$ , $K_r = 2000\text{MPa}$ , $F\lambda f = 1$ .....	118
Figure 7. 5 Height of the energetic barrier with respect to the temperature, for diameters of rubber particles shown in the legend. ....	120
Figure 7. 6 Values of activation time for the isothermal curves conducted on Sample A ....	121
Figure 7. 7 Arrhenius plot fitting the experimental data of Sample A .....	122
Figure 7. 8 Probability of cavitation versus $1000/T$ for different rubber particles' diameters	124
Figure 7. 9 Zooming of the isothermal zone in Figure 7.8.....	125



## Introduction

Polymers are present in every aspect of our life, thanks to their exclusive properties they have gained a lot of importance in a wide variety of applications such as construction, transport, electronics, packaging, and many other sectors. Polymeric materials are not just used because of their light weight, corrosion resistance, easy process production, they are mainly utilized because of their ability to absorb energy and deform before reaching fracture, this ability is what is defined as toughness.

When toughness is present, polymers show a ductile fracture, a failure of the material that does not represent an issue, because it is not abrupt, but can be predicted. However, not all the polymeric materials show enough toughness, some of them are affected by a brittle behaviour giving rise to an unpredictable fracture.

In the latest 1940s, the idea of improving the properties of unpromising polymeric materials, subjected to brittle behaviour such as Polystyrene and Epoxy Resins have become of important interest in the plastic market. One way of increasing the range of applications of polymeric materials was the addition of 5 to 20% of rubber particles, dispersed into a matrix, that has led to what are called “Rubber-toughened Plastic”.<sup>1</sup>

These RT-plastics are composite materials composed of a rigid plastic matrix with a high glass transition temperature ( $T_g$ ) and a dispersed phase, made of rubber, with a lower  $T_g$ . These composite materials have a better balance of properties than the parent polymers: increased fracture resistance, elongation at break and impact strength, of course these improvements are gained by paying a price in tensile strength, modulus and melt viscosity, however negligible. This combination of properties has led to a significant diffusion of plastic in different field of applications. Despite that, rubber particles modification of polymers has a lot of questions still to be answered.

Indeed, many parameters are involved in this modification process and can influence toughened plastics behaviour such as: rubber and matrix composition, rubber particles content and dimensions, morphology of the rubber toughened polymer (presence of inclusions), compatibility and adhesion between matrix and particles. Attention should be given to some of these parameters due to their extreme importance in the toughening

of polymeric materials. The adhesion between the two phases should be strong and rubber particles must be finely dispersed to be effective in the mechanism. During numerous studies, the optimum values of particles dimension have been found, and they usually vary in the range of 0.1 and 2  $\mu\text{m}^2$ . The interfacial adhesion and the structure of the separate phase must be controlled to ensure the best balance of properties. This balance is strictly related to the polymers' compatibility, in fact toughness can be achieved only if the matrix and the rubber are neither completely compatible, giving rise to intermediate properties between those of the constituents, nor completely incompatibles, in which a fine dispersion cannot be achieved, influencing the optical, mechanical, and rheological properties. To ensure the sufficient degree of compatibility, copolymers are used, indeed graft and block copolymers are used to modify the properties of the interface between the two components, instead random copolymers to modify the properties of the single-phase, matrix or rubber particles.

The only way to study and inspect the toughening mechanism is to give attention also to the deformation mechanism of rubber reinforced plastics, in fact they are subjected to three principal mechanisms: shear yielding, crazing and rubber particle cavitation which are all affected by stress and temperature application.<sup>3</sup>

Shear yielding is related to a distortion of shape without significant change in volume, it starts with the formation of a localized shear band inclined of 45° with respect to the direction of application of stress. Instead, crazing mechanism will play an important role when the stress applied overcomes the elastic region and it is related to a change in volume. Small cracks oriented perpendicularly to the direction of the stress applied arise and instead of coalescing to form a real crack they are stabilized by fibrils of oriented polymeric material, which prevent them to increase their dimensions.

Generally, these two mechanisms of deformation are possible, but since polymers are viscoelastic materials whose critical stress values are time and temperature dependent, they are in competition. This is true for both homogeneous glassy polymers and rubber toughened plastics, but when rubber particles are introduced in a glassy polymer, the stress concentration around them will generate a lot of microscopic crazes that will not be able to propagate into the matrix due to the low value of stress. This “multiple

crazing” gives rise, at the macroscopic level, to the stress whitening of the material. Mechanism that will also affect the stress-strain behaviour increasing the area under the curve and consequently the toughness. In this thesis, the third mechanism of deformation, the so called “rubber particle cavitation” will be treated in detail. The goal is to provide an insight of the cavitation phenomenon studied through a rheological approach.

Rubber particle cavitation is one of the deformation processes present in ABS copolymers: dispersed rubber particles when subjected to a triaxial negative hydrostatic stress, usually generated by a significant mismatch of thermal expansion coefficient between matrix and dispersed phase, can give rise to the formation of cavities inside the rubber, allowing the release of volumetric strain present.

Even if, cavitation is a very peculiar phenomenon restricted to a small class of materials, it is extremely important due to the enormous contribution to the fracture resistance of rubber reinforced polymers. Indeed, cavitated rubber particles play an important role in the energy absorbing deformation mechanism because not only reduce the shear yield stress of polymer, but also act as nuclei for craze initiation. Fracture behaviour of rubber toughened materials is strictly related to the interactions of deformation mechanisms, shear yielding and multiple crazing, with the cavitation phenomenon. When particles are too small, the dilatational stress required to allow their cavitation increases reducing the probability of forming internal voids, this actually affects the impact behaviour of polymers that will suffer a decrease of the yield zone and consequently a reduction of the toughness of the material.

In this work, the rheological studies performed to inspect the cavitation phenomenon have provided interesting results concerning the time dependency of this phenomenon and the position of the glass transition temperature of the rubbery phase in ABS copolymers, which will ensure the development of future studies dedicated to this fundamental aspect of rubber toughened materials.



## CHAPTER 1

### Deformation mechanism in homogenous polymeric materials

Polymers are long macromolecular chains composed of different monomers, whose total molecular weight can reach even millions. When they are subjected to stress application, they show different behaviour according to their chemical structure, molecular weight, degree of crystallinity, number of crosslinks and many other characteristics. One of the simplest ways to inspect the mechanical resistance of polymeric materials is the tensile test. The dog-bone shaped specimen is subjected to a tensile force, the material will slowly extend until it fractures, during the test extension and stress applied are monitored giving rise to the stress-strain engineering curves.

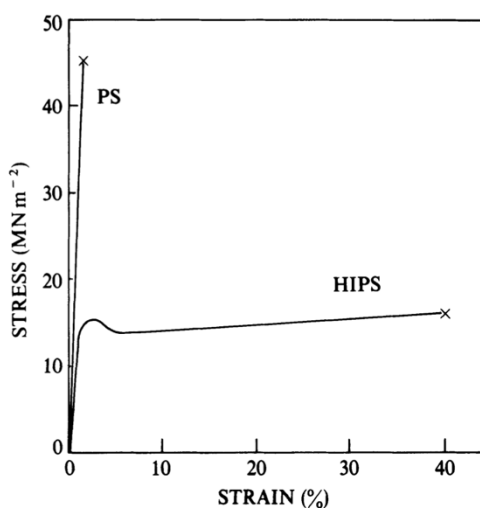


Figure 1. 1 Stress-strain curves for PS and HIPS <sup>2</sup>

Figure 1.1 denotes how it is important to analyse the stress strain curve, especially in terms of toughness. Two different behaviours are shown, PolyStyrene shows a linear zone corresponding to an elastic deformation in which once the stress is removed, we can recover the original shape, exception made for the last point of the curve that represents the failure of the material. The elastic deformation is denoted by a proportionality between stress and strain, in which the material obeys to Hooke's Law, this behaviour is rate and time dependent, but reversible.

The High Impact PolyStyrene, that is the rubber reinforced PolyStyrene, has a curve with an initial linear zone (elastic deformation), after a small maximum in the curve

conventionally known as the yield point, the region of plastic deformation began, in which recover is not possible anymore. In this region of almost constant stress, the applied deformation is just partly reversible.

The area below the curve represents the energy per unit volume required to cause the fracture of the material, indeed PolyStyrene shows a brittle behaviour, low values of strain and consequently small energy per unit volume (toughness), the High Impact PolyStyrene shows a toughened behaviour, high value of strains and increased area below the curve that will be responsible for an increase in toughness.

## 1.1 Elastic deformation

As already anticipated in the previous paragraph, the elastic deformation can be described by Hooke's Law which states the proportionality between stress and strain in uniaxial tension condition. This proportionality between the stress  $\sigma$  and the strain  $\epsilon$  in polymers can be expressed in terms of the useful Young's modulus, given by:

$$E = \frac{\sigma}{\epsilon}$$

(1.1)

The use of this parameter as indication of the stiffness of the material must be restricted to specific applications in which the material is subjected to uniaxial tensile or compressive loading, because not always stress and strain are related in this simple way. In order to describe the elastic behaviour of isotropic solids, whose properties are identic in all directions, three elastic constants are usually used:

- Young's modulus
- Shear modulus  $G$
- Poisson's ratio  $\nu$

The shear modulus relates the shear stress applied to the shear strain; Poisson's ratio instead accounts for the lateral contraction of the material during uniaxial tension. These parameters can be related through the following equation:

$$G = \frac{E}{2(1 + \nu)}$$

(1.2)

To account also for the resistance of the material towards compression, the bulk modulus can be used and expressed as function of Young's modulus and Poisson's ratio:

$$K = \frac{E}{3(1 - 2\nu)}$$

(1. 3)

The physical properties of polymeric materials are not always constant, in most of the cases polymers' properties are extremely sensitive to temperature, structure and testing conditions. Indeed, polymers show stress strain curves that vary for both temperature and rate of testing. For instance, the Young's modulus decreases as the temperature is increased and this produce an improvement of ductility, instead increasing the rate of testing produces the same effect of reducing the testing temperature, so it produces an increase of the Young's modulus.

## 1.2 Plastic deformation

When a polymeric material overcomes the yield point, the elastic deformation does not occur anymore, but a plastic deformation arises. In this plastic region, the material cannot recover the original shape, but it is subjected to an irreversible deformation. Different mechanisms of plastic deformation can arise in the material, after the application of a stress, these are shear yielding and crazing mechanisms.

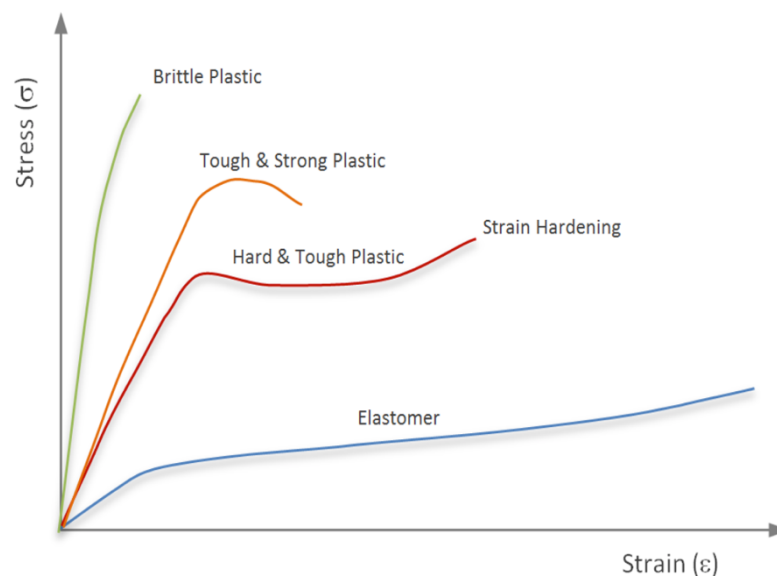


Figure 1. 2 Stress-strain behavior of polymers<sup>30</sup>

These both involve a localised or inhomogeneous plastic deformation, possible due to strain softening or other geometrical considerations. The main difference between shear yielding and crazing is related to the volume, in particular shear yielding occurs at constant volume, on the other hand crazing is characterized by an increase of volume.

### **1.3 Viscoelasticity**

The behaviour of polymers cannot be restricted just to the elastic deformation, because these materials usually display a peculiar behaviour identified by the term “viscoelasticity”. Viscoelastic materials, as suggested by their name, combine two different ways of response to the application of a stress. The term “viscous” is related to their ability to deform slowly when exposed to an external force, like water, viscous materials resist shear flow and strain linearly with time and once the material is deformed, there is no way of restoring the undeformed configuration. The term “elastic”, instead, is related to the fact that once the elastic material is deformed with the application of a stress, the removal of the stress applied leads to the recovery of the original configuration.

Viscoelastic materials are those substances having both elastic and viscous component, and whose properties exhibit a time scale and strain rate dependency. Viscoelasticity is typical of polymeric materials, and one technique able to inspect the viscoelasticity of polymers is the dynamic mechanical analysis. In particular, by applying a small oscillatory stress and measuring the resulting strain three different conditions can be obtained, according to the response of polymeric materials:

- Purely elastic materials have stress and strain in phase, so the response is the direct consequence of the stress applied
- Purely viscous materials show a stress-strain lag of 90-degree phase, consequently the strain is not the direct consequence of the stress applied
- Viscoelastic materials exhibit a hybrid behaviour, a response that is somewhere in the middle of the other two behaviours

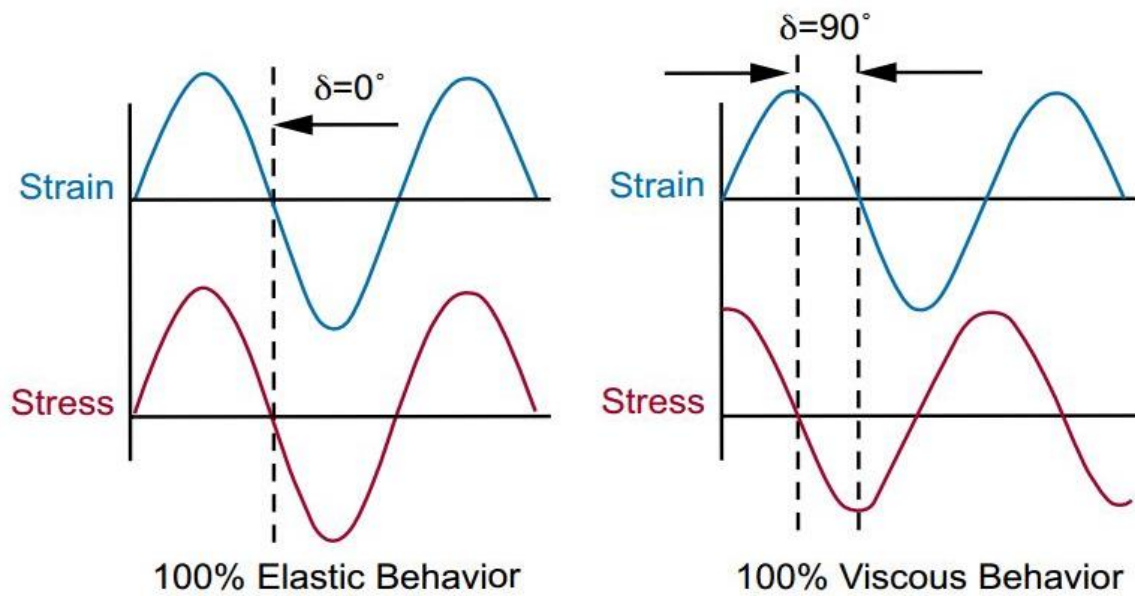


Figure 1.3 Elastic and Viscous behaviour<sup>31</sup>

In Figure 1.3 it is shown the elastic and viscous response of a material subjected to an oscillatory stress expressed by the following equation in terms of time and frequency:

$$\sigma = \sigma_0 \sin(\omega t) \quad (1.4)$$

If the material is perfectly elastic the Hooke's Law, in which stress and strain are linearly related by the Young's modulus  $\sigma = E\epsilon$  (1.5), can be applied and the strain should be expressed as:

$$\epsilon = \epsilon_0 \sin(\omega t) \quad (1.6)$$

In which  $\epsilon_0$  is the ratio between  $\sigma_0$  and the Young's modulus. The linearity of elastic materials is also expressed by the absence of any lag phase between stress and strain, so defining the angle between the two sinusoidal curves as  $\delta$ , in case of elastic material it is equal to 0.

Same consideration can be done for a viscous response, here however the Hooke's Law is not anymore valid, so a viscous material can be studied considering the Newton's Law in which the stress is proportional to the strain rate and independent of the strain:

$$\sigma = \eta \frac{d\epsilon}{dt} \quad (1.7)$$

Where  $\eta$  is the viscosity of the material and the stress is now out of phase with respect to the strain of 90 degrees:

$$\sigma = \sigma_0 \text{sen}(\omega t + 90^\circ) \quad (1.8)$$

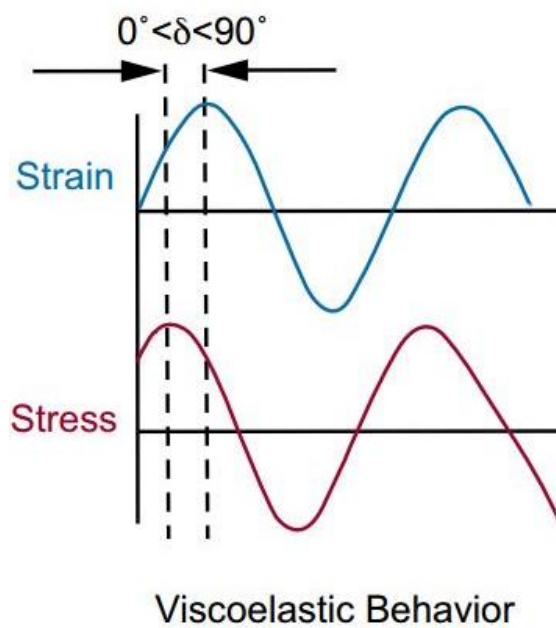


Figure 1.4 Viscoelastic Behaviour<sup>31</sup>

For a viscoelastic material, characterized by a hybrid behaviour between the elastic and the viscous response, the stress is still out of phase and can be expressed in a similar way as in Equation (1.4):

$$\sigma = \sigma_0 \text{sen}(\omega t + \delta) \quad (1.9)$$

But the main difference is given by the presence of a lag phase comprised between 0 and 90 degrees.

After having an idea of how viscoelastic materials respond, an attention must be given to the variables involved during the experiments. In case of an elastic material, the stress is directly proportional to the stress by a variable called Young's modulus, that provides

information about the strength of the material subjected to an external force. When a viscoelastic material is analysed, the Young's modulus necessitates a different expression, taking into account the combination of two contributions: viscous and elastic. This new modulus can be expressed in terms of complex modulus, in which a real and imaginary term are present:

$$E^* = E' + iE'' \quad (1.10)$$

In this equation  $E'$  represents the storage modulus and can be expressed in the following way:

$$E' = \frac{\sigma_0}{\epsilon_0} \cos\delta = E^* \cos\delta \quad (1.11)$$

And  $E''$  is representing the loss modulus, defined as:

$$E'' = \frac{\sigma_0}{\epsilon_0} \sin\delta = E^* \sin\delta \quad (1.12)$$

Dividing Equation (1.12) by Equation (1.11) another important variable can be retrieved:

$$\tan\delta = E''/E' \quad (1.13)$$

These rheological parameters can be summarized in the following image:

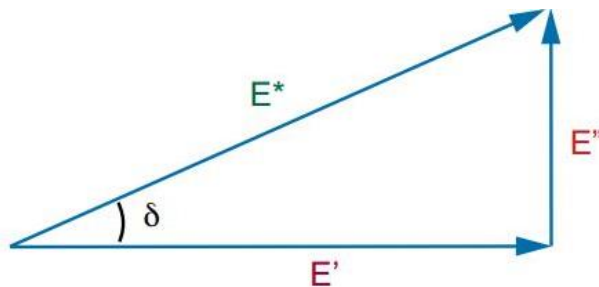


Figure 1.5 Geometrical approach to complex modulus<sup>31</sup>

From which with the help of a dynamic mechanical analysis a lot of information related to the relaxation behaviour of polymers can be retrieved.

## 1.4 Shear yielding

Polymers are capable of exhibiting yielding, but in some cases distinguish between elastic and plastic deformation, that are separated by the yield point, is not so easy. Recover of the original configuration, can be possible just if enough time for molecular relaxation is provided, and small deformations were applied. When large deformations are applied, the recovery can be achieved through a heating process above the glass transition temperature of the polymeric material. The yield point denoting the change from elastic to plastic deformations, is responsible also for a decrease of the stress with increasing strain giving rise to the so called “strain softening” phenomenon.

Going in more details, shear yielding is a physical phenomenon that takes place when polymer start to deform plastically under an applied stress. Specifically, shear deformation consists of a change of shape without significant change in volume and it becomes important when the failure mechanism of a polymer is taken into consideration. Plastic deformation in polymers starts with a localized shear band inclined with respect to the direction of application of the stress, usually in a tensile test the shear band is inclined of about  $45^\circ$ . This deformation occurs in absence of volume variation, thanks to the sliding of different portion of the material.

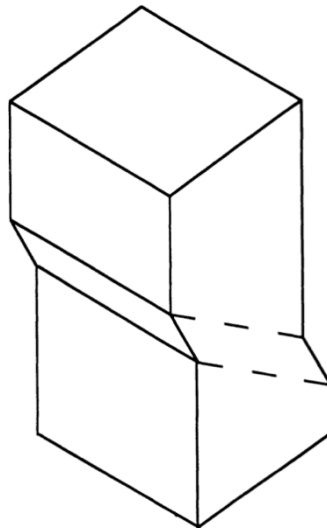


*Figure 1. 6 Schematic representation of a shear band<sup>32</sup>*

The tensorial nature of the deformation mechanism must be considered, because it is the only way to describe the three fundamental types of deformation:

- Tension or compression

- Shear deformation
- Increase or decrease in volume

The stress tensor is composed of nine components, in which  $\sigma_{ij}$  refer to the stress acting in the direction  $j$  on the face having a normal in the  $i$  direction.

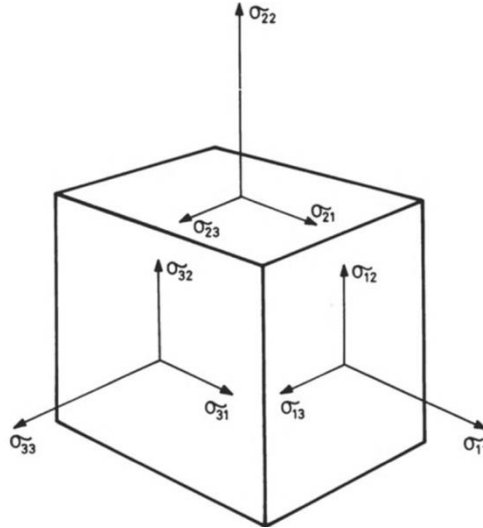


Figure 1. 7 The nine components of the stress tensor<sup>2</sup>

$$\text{Stress Tensor} = \begin{bmatrix} \sigma_{11} & \sigma_{12} & \sigma_{13} \\ \sigma_{21} & \sigma_{22} & \sigma_{23} \\ \sigma_{31} & \sigma_{32} & \sigma_{33} \end{bmatrix}$$

(1. 14)

This matrix can reduce its components to six, considering the symmetry of the shear stress  $\sigma_{ij} = \sigma_{ji}$ , moreover choosing a suitable reference axis, the shear stresses can be reduced to zero and the matrix can be expressed in the forms of principal stresses:

$$\begin{bmatrix} \sigma_{11} & 0 & 0 \\ 0 & \sigma_{22} & 0 \\ 0 & 0 & \sigma_{33} \end{bmatrix} = \begin{bmatrix} p & 0 & 0 \\ 0 & p & 0 \\ 0 & 0 & p \end{bmatrix} + \begin{bmatrix} \sigma_{11} - p & 0 & 0 \\ 0 & \sigma_{22} - p & 0 \\ 0 & 0 & \sigma_{33} - p \end{bmatrix}$$

(1. 15)

In which the first matrix refers to the hydrostatic component, represented by the mean stress, which is a pressure term able to alter the volume of the material without changing the shape:

$$p = \frac{1}{3}(\sigma_{11} + \sigma_{22} + \sigma_{33}) = -\sigma_m$$

(1. 16)

and the second matrix represents the deviatoric component able to alter the shape without affecting the volume.

Aware of the tensorial nature of the stresses, the yielding criterion for polymers can be introduced and expressed through Von Mises criterion that predicts a yielding occurring when the shear strain energy in the material reaches a critical value. However, in case of polymeric materials a modified version that takes into account the pressure dependency is necessary because the yield stress is not independent of the hydrostatic component of the stress tensor. The critical value of the shear strain energy can be expressed as:

$$\tau_{oct} = \frac{1}{3} [(\sigma_{11} - \sigma_{22})^2 + (\sigma_{22} - \sigma_{33})^2 + (\sigma_{33} - \sigma_{11})^2]^{\frac{1}{2}} = \tau_0 - \mu_m \sigma_m \quad (1.17)$$

where  $\tau_{oct}$  represent the ‘‘octahedral shear stress’’ and  $\tau_0$  and  $\mu_m$  are materials constant. The octahedral shear stress is the stress acting on a plane having a normal that makes the same angle to all three principal stress direction, explicitly  $|\sigma_{11}| = |\sigma_{22}| = |\sigma_{33}|$ . According to this criterion the shear yielding occurs when the octahedral shear stress reaches a critical value. In the three-dimensional principal stress space, the modified version of Von Mises gives rise to a cone, whose tip defines the conditions for which there can be yielding under the influence of hydrostatic stress alone.

## 1.5 Eyring’s model

Shear yielding is due to the sliding of macromolecules or segments of polymers subjected to the action of external stresses, these movements can occur just overcoming an energy barrier and passing through an activated state, that can be actually described with an Arrhenius like equation.

Since shear yielding in polymers is rate and temperature dependent, Eyring’s model comes to help in order to correlate these effects to the flow stress trough a molecular model of the flow mechanism. The theory behind this model is essentially an extension of the well-known Arrhenius approach to the chemical rate processes, which considers that reacting molecules must pass over an energy barrier in order to transform into a product. Eyring adopted a similar approach to treat viscous flow and plastic

deformation, he considered each flowing molecule passing over a symmetrical energy barrier as it squeezes past its neighbours into a new position, so the fundamental idea is that the macromolecule has to overcome a certain energy barrier in order to jump from an equilibrium position to another. When a shear stress is applied a net flow in one direction is created, indeed the stress does work on the molecule increasing its energy when it moves in the forward direction, but it reduces its energy when the molecule moves in the reverse direction. This rate and temperature dependent process can be described using Eyring equation which expresses a sort of deformation velocity as function of temperature and stress applied:

$$\dot{\epsilon}_y = \dot{\epsilon}_0 \exp\left(-\frac{\Delta H}{RT} + \frac{\sigma_y V^*}{2RT}\right) \quad (1.18)$$

In which the parameters involved are:

- $\dot{\epsilon}_y$  plastic strain rate
- $\dot{\epsilon}_0$  pre-exponential constant
- $\Delta H$  activation energy or also called enthalpy barrier, it is the energy required to allow the deformation process
- R the gas constant
- T the temperature in Kelvin
- $\sigma_y$  is the yield stress applied
- $V^*$  the activation volume, that has not to be confused with the physical volume, multiplied by the stress represents the mechanical work provided to the system that enables the deformation in the direction of the stress applied

In absence of stress, the polymer's segments rarely will jump overcoming the barrier, instead when a shear stress  $\sigma_s$  is applied, such as the maximum shear stress at yield  $\sigma_s = \sigma_y/2$  (1.19), the enthalpy barriers are changed into:

- $(\Delta H - \sigma_s V^*)$ , forward barrier
- $(\Delta H + \sigma_s V^*)$ , backward barrier

In this way the polymer jumps over the barrier at an equal rate forward and backward, giving rise to a process that will start all over again. Consequently, yielding can be seen as the result of the movement of polymer's segments jumping from one equilibrium position to another one.

## 1.6 Crazing

Different mechanism with respect to the shear yielding is crazes formation. Crazing is also a localized yielding process, that gives rise to the formation of microcracks that are actually bridged by fibrils of polymeric material and require the presence of a hydrostatic or dilatational component of the stress tensor.

When a tensile stress is applied and the elastic limit is overpassed, the material gives rise to the formation of small holes in a plane perpendicular to the direction of the maximum principal stress applied, ready to form an incipient crack. However, coalescence does not occur, because the small holes are stabilized by the presence of plastically deformed fibrils of oriented polymeric material which span the gap and prevent the propagation. The network formed by the interpenetration of fibrils and voids is what has been called as craze.

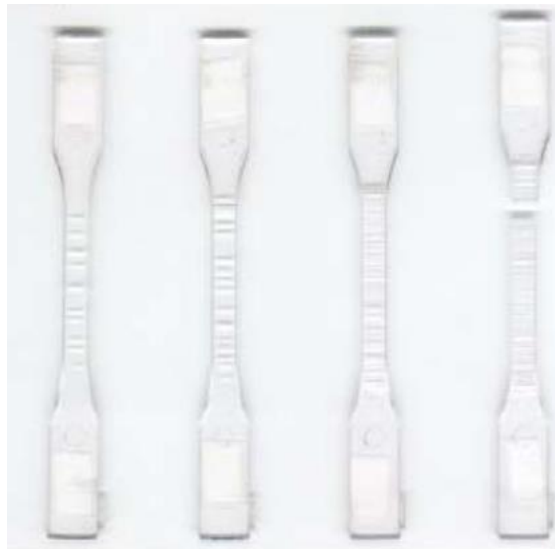


*Figure 1. 8 Evolution of crazes in Polystyrene*

Nucleation of crazes is related to the defects and impurities present at the microscopic level that cause the concentration of stress, for instance flaws, cracks, or internal foreign sites such as air bubbles. Under the application of suitable external stresses, they can

activate a locally yielding process while the surrounding material is still in the elastic regime. Indeed, crazes will be formed when the plastic deformation near the defect is not able to propagate in the material giving rise to the formation of micro voids. Once crazes are formed, they will start to propagate on a plane normal to the direction of application of stress and increase their dimensions (i.e., thickness) intersecting the polymer's fibrils. Thanks to the transmission of loads to the fibrils, crazing mechanism represent an important energy absorbing mechanism.

Crazes will form just under condition of hydrostatic tension because an increase in volume is not possible under compression in which shear yielding can actually occur. The criteria for crazes formation were proposed, in terms of biaxial stress experiment conducted on PMMA, by Sternstein and Ongchin<sup>4</sup>:

$$\sigma_b = |\sigma_{11} - \sigma_{22}| = A(T) + \frac{B(T)}{\sigma_{11} + \sigma_{22}} \quad (1. 20)$$

In this equation  $\sigma_b$  is the biaxial stress applied,  $A(T)$  and  $B(T)$  temperature dependent quantities.

In order to have a more general criterion able to represent the maximum shear stress a modification was introduced by Bowden and Oxborough<sup>4</sup>, their approach states that crazing occurs when the strain attains a critical level, in any direction, and this level is strictly related to the hydrostatic component of the stress.

The modification of the maximum shear stress was expressed in the following way:

$$\sigma_{11} - \nu(\sigma_{22} + \sigma_{33}) = C(t, T) + \frac{D(t, T)}{\sigma_{11} + \sigma_{22} + \sigma_{33}} \quad (1. 21)$$

Where  $\nu$  is the Poisson's ratio and  $C(t, T), D(t, T)$  are time and temperature dependent quantities. Writing the Young's modulus and the major principal strain the following expression can be obtained:

$$E\varepsilon_{11} = \sigma_{11} - \nu(\sigma_{22} + \sigma_{33}) \quad (1.22)$$

And therefore, the critical strain criterion can be expressed as a combination of *Equation (1.21)* and *(1.22)*:

$$\varepsilon_{11} = \frac{1}{E} \left[ C(t, T) + \frac{D(t, T)}{\sigma_{11} + \sigma_{22} + \sigma_{33}} \right] \quad (1.23)$$

Plastic deformation and local energy absorption are involved in craze initiation, propagation, and breakdown. However, these micro mechanisms are localised and restricted to a small volume of material, so in order to increase the toughness of polymeric material it is necessary to ensure a sufficiently large volume in which this energy dissipation mechanisms can occur.

### **1.7 Interaction between shear bands and crazes**

The type of deformation mechanism that can occur in a polymeric material is not just the result of characteristic molecular structure such as entanglements or crosslinks able to reduce the mobility of molecules, but it is also determined by the stress conditions able to favour shear bands or craze formation.

The two deformation mechanisms “shear yielding” and “crazing” are both possible and according to the stress conditions and to the critical value, usually dependent on time and temperature, enter into competition. The interactions, between the two processes, are fundamental in the analysis of toughness and fracture resistance, especially because they determine the transition between ductile and brittle behaviour.

Competition between the two mechanisms can be analysed in *Figure 1.9* where a complete failure envelope under biaxial stress is shown. The graph reported shows the projection of  $\sigma_1$  and  $\sigma_2$  principal stresses expressed by Von Mises criterion in case of shear yielding and the criterion for crazing expressed in *Equation (1.20)*. In the first quadrant, subjected to biaxial tension, the polymer fails in condition of crazing and brittle fracture will occur at a stress well below the corresponding stress in condition of

shear yielding. In the third quadrant, the polymer is subjected to biaxial compression, no increase of volume and consequently no crazing will be possible, indeed shear yielding will dominate. In the second and fourth quadrant, the two envelopes intersect, so shear yielding, and crazing will occur simultaneously. To achieve this situation *Equation (1.17)* and *Equation (1.23)* must be both satisfied, and the stress cannot overcome the level required to cause fracture.

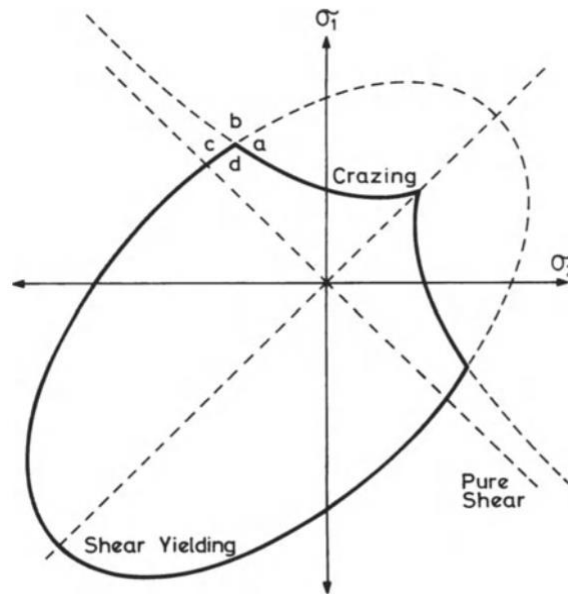


Figure 1.9 Failure envelope under biaxial stress<sup>2</sup>

In these regions of the diagram, we will have the transition between brittle and ductile behaviour of the material, interactions between crazes and shear bands are expected especially in the zone of the envelope denoted by 'a'. Interactions can assume different forms:

- A craze will meet an existing shear band and its growth is stopped due to the high molecular orientation within the shear band
- New shear bands will initiate from the tip of the crazes, where stress is concentrated and, these bands will again hinder the expansion of crazes

The relative positions of failure envelopes are influenced by various factors, such as the temperature, strain rate and magnitude of the third principal stress  $\sigma_{33}$ . For example, increasing temperature, shear yielding is usually promoted at the expense of crazing, while increasing the strain rate generally promotes a more brittle response from the polymer. If we consider the effect of  $\sigma_{33}$ , the hydrostatic pressure can increase the

crazing envelope with respect to the shear one, promoting the ductility of the polymer itself.

## CHAPTER 2

### **Rubber toughened polymers**

It is well known that glassy thermoplastic polymers, like polystyrene (PS), styrene-acrylonitrile (SAN) and polymethylmethacrylate (PMMA) can be blended or alloyed with particles of polybutadiene rubber to give rise to different new materials such as acrylonitrile-butadiene-styrene (ABS), high impact polystyrene (HIPS) and rubber toughened polymethylmethacrylate (RT-PMMA). These materials usually called "rubber toughened polymers" stand out because of their improved mechanical properties and impact toughness with respect to the parent ones.

In this thesis attention will be dedicated to acrylonitrile-butadiene-styrene copolymers (ABS), opaque thermoplastic polymers, strong and durable even at low temperatures.

#### **2.1 ABS Acrylonitrile-Butadiene-Styrene**

Commercially available since 1940s, ABS was first developed during World War II in the attempts to produce bulletproof plastic sheets. It was patented in 1948 and introduced to commercial markets by the Borg-Warner Corporations. Essential properties of ABS are the light weight and ability to be injection moulded and extruded that make it useful in manufacturing products such as pipe systems, musical instruments, luggage, automotive interior parts, and many other applications. It is useful in different applications that require a hard, tough and heat resistant engineering plastic.

ABS is a copolymer made from the monomers Acrylonitrile, 1,3 Butadiene and Styrene, its chemical resistance, heat and ageing stability depend on the acrylonitrile, while its toughness and impact resistance are developed thanks to the introduction of butadiene rubber. Styrene is instead responsible for copolymer rigidity, glossy surface and easy processability.

Proportions of these three monomers can vary from 15% to 35% of acrylonitrile, 5% to 30% of butadiene and 40% to 60% styrene. At the end a long chain of polybutadiene will be crisscrossed with shorter chains of styrene-co-acrylonitrile, the presence of polar nitrile groups in the neighbouring chains, increases the attraction between chains,

binding them together and increasing the final strength of ABS with respect to the pure polystyrene.

The incorporation of a low  $T_g$  rubber reduces the modulus, the hardness but improves the toughness, however, makes the material susceptible to oxidation and degradation, making the addition of chemical compounds necessary.

## **2.2 Production of ABS**

All products made of ABS commercially available are produced with two different production technologies: mass and emulsion. These two technologies are able to produce materials with peculiar, but different properties. Mass technology is usually preferred in case of material with high mechanical properties produced preferably through extrusion. ABS products derived from mass technology show a good balance between impact resistance and modulus, so they provide a high mechanical resistance and high value of elastic modulus. Emulsion products provide an optimum balance between esthetical and mechanical properties, combination typically required for those materials produced through injection moulding technique.

The diverse performances present between emulsion and mass product are essentially due to the different morphology, distribution and dimension of the rubber particles dispersed into the matrix. ABS products derived from the emulsion technology show a bimodal distribution of spherical particles, whose mean value of diameter is slightly lower than those produced through mass technology. Rubber particles of mass products, distinguish themselves for a “salami” morphology and a monomodal distribution. One of the main limitations of the mass technology is the minimum dimension of particles that can be obtained. Indeed, rubber particles are obtained through an “in situ mechanism”, in which considering equal flux characteristics (intensity, shear and elongational geometry) and interfacial tension, the only way to reduce the diameter of particles is to increase the viscosity ratio between SAN and rubbery phase. SAN viscosity is dictated by the “melt flow index” required, the rubber viscosity instead is dependent on the production process, in which low value of rubber viscosity make impossible the last refining step.

In order to overcome this limitation, new technologies have been developed, in particular these ones do not necessitate the refining step for the rubbery phase and consequently expand the range of rubbers that can be used in the production of ABS from mass technology. These improved technologies allow to reduce the viscosity of the polybutadiene rubber, also involving a change in the final morphology of ABS that will be now similar to those obtained through emulsion.

However, another problem occurs in these peculiar technologies: reducing the viscosity of the rubber allows to obtain smaller diameters of the particles, this will increase their tendency to agglomerate, modifying irreversibly the mechanical and elastic properties of the final products. Consequently, in order to stabilize these smaller particles, it is necessary to increase the concentration of grafting copolymer used, improving in this way also the compatibility between the two polymeric phases constituting the material.

### **2.3 Toughening mechanism in rubber reinforced polymers**

The property of toughness, regarded as the ability of a material to absorb energy and plastically deform before fracture, have become a fundamental factor in the selection of material for specific purpose. The continuous research of materials with better properties is related not just to the discover of new materials but also to the modification of those already present. Focusing on the plastic market, the toughness requirement has been achieved thanks to a relatively simple modification of the homogenous glassy polymer, called the rubber toughening mechanism. This strategy is based on the idea of maximizing the volume of material participating in the process of dissipation of a large amount of energy.

Basically, this mechanism is based on the dispersion of a small quantity of rubber particles in a polymer matrix, having lower stiffness than the matrix itself. Usually, the rubber's quantity varies in the range of 5 to 20 %, and the dimension of particles goes from 0.05 to 5  $\mu m$ , moreover the effective rubber content can be higher than the amount added, due to the possible inclusion of rigid matrix.

Adhesion between rubber particles and matrix is essential to ensure a good transfer of properties and it is not always possible with the matrix and the rubber alone because usually polymers chemically different are immiscible and incompatible. Compatibility

is usually achieved with the introduction of a grafted copolymer. Grafted copolymer has two functions:

- Acts as surfactant for dispersion of particles and consequently affects the final dimension
- Ensures the adhesion between matrix and dispersed phase during deformation

Rubber toughened polymers are composite materials with a complex structure that show an increased fracture resistance, paying a negligible extent in stiffness due to the rubber presence. At small strains the deformation mechanism is governed by matrix properties, instead the mechanical response to deformation at high values of strain is associated to the rubbery phase that indeed is responsible for the improved toughness.

Some thermoplastics, especially polystyrene compound, are usually subjected to a multiple crazing toughening mechanism, while a larger family of materials usually show shear yielding phenomenon as deformation mechanism. Furthermore, both deformations are accompanied by another important mechanisms that is the cavitation of rubber particles dispersed into the matrix. Indeed, it is generally known that the principal mechanisms responsible for an improvement of the toughening behaviour and the energy absorption capability of polymeric materials are shear yielding, crazing, and rubber particles cavitation. Even if shear yielding and crazing under specific conditions are just in part recoverable, they are usually described as irreversible processes. Cavitation phenomenon is actually irreversible because it involves the breaking of chemical bonds of the rubber that cannot be recovered by heat or time.

As already anticipated in the previous chapter, shear yielding does not produce a change in density or volume because it occurs without loss of intermolecular cohesion, while crazing and cavitation involve void formation and local increase of volume. Despite the differences the overall effect of shear yielding, and crazing is the improvement of the capability of absorbing energy of rubber toughened polymers thanks to a combination of strain hardening and cavitation present under the application of a load.

In order to have a general idea about the toughening mechanism accomplished in rubber reinforced polymers, in the following paragraphs attention will be given to multiple crazing and shear yielding, that usually occur simultaneously. Furthermore, a small introduction on the effect of rubber particles on the stress field is provided before giving

attention to the toughening mechanism obtained with the modification of the polymeric matrix.

## 2.4 Effect of rubber particles on stress field

Rubber particles, dispersed into the glassy polymer, are responsible for the alteration of the stress field acting in the matrix, consequently they allow a modification of the deformation mechanisms involved in the matrix itself. In order to provide an idea about the alteration involved an analysis of the stresses can be used.

The addition of rubber particles into homogenous glassy polymers alters the stress field around the inclusion itself, due to the lower shear moduli of the rubber with respect to the material of the matrix. Any discussion about rubber toughening must be coupled with an understanding of the inhomogeneous stress field generated around the particles acting as stress concentrators.

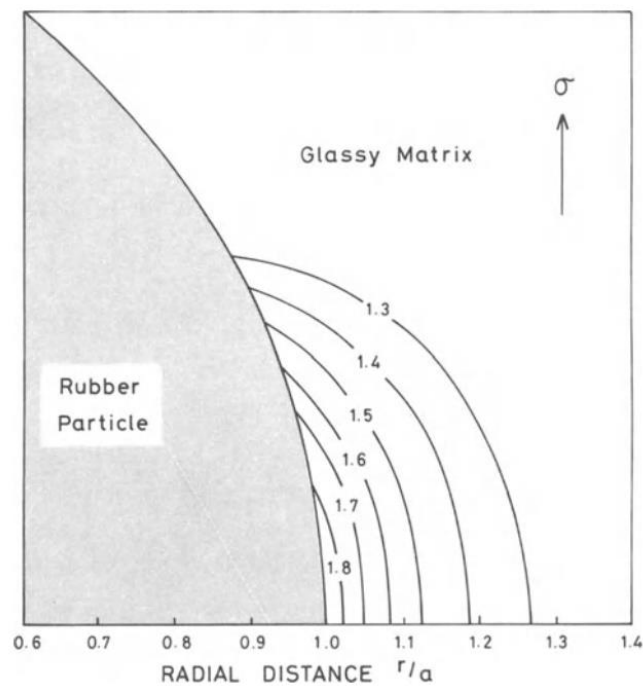


Figure 2. 1 Contour map showing stress concentration<sup>2</sup>

The simplest model to describe the stress analysis around a rubber particle has been proposed by Goodier, in case of an isolated spherical particle embedded in an isotropic solid body. The spherical particle is assumed to be homogenous, isotropic, and perfectly bonded to the matrix, moreover the matrix is subject to a uniform uniaxial tension  $\sigma$  at

all points remote from the rubber particle. This analysis applied to an isolated rubber particle in High Impact PolyStyrene under uniaxial tension is shown in *Figure 2.1*.

The figure shows that maximum stress concentrations occur at the equator of the rubber particle, and they fall with increasing distance from the surface of the particle itself. The extension of the stress concentration zone depends on the particles' dimensions, but the intensity of the stress concentrated will not depend on it, indeed particles with different dimensions but same shape can give rise to the same intensification of stress.

The contour map reported emphasizes the localized nature of the stress field, however stress field's importance relies on the capacity to generate crazes and shear bands, and consequently affect the deformation mechanism, not on its extent.

## **2.5 Multiple crazing and shear yielding**

Multiple crazing theory was first introduced by Bucknall and Smith in 1965<sup>5</sup>, after numerous experimental observations of the fracture of glassy polymers.

The basis of this theory relies on the ability of rubber particles to promote and control the nucleation and the growth of crazes, since they act as stress concentrators in the matrix. When a rubber toughened material is subjected to tensile stress, crazes are initiated near the equators of rubber particles, where points of maximum principal strain are usually located. Once they are formed, propagation will start following the planes of maximum principal strain and will continue until the stress concentration at the tip falls below the critical level for propagation or when they income into large rubber particles or other obstacles, such as shear bands. Basically, a large number of small crazes are generated due to the presence of rubber particles, instead in the unmodified parent polymer a small number of large crazes would have been present causing the failure of the material. This deformation mechanism is coupled by a significant dissipation of energy and a toughening behaviour.

Multiple crazing is responsible also for a macroscopic modification of the material, in fact the generation of small crazes around the rubber particles determine a change in the aspect, giving rise to the "stress whitening" phenomenon, responsible for an increased opacity and brighter colour than the parent polymer as it occurs in HIPS (*High Impact Polystyrene*).

The multiple crazing theory is well founded on experimental evidence, however some behaviours remain without explanation, for instance the marked necking in tensile yielding experiments of some toughened plastics such as ABS. To explain this behaviour a postulation that shear yielding mechanism also contribute to the tensile deformation of reinforced rubber plastics is required.

The suggestion that rubber toughening is also related to the shear yielding in the matrix was proposed by Newman and Strella in 1965<sup>6</sup>, based on the experimental studied conducted on ABS that showed rubber particles distortion in tensile specimens. However, shear yielding theories do not explain stress whitening, density changes, elongation in absence of necking and other characteristics of rubber toughened plastics. So, shear yielding contributes in some extent to these effects, especially in those materials that show a more ductile matrix, in these ones crazes and shear bands interactions appear to be more important, since shear bands are oriented parallel to the direction of stress application, they are normal to the plane of crazes, consequently, shear bands will act as obstacle to craze propagation, increasing the toughness.

Materials subjected to both shear yielding and crazing, that occur simultaneously are influenced in their deformation behaviour by the dimensions and morphology of the rubber particles. For instance, considering HIPS and ABS, their overall deformation is affected by the contribution of the two mechanisms. In HIPS crazing dominates, and there is a little contribution coming from shear yielding, on the other hand, in ABS crazing and shear yielding occur simultaneously so that the specimen can show both stress whitening and necking. Indeed, taking into account the morphology of rubber particles, it can be noticed that bigger particles full of matrix inclusions favours crazes nucleation, instead smaller particles without inclusion allow the shear yielding, so in these materials the maximum allowable toughening effect can be achieved just realizing a bimodal distribution of rubber particles.

Shear yielding and multiple crazing in rubber reinforced polymers are coupled with the cavitation phenomenon, in particular when a material tends to deform in shear yielding condition, the presence of rubber particles able to cavitate enables the build-up of local hydrostatic tension that are produced by the release of localised shear processes moreover, since shear yielding occurs under biaxial stress state, cavitation (induced by

the presence of triaxial stresses) is able to favour local shear yield deformations. While in those material subjected to multiple crazing, crazes formation is favoured by the presence of rubber particles that, when fibrillation mechanism occurs, contribute also to the craze's stabilisation and to the formation of continuous planar bands running through the material.

## **2.6 Introduction about cavitation of rubber particles**

A small introduction about cavitation phenomenon is presented in order to give an idea of the toughening mechanism involved in rubber reinforced plastics, indeed cavitation phenomenon will be treated later in detail.

Rubber particle cavitation has become important after several years of research and this is now considered as one of the causes contributing to stress whitening and toughening in many polymeric materials. When rubber particles are introduced into a glassy matrix, they act as concentrators of the stress applied to the toughened materials, however this concentration of stress can also be responsible for the generation of a hydrostatic stress inside the rubber, allowing the formation of a void inside the particles, this phenomenon is called "cavitation".

Cavitation phenomenon was first observed, by H. Breuer<sup>7</sup> in BASF, during the analysis of a matrix of Poly-Vinyl-Chloride reinforced with Methyl-Acrylate-Butadiene-Styrene. The idea was retrieving information about the deformation mechanism such as crazes and shear bands, but the images obtained with the TEM (transmission electron microscope) showed micro voids in rubber particles, since then a lot of other studies have been dedicated to this peculiar phenomenon.

Rubber cavitation plays an important role in the toughening mechanism, first it contributes to dissipate the energy and, in this way, increasing the toughness, but its primary effect is the variation of the stress field to which the matrix is subjected. For instance, the region of matrix included between two particles is subjected to hydrostatic conditions, that can be released when cavitation occurs. Indeed, the formation of a micro void inside the particle is able to cancel the dilatational stress generated, subjecting the matrix to a planar stress. This can give rise to the nucleation of shear bands in regions of the material where in absence of cavitation, shear yielding would have not been

possible. Cavitation not only reduces the resistance of the polymer towards volumetric expansion under the application of a dilatational stress, but it also provides free surfaces useful for craze initiation.

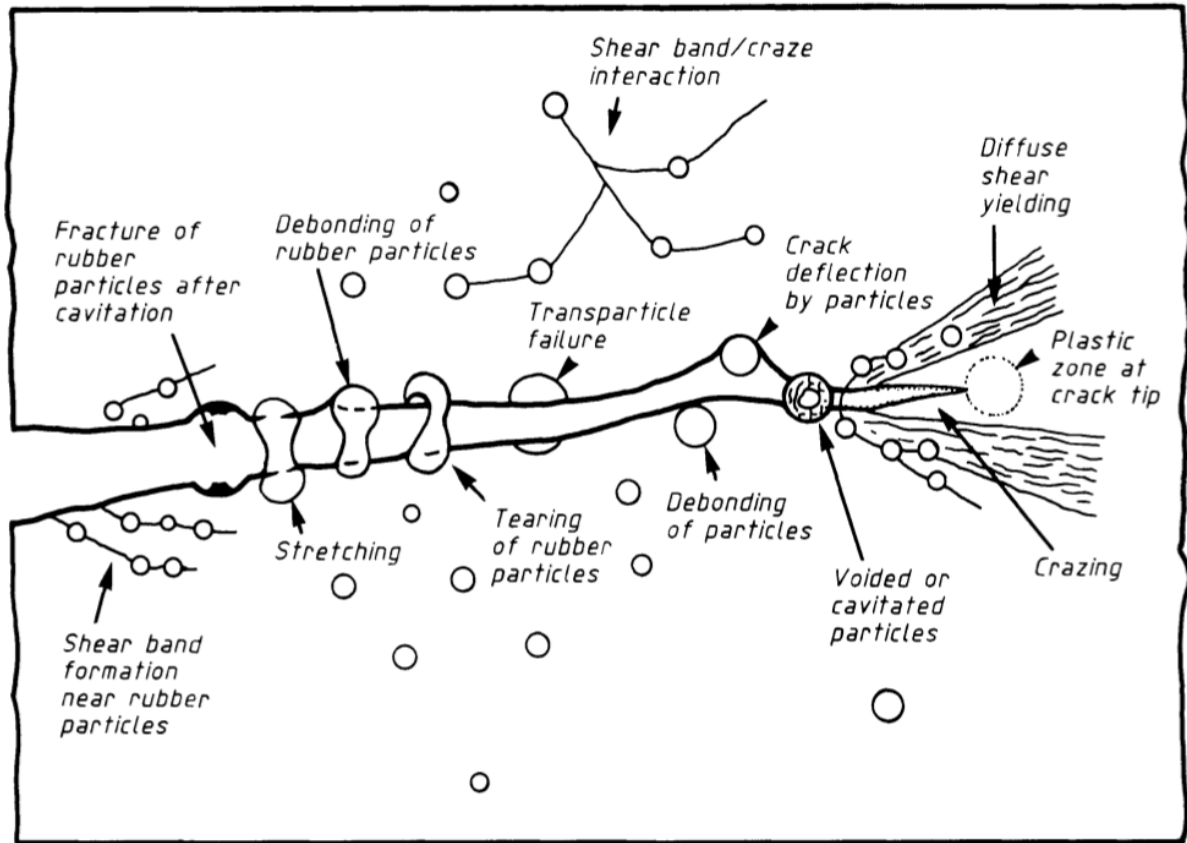


Figure 2. 2 Crack toughening mechanism in rubber reinforced polymers<sup>32</sup>

## **Cavitation of rubber particles in rubber toughened polymers**

Rubber particles cavitation affects the deformation and fracture behaviour of rubber modified plastics contributing to their improvements in both thermoplastics and thermosets. Cavitation of rubber particles plays an important role in the toughening process not just when shear yielding is the main deformation mechanism, but also when crazing is the dominant deformation mechanism. In order to have a general idea about the effect of rubber particle cavitation on the toughening mechanism, it is necessary to consider the interactions between cavitation and the other ways of deformation.

In 1993, A. Lazzeri and C. Bucknall proposed a theory able to explain the effect induced by the presence of cavitation of rubber particles. According to their work the deformation mechanism starts with the rubber particle cavitation, that represent an essential condition for extensive shear yielding of the matrix under intense conditions such as the notched impact test. Moreover, the brittle-tough transition temperature is affected by the particles' dimensions, decreasing the size also the temperature will decrease but only down to a critical size of particle dimension of about  $0.2 \mu\text{m}$ , below which the particle shows difficulties in cavitation development.

Starting with the model for particle cavitation, the interactions between particle cavitation and the other mechanisms are then discussed, considering in this way the deformation behaviour present in rubber reinforced plastics, other considerations will be provided considering the parameters influencing the cavitation phenomenon.

Moreover, a brief paragraph dedicated to the notched impact behaviour must be considered due the extremely important influence of cavitation on it and the information about fracture resistance that can be retrieved.

### **3.1 A model for particle cavitation**

The cavitation phenomenon has been observed in many toughened plastics over the years, but just a model has been proposed to describe the energy involved in this mechanism. The energy balance criterion for cavitation has been provided by A. Lazzeri

and C. Bucknall in 1993<sup>8</sup> and includes the terms relative to the energy stored by the matrix and those released in the void expansion. The principle of this model is that the particle will be able to cavitate just when the energy released during cavitation is greater than the energy needed to form the void.

The model is based on two basic assumptions:

- Largest defect in a typical rubber particle under triaxial tension are micro-voids whose dimensions are in the order of nanometers
- Expansion of micro-voids is possible just if the release of the stored strain energy density is sufficient to both increase the surface area of the void and to stretch the surrounding layers of rubber biaxially

Before introducing the energy balance, an assumption is made for convenience of calculation: the rubber toughened polymer is treated as an assembly of spherical elements, in which the rubber particle has a radius  $R$  and is surrounded by a concentric shell of the matrix polymer with an external radius  $Q$ . This configuration is shown in the figure reported below.

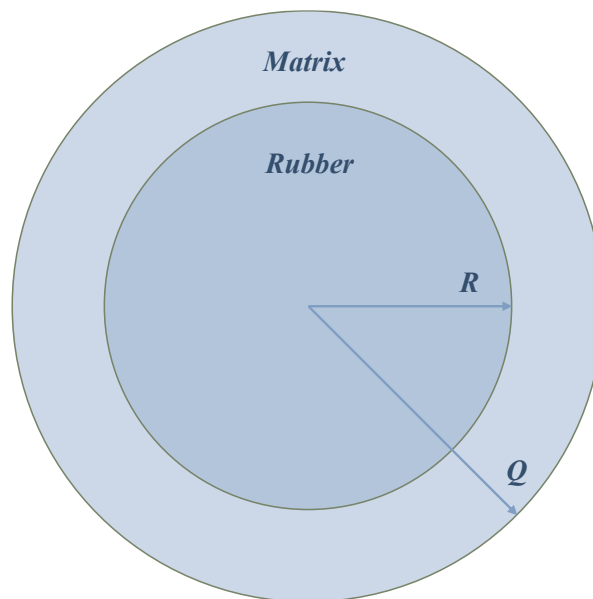


*Figure 3. 1 Composite spherical element used in the model*

The energetic model will consider numerous parameters, in particular the elastic properties that are defined by shear and bulk moduli, they are expressed respectively as  $G$  and  $K$ . The rubber and matrix phases are assumed homogenous, isotropic, and well bonded one to the other, because otherwise the stress condition required for cavitation

inside the rubber particle will not occur and interfacial debonding will be favoured. Since rubber has very low shear moduli but high bulk moduli, under uniaxial or biaxial tension, the particles alone can reach extension ratios exceeding of about five times at low stress, which are able to produce volume strain of about 0.5 %. On the other hand, when they are dispersed into the matrix, they are easily subjected to triaxial stress, and the volume strain generated can rise to 1 %. These dilatational strains can be enough to overcome the weak Van der Waals forces attracting neighbouring chains in organic polymers, inducing cohesive failure in the rubber, whose expansion is aided by the mobility of the rubber molecules.

To simplify the calculation the void is assumed to be a sphere of radius  $r$  concentric to the rubber particle well bonded to the matrix.

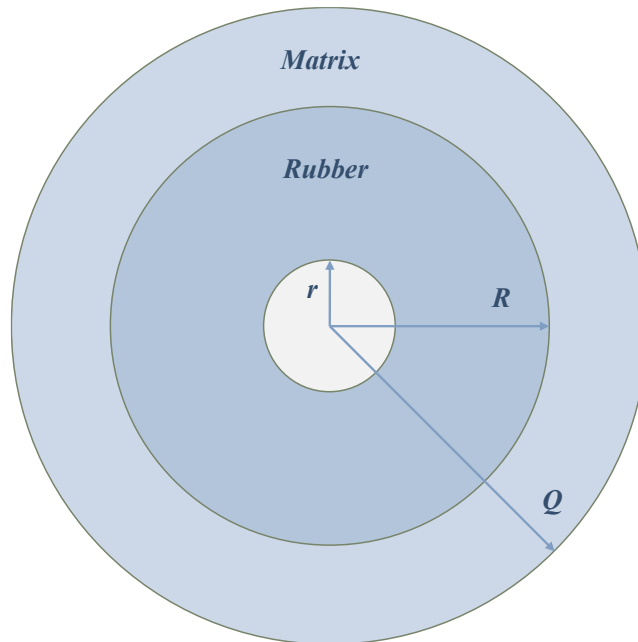


Figure 3. 2 Composite spherical element used in the model, after cavitation (formation of the void)

Supposing that cavitation is initiated by a critical mean stress able to produce a volume strain in the rubber, the strain energy of the particle before cavitation is expressed as:

$$U_0 = \frac{4}{3} \pi R^3 W^* = \frac{2}{3} \pi R^3 K_r \Delta v_0^2 \quad (3. 1)$$

In which  $W^*$  and  $K_r$  are respectively the stored energy density and the bulk modulus of the rubber,  $\Delta v_0$  is the volume strain in the rubber phase immediately before cavitation. The matrix is supposed to do not provide additional external work considering the radius

of the rubber particle remaining constant even during the expansion of the cavity. Considering the volume fraction of the void as  $\frac{r^3}{R^3}$ , the volume strain within the cavitated particles can be calculated as  $(\Delta v_0 - \frac{r^3}{R^3})$ . Moreover, the formation of this cavity will introduce two additional terms to the strain energy of the particle, one is related to the surface energy of the rubber particle ( $4\pi r^2 \Gamma$ ), the other to the energy required to stretch biaxially the rubber and allow the expansion of the void ( $\int W_s^* dV$ ).

The total energy  $U$  of the cavitated rubber particle is:

$$U(r) = \frac{2}{3} \pi R^3 K_r \left( \Delta v_0 - \frac{r^3}{R^3} \right)^2 + 4\pi r^2 \Gamma + \int W_s^* dV \quad (3.2)$$

The second term related to the surface energy of the rubber particle in which  $\Gamma$  is the surface tension of the rubber, the third term represent the shear strain energy able to stretch the rubber ensuring the expansion of the cavity after cavitation. To calculate the shear strain energy density, the rubber-like elasticity theory is considered, the rubber concentric shell of radius  $a$  is subjected to an equibiaxial extension to the final radius  $b$ , due to the formation of the cavity:

$$W_s^* = \frac{G_r}{2} (\lambda_1^2 + \lambda_2^2 + \lambda_3^2 - 3) \quad (3.3)$$

In equibiaxial extension, the principal extension ratios are  $\lambda_1 = \lambda_2 = \lambda$  and  $\lambda_3 = \frac{1}{\lambda^2}$  where  $\lambda = b/a$ . The  $W_s^*$  can be rearranged in the following expression, in which the  $G_r$  represents the shear modulus of the rubber:

$$W_s^* = \frac{G_r}{2} (2\lambda^2 + \lambda^{-4} - 3) \quad (3.4)$$

The extension ratio of a thin spherical shell and its radial distance from the centre of the cavitated particle  $b$  are related by the following expression:

$$\rho_a a^3 = \rho_b (b^3 - r^3) \quad (3.5)$$

Rearranging, thanks to expression of the extension ratio, b can be expressed:

$$b = a\lambda = r\lambda \left( \lambda^3 - \frac{\rho_a}{\rho_b} \right)^{-\frac{1}{3}} \quad (3.6)$$

Keeping in mind that  $dV = 4\pi b^2 db$ , the shear strain energy of a cavitated particle is:

$$U_s = \int_{b=r}^R 4\pi b^2 W(b) db \quad (3.7)$$

Combining *Equation (3.4), (3.6) and (3.7)*, the shear strain energy is indicated in the following equation in which  $\rho$  represents the density ratio and is equal to  $\frac{\rho_a}{\rho_b}$ , and  $\lambda_f$  represents the extension ratio at failure in equibiaxial extension:

$$U_s = 2\pi r^3 \rho G_r \int_{\lambda=\lambda_f}^1 \frac{\lambda^2 (2\lambda^2 + \lambda^{-4} - 3)}{(\lambda^3 - \rho)^2} d\lambda \quad (3.8)$$

In the abbreviated form the shear strain energy can be written as:

$$U_s = 2\pi r^3 \rho G_r F(\lambda_f) \quad (3.9)$$

The function  $F(\lambda_f)$  has values in the range of 0.7 to 1.3, when the extension ratio at failure goes from 2 to 6. The treatment done till now, neglects the central part of the rubber particles highly stretch to value beyond  $\lambda_f$ , and consequently fails. To write the expression for the energy require to rupture this region,  $W_{sf}^*$  shear strain energy density at failure and  $a_f$  radius of the stretched zone at the centre of the particle must be considered, the radius can be retrieved from the *Equation (3.6)*:

$$U_{sf} = \frac{4}{3} \pi a_f^3 W_{sf}^* \quad (3.10)$$

Since  $U_s$  and  $U_{sf}$  are proportional to  $r^3$  they can be combined, by an appropriate modification of  $F(\lambda_f)$ , into a single equation.

The energy of the cavitated rubber particle can be finally expressed:

$$U(r) = \frac{2}{3} \pi K_r R^3 \left( \Delta v_0 - \frac{r^3}{R^3} \right)^2 + 4\pi r^2 \Gamma + 2\pi r^3 G_r \rho F(\lambda_f) \quad (3.11)$$

*Equation (3.11)* provides information about the energy involved in the cavitation process, specifically this energetic balance is strictly dependent on the initial volume strain  $\Delta v_0$  and the rubber particle radius. When the volume strain is sufficiently high it passes through a small maximum, proceeding versus a more pronounced minimum. This minimum in the energy will originate when the volume strain due to the cavity  $\frac{r^3}{R^3}$  approaches the original dilatational strain in the rubber phase, indeed when  $\left( \Delta v_0 - \frac{r^3}{R^3} \right) \rightarrow 0$ . *(3.12)*

Rearranging *Equation (3.11)*, the influence of the surface energy term on the total energy U can be simpler to analyse:

$$U(r) = \frac{2}{3} \pi K_r R^3 \left[ \left( \Delta v_0 - \frac{r^3}{R^3} \right)^2 + \frac{6\Gamma}{K_r R} \left( \frac{r^2}{R^2} \right) + \frac{3G_r g \rho F(\lambda_f)}{K_r} \left( \frac{r^3}{R^3} \right) \right] \quad (3.13)$$

In the previous equation the total energy U decreases by increasing the radius of the rubber particle R, in this way also the initial volume strain will decrease giving rise to a lower stress required to cavitate the rubber particles.

Dividing the *Equation (3.13)* of the total energy U by *Equation (3.1)* the reduced energy can be obtained:

$$\frac{U}{U_0} = \frac{1}{\Delta v_0^2} \left[ \left( \Delta v_0 - \frac{r^3}{R^3} \right)^2 + \frac{6\Gamma}{K_r R} \left( \frac{r^2}{R^2} \right) + \frac{3G_r g \rho F(\lambda_f)}{K_r} \left( \frac{r^3}{R^3} \right) \right] \quad (3.14)$$

Plotting the normalized energy expressed in *Equation (3.14)* as function of the reduced variable  $\frac{r}{R}$ , the parametric curves reported in *Figure 3.3* are reported:

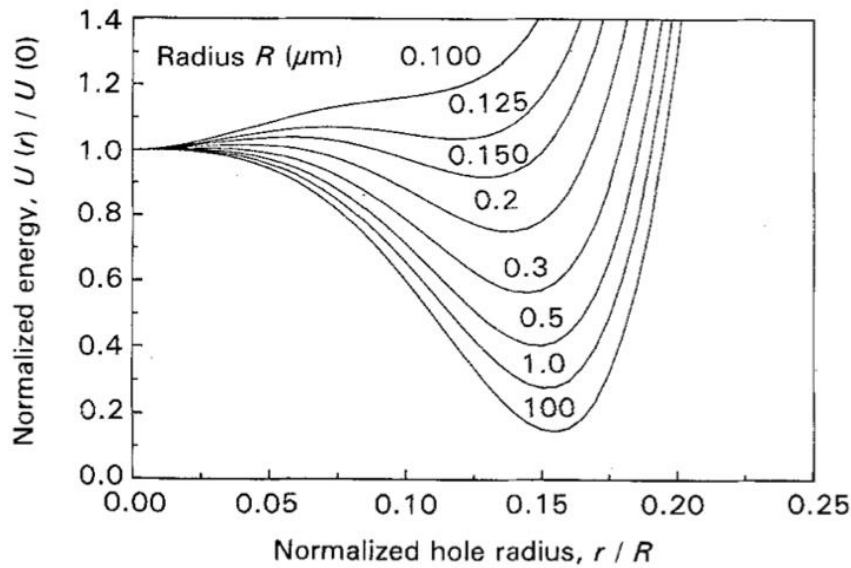


*Figure 3.3* Normalized energy of a cavitated particle as function of  $r/R$ , keeping the volume strain constant at  $0.004^{26}$

*Figure 3.3* shows the reduced calculated energy for a cavitated rubber particle with respect to the normalized radii, keeping constant the initial volume strain  $\Delta v_0$  and plotting a series of fixed radius of the rubber particle, in this way no further work is done by the matrix and all the energy changes take place in the particle itself. The data plotted are obtained considering a rubber with shear modulus  $G = 0.4 \text{ MPa}$ , bulk modulus  $K = 2000 \text{ MPa}$ , surface tension  $\Gamma = 0.03 \text{ Nm}^{-1}$ ,  $\rho = 1$  and the function depending on the failure in equibiaxial tension  $F(\lambda_f) = 1$ . As  $R$  decreases the surface energy term becomes more important giving rise to a shallower minimum of the energy that will move to lower value of  $r/R$ . Equilibrium is reached before the stored strain energy falls to zero.

In the end, considering a radius of the rubber particle in the range between  $0.1$  and  $100 \mu\text{m}$ , the reduced energy shows a minimum progressively pronounced increasing the radius, indeed particles showing a minimum in this energetic balance will be more inclined in starting the cavitation.

The behaviour of a rubber particle during cavitation can be easily understood by holding the radius of the particle fixed at  $0.1 \mu\text{m}$  and plotting a series of fixed volume strains.

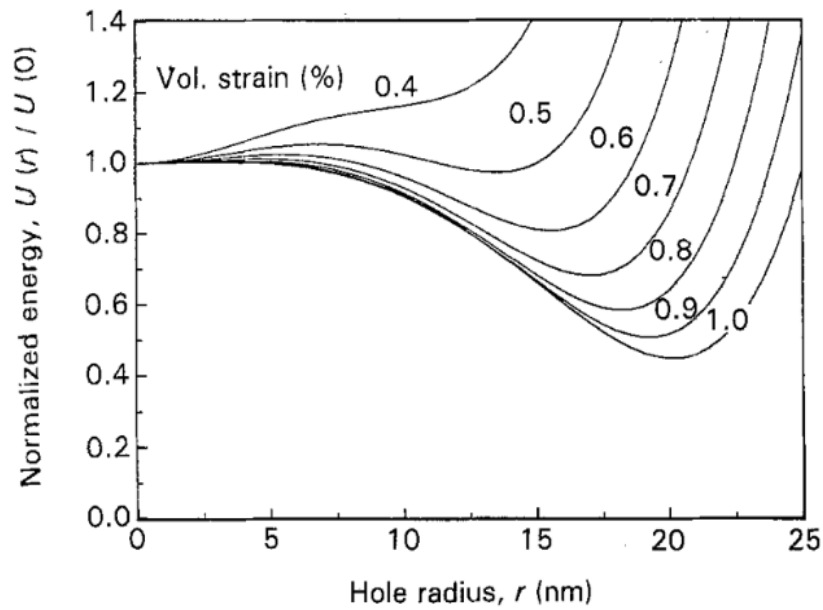


Figure 3. 4 Normalized energy of a rubber particle as function of  $r/R$ , keeping a series of volume strain constant during cavitation<sup>26</sup>

Figure 3.4 shows the normalized energy as function of the hole radius in case of a rubber particle with fixed radius and fixed series of volume strains.

At higher volume strain the energy decreases rapidly by increasing the void size, reaching a minimum that corresponds to the condition in which the volumetric strain energy store in the rubber phase tends to zero, as expressed in Equation (3.12). The zone beyond the minimum shows a rapid rise in the energy because at fixed volume strain a further increase in the void could be achieved just with a compression of the rubber against the surrounding matrix. Important to notice in Figure 3.4 is the behaviour of the energy minimum that becomes less pronounced when the applied volume strain is reduced, until the minimum disappears, and the formation of a void becomes impossible without increasing the energy of the particle above a void free state.

This information provides an important requirement for the beginning of cavitation: a particle will have the possibility to cavitate just if it is able to reach a state of lower energy in forming the void, represented by the presence of the minimum in the energetic balance.

The analysis of this model is not complete, some considerations about the work done by the matrix and the critical conditions to cavitation, in terms of particle radius, volume strains and shear modulus of the rubber, must be provided.

### 3.2 Criteria for cavitation

The energetic model proposed in the previous paragraph identifies two criteria required for rubber particle cavitation. One necessary condition is purely thermodynamic, and it is related to the fact that the energy released during the void formation must exceed the energy needed in the formation of the void. The second one is kinetic and derives from the prediction of a small maximum in the energy balance equation when a rubber particle cavitates. This latter criterion is extremely important because it increases the resistance of rubber particles towards cavitation even when the thermodynamic criterion is satisfied. Indeed, this evidence has led to the possibility that the rate of initiation of voids is actually limited by an energy barrier.

Also, cavitation as many other chemical and physical rate processes, is affected by a dependency of the kinetics of conversion, from one state to another, upon the height of the energy barrier coupled with the energy available to make possible the overcoming of the barrier. However, in most of the cases cavitation is initiated by cooling and consequently it is subjected to a height of the energy barrier not fixed, but dependent on the temperature applied.

Considering the absence of any external stress, in a thermal contraction experiment the initial volume strain has to be considered proportional to  $\Delta T$ , the difference between the current temperature  $T$  and the solidification temperature  $T_{solid}$  of the matrix, which can be equated to the glass transition temperature  $T_g$ . The mean stress can be calculated following the scheme proposed in *Figure 3.1*, from which the volume fraction of rubber  $\phi$  can be expressed as :

$$\phi_r = \left(\frac{R}{Q}\right)^3 \quad (3.15)$$

The mean stress can be then calculated as proposed by Bucknall et Al.<sup>9</sup>:

$$\sigma_{hr} = \frac{(\beta_r - \beta_m)\Delta T}{\frac{1}{K_r} + \frac{4G_m\phi_r + 3K_m}{4G_mK_m(1 - \phi_r)}} \quad (3.16)$$

In which  $G_m$  and  $K_m$  are the shear and bulk moduli of the matrix, applying Hooke's law the initial volumetric strain energy density in the particle can be retrieved:

$$U_0 = \frac{\sigma_{hr} \Delta V_r}{2} = \frac{\sigma_{hr}^2}{2K_r} = \frac{K_r \Delta V_r^2}{2}$$

(3.17)

Considering the relationship between the mean stress and the volume strain, it is possible to see the dependency of the initial store energy available for void formation from the temperature, it actually increases with  $(\Delta T)^2$ . Indeed, the contribution from the stored energy becomes progressively larger upon cooling, while the cavity formation energy, derived from the summation of the rubber stretching and surface energy term in the energy balance, remains insensitive to temperature changes. This is illustrated in the figure reported below.

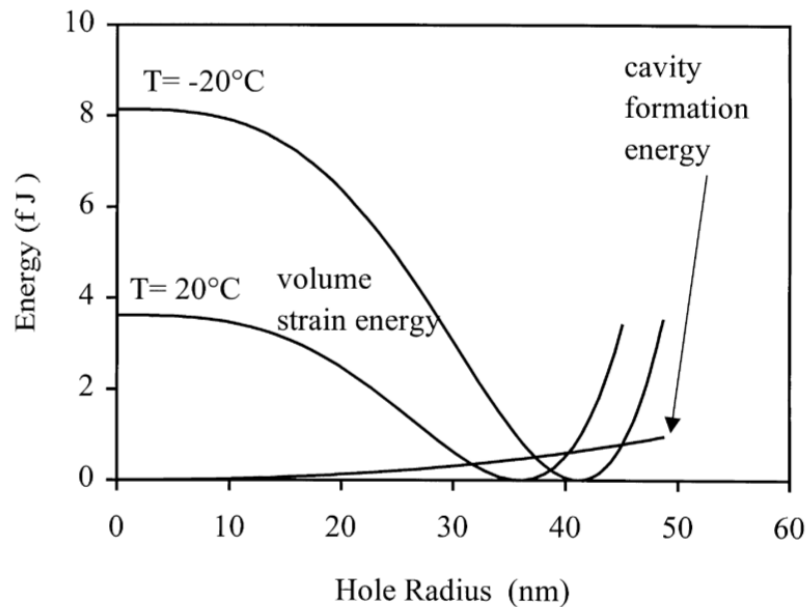


Figure 3.5 Contributions from volume strain energy and cavity formation energy to the total energy of a rubber particle at -20 and +20 °C, for calculations made with  $\Gamma_r = 20 \text{ mJ m}^{-2}$ ,  $R=100 \text{ nm}$ ,  $G_r = 0.5 \text{ MPa}$ ,  $K_r = 2 \text{ GPa}$ ,  $K_m = 4 \text{ GPa}$ ,  $G_m = 1.2 \text{ GPa}$  and  $\phi_r = 0.16$ <sup>28</sup>

This plot emphasizes the fact that there is enough energy to cause cavitation even at 20°C, if just the thermodynamic criterion is considered, because the energy minimum of  $U_0$  is well below this temperature.

In this range of temperatures, the surface energy and the rubber content do not produce any significant effect on the energy minimum. The same consideration is not true for the height of energy barrier which increases considerably passing from a surface energy of 20 to 35  $mJ m^{-2}$ , or decreases when the temperature is reduced as shown in the next figure.

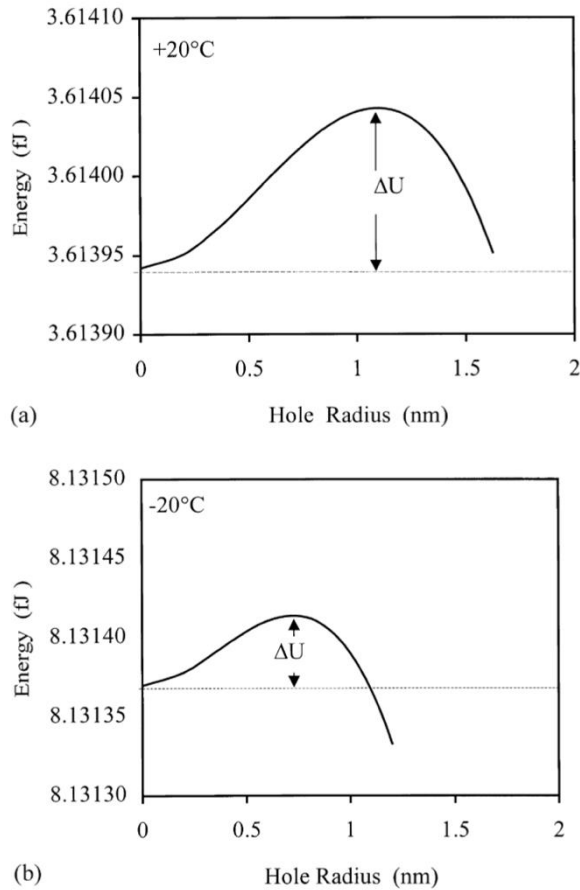


Figure 3. 6 Initial sections of calculated energy void size curves based on Figure 3.5, comparing energy maxima at (a) +20 °C and (b) -20 °C<sup>28</sup>

In absolute terms, the height of these energy maxima is really small, but it plays an important role in controlling the initiation of void formation. Rubber particle cavitation is promoted at an appreciable rate when the energy barrier is low and enough mechanical and thermal energy, derived from differential cooling and/or mechanical loading, is available to surmount this barrier.

### 3.3 Parameters influencing cavitation phenomenon

Voids formation and growth in rubber particles is not just the result of the presence of occasional defects that act as stress concentrators, but it is also related to intrinsic properties of rubber that actually control the ability to absorb and dissipate energy contributing to the fracture resistance. Indeed, under the application of a stress, in particular triaxial stresses the resistance of rubber to dilation, due to weak Van der Waals interactions, becomes unstable because of the inhomogeneous distribution of polymeric chains, raising in this way the capability of the rubber to form micro voids.

Consequently, understanding all the parameters influencing the cavitation is essential to have a general view on this important phenomenon.

#### Rubber characteristics and content

Rubbery materials belong to the that family of polymeric material called “elastomers”, they consist of long flexible chains, usually amorphous and slightly crosslinked, with a glass transition temperature well below the room temperature. Rubber chain-like molecules, when crosslinked, are inter-connected at various points giving rise to a loose molecular network.

The glass transition temperature  $T_g$ , denoting the transition between the glassy and the rubbery behaviour, is typically in the range of  $-60^\circ\text{C}$  and  $-100^\circ\text{C}$ . The intermolecular forces between the polymer chains are rather weak, but when the material is stressed, the chains are forced to assume rare conformations with respect to the original state of configuration. Once the stress is removed the rubber macromolecules are able to return to the original shape, recovering completely the large deformation applied. Thus, among all the important properties of elastomer it is important to consider the low Young's modulus and very high elongation at break when compared with other polymers.

The toughening mechanism is influenced by the rubber content inside the matrix and this effect is mainly determined by the possible interactions between stress concentrations and average stresses present in the matrix. In fact, when a stress is applied on the rubber reinforced polymer, a misfit of the stress state is generated around the rubber particle, mainly due to the different elastic properties between particles and

matrix. This misfit will generate also a non-uniform distribution of stress in the matrix that will actually be concentrated at the equatorial plane of the low-modulus particles, increasing the average stress carried by the stiffer matrix.

The interactions between the stresses acting around the particles and those present into the matrix and the pressure differences built up inside the material are responsible for a reduction of yield stress, stress that can be further reduced by cavitation of the rubber particles. Indeed, when cavitation occurs the triaxial stresses to which the rubber is subjected are relieved, and the cavitated particles transfer loads onto the matrix increasing again the average stresses already present.

Increasing the rubber particles content favours the plastic deformation of the matrix, because it produces an increase of the average stresses into the matrix that will be coupled with a higher probability for the cavitation phenomenon. Furthermore, these high average stresses in the matrix will be released only when crazing or orientation hardening will begin, consequently increasing the rubber content will not influence just crazes' initiation but also its propagation. Cavitation phenomenon inside the rubber particles will not induce the disappearing of the stress concentrations around the particles but will induce the formation of shear bands and crazes that will actually reduce the concentrations of stresses around the particles. Rubber content and also rubber particle volume fraction both have a strong effect on the kinetics involved in the deformation mechanisms, that will be affected also by the strain rate and temperature, parameters that will be later discussed.

### *Rubber particles size*

Keeping in mind that both matrix and rubber particles play an important role in the phenomenon of toughening, it seems adequate to dedicate a small paragraph to the role of particle size.

Particle size can affect the deformation behaviour of rubber reinforced polymers in three different ways:

- Influencing the critical volume strain required for cavitation
- Influencing the critical tensile strain to initiate craze
- Affecting the volume strain able to cause debonding of particles

Rubber particles size is not unique for all the types of polymers, but each of them will be characterized by an optimum value that is closely related to the nature of post yield deformation mechanism of the matrix, in most of the cases triggered by rubber particle cavitation. The effectiveness of a toughening process is strictly related to the dimensions of the particles introduced into the matrix, in order to have the best improvement it is necessary to consider the type of material chosen as matrix. In case of brittle polymers, as the Polystyrene, generally subjected to multiple crazing it is required the use of relatively large particles of about several microns. On the other hand, ductile polymers such as Polycarbonates are characterized by shear yielding deformation mechanism, their toughening can be achieved by the addition of relatively smaller rubber particles with respect to those material subjected to crazing.

As already shown in the paragraph dedicated to the model for particle cavitation, the energy balance proposed by Lazzeri and Bucknall relates the critical volume strain at cavitation to the radius of the rubber particles, to the shear modulus, the surface energy and also the failure strain of the rubber. This means that critical volume strain at cavitation is influenced by particles dimensions, because larger are the particles, higher will be the stored energy and lower will be the stresses required to initiate cavitation.

When multiple crazing is the main deformation mechanisms, larger particles are preferred because they can form bridging rubber fibrils and provide stability to crazes, consequently the critical volume strain does not control just the cavitation initiation but also the multiple crazing process. On the other hand, the effect of particle size on ductile polymers is not so significant as in brittle matrix, due to the existence of a dual deformation mechanisms.

### Particle morphology

Rubber toughened materials are characterized by different morphology of the dispersed phase that can go from simple homogenous spheres to complex combinations of rubber and rigid inclusions. The presence of inclusions affects mechanical properties because it increases the volume fraction of particles and consequently decreases the volume fraction of the load bearing matrix, it confines the void propagation into the rubber phase and provides anchor points to rubber fibrils. Rubber particles with presence of inclusions

are usually required in case of a brittle matrix, such as PolyStyrene, in which large homogenous rubber particles weaken the matrix after cavitation, effectively acting as spherical voids and making little contribution to strength since particles will first craze and then fracture. In order to overcome this problem, inclusions are introduced into the particles, in this way cavitation will result into fibrillation of rubber membranes and reinforcement of the surrounding crazes.

Materials, subjected preferentially to shear yielding phenomenon, are usually characterized by the presence of small homogenous rubber particles. This particles' morphology, upon cavitation, shows the presence of growing spherical voids that will actually minimize the surface energy of the particles, increasing their tendency to cavitation.

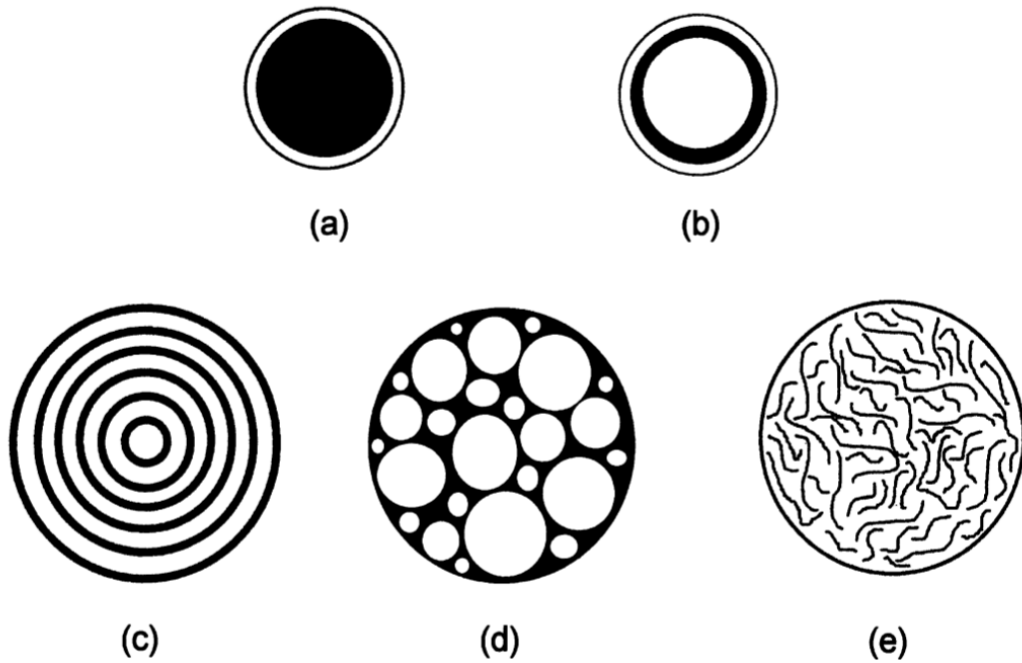


Figure 3. 7 Schematic diagram showing typical morphologies of rubber particles: (a) soft core-hard shell, (b) hard core-soft shell-hard shell, (c) onion morphology, (d) salami particle, (e) can of worms morphology<sup>3</sup>

### Strain rate and temperature

Shear yielding and crazing deformation mechanisms are both rate processes in which both raising the strain rate or decreasing the temperature, produces an increase of yield and craze growth stress. Cavitation phenomenon is relatively insensitive to changes in strain rate, exceptions occur near the  $\alpha$ - transition of the rubber phase where the shear modulus  $G_r$  increases strongly decreasing the time scale and consequently raising the

energy. Cavitation stresses are more sensitive to strain rate changes because they are not determined only by cavitation strains but also by the moduli of the rubbery and glassy phase, which are themselves time dependent.

The effect of temperature is a little more complicated because the shear modulus varies with it. At high temperature  $G_r$  has a value between 0.1 to 1.0 MPa, while at low temperature, below the  $\alpha$ -relaxation temperature the rubber shear modulus increases to 1000 MPa. One condition to be fulfilled, in order to make effective the toughening of the material, is to have a shear modulus of the rubber phase well below that of the glassy matrix, larger the misfit more favoured will be the initiation of cavitation and consequently the toughening. Optimum values to ensure cavitation are  $G_r \leq 0.5$  MPa, because higher value of modulus will cause an increasing resistance of rubber to stretch that can cause a complete suppression of the hole formation.

Furthermore, temperature has a direct effect on the critical strain at cavitation because decreasing the temperature increases the misfit of thermal expansion coefficients between matrix and dispersed phase. This misfit generates a hydrostatic stress in the rubber and compressive stresses in the matrix, which together favour the initiation of cavitation.

To conclude, at very high temperatures or low strain rates cavitation is suppressed and shear yielding phenomenon is predominant. At intermediate strain rates and temperatures, a co-existence between shear yielding and cavitation occurs, while at high strain rates or low temperatures cavitation is strongly preferred and it triggers extensive rubber deformation, rupture, and fibrillation in the particles.<sup>10</sup>

### **3.4 Effect of cavitation phenomenon on yielding behaviour**

During several experiments, a great number of laboratories have shown that the formation of cavities in rubber particles of many polymers is concentrated in those regions characterized by high shear strain. Polymers have a peculiar behaviour, they exhibit a tendency to extend and strain hardening, thanks to the presence of the molecular orientation process. In polymers, the cavitation phenomenon is stabilised by different conditions such as orientation hardening and strengthening, this allows a dissipation of energy that will give rise to the formation of a necking within the stressed

region. Numerous studies conducted on materials undergoing plastic deformation, accompanied by void formation, were carried out by Berg and later by Gurson. Based on their theory in which materials, undergoing plastic deformation coupled with void development, were treated as continuum a slightly modification was proposed by A. Lazzeri and C. Bucknall<sup>8</sup> to analyse rubber toughened polymers.

Understanding the kinetics of yielding requires the analysis of microscopic behaviour and its macroscopic response, the authors considered an element of ductile polymer containing several micro voids, that can be treated as homogenous as already showed in *Figure 3.8*.

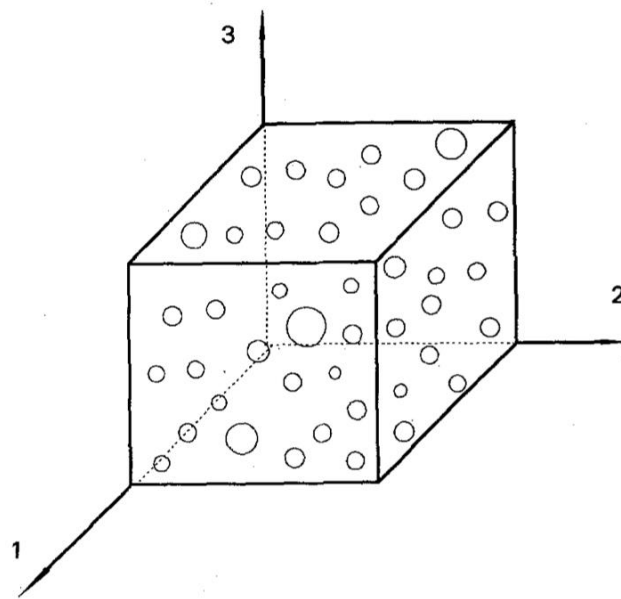


*Figure 3. 8 Element of ductile polymer with a large number of micro voids<sup>8</sup>*

As already mentioned in the shear yielding section, a homogenous rigid-plastic material in which the pressure has no effect on yielding, the Von mises criterion is considered. This criterion is able to combine the three principal stresses into an equivalent stress, this one will be then compared with the yield stress of the material in order to examine the failure condition of the material.

$$\sigma_e = \sqrt{\frac{(\sigma_{11} - \sigma_{22})^2 + (\sigma_{22} - \sigma_{33})^2 + (\sigma_{33} - \sigma_{11})^2}{2}}$$

(3. 18)

This equivalent stress, however, is not able to describe adequately the yield behaviour of polymers and must be modified taking into account that polymers are affected by a

pressure dependency, that can be rewritten in terms of equivalent stress  $\sigma_e$  and mean stress  $\sigma_m$  in:

$$\sigma_e^2 = (\sigma_0 - \mu\sigma_m)^2 \quad (3.19)$$

In which  $\sigma_0$  is the yield stress in absence of hydrostatic pressure and  $\mu$  is the material constant able to characterize the pressure sensitivity of yielding, and it is related to the compressive and tensile values of uniaxial yield stress:  $\sigma_C$  and  $\sigma_T$ . This material constant is reported in the following equation:

$$\mu = 3 \left( \frac{\sigma_C - \sigma_T}{\sigma_C + \sigma_T} \right) \quad (3.20)$$

For many polymers the material constant is taken as equal to 0.39. Taking into account the yield stress obtained by Von Mises yield criterion, the simple yield function can be retrieved. This function is able to describe the location in stress space of points for which the material undergoes plastic yield:

$$\Phi = \frac{\sigma_e^2}{\sigma_y^2} - 1 = 0 \quad (3.21)$$

In which the yield stress can be expressed in terms of delta Kroneker as:

$$\sigma_y^2 = \frac{3}{2} \delta_{ij} \delta_{ij} \quad (3.22)$$

Also, *Equation (3.21)* must be modified to consider the pressure dependency, its expansion provides:

$$\Phi(\sigma_e, \sigma_m) = \frac{\sigma_e^2}{\sigma_y^2} + g(\sigma_m) - 1 = 0 \quad (3.23)$$

In which  $g(\sigma_m)$  represents its pressure dependence:

$$g(\sigma_m) = \frac{\mu\sigma_m}{\sigma_0} \left( 2 - \frac{\mu\sigma_m}{\sigma_0} \right)$$

(3. 24)

The yield surface can be represented in the form of a cone in stress space that intersects 1-2, 1-3 and 2-3 planes to form distorted ellipses.

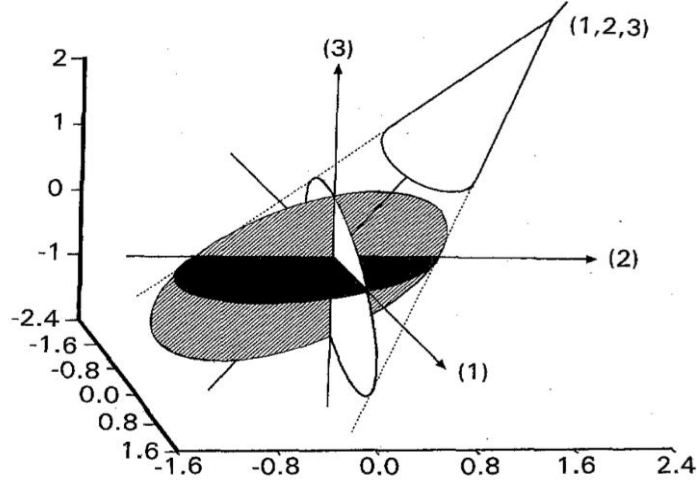


Figure 3. 9 Pressure modified von Mises yield surface of a non cavitating polymer<sup>8</sup>

The yield surface shown in *Figure 3.9* coincides with the pressure independent von Mises criterion for  $\mu = 0$  and  $g(\sigma_m) = 0$ , indeed the cone goes back to the shape of a circular cylinder.

Gurson has proposed the following expression for the yield function in case of a pressure independent material containing spherical voids:

$$\Phi = \frac{\sigma_e^2}{\sigma_y^2} + 2f \cosh\left(\frac{3\sigma_m}{2\sigma_y}\right) - f^2 - 1 = 0$$

(3. 25)

In which  $f$  is the current volume fraction of voids, equivalent and mean stress are considered as “macroscopic” quantities, while the yield stress is considered as the “microscopic” matrix flow stress.

To describe pressure dependent material *Equation (3.23)-(3.25)* can be combined in order to provide a yield function able to also consider the presence of spherical voids.

$$\Phi = \frac{\sigma_e^2}{\sigma_0^2} + \frac{\mu\sigma_m}{\sigma_0} \left( 2 - \frac{\mu\sigma_m}{\sigma_0} \right) + 2f \cosh\left(\frac{3\sigma_m}{2\sigma_0}\right) - f^2 - 1 = 0$$

(3. 26)

In which  $\sigma_0$ , for pressure independent material, substitutes the tensile yield stress. Gurson's analysis can be adapted to describe the cavitation phenomenon in polymeric materials.

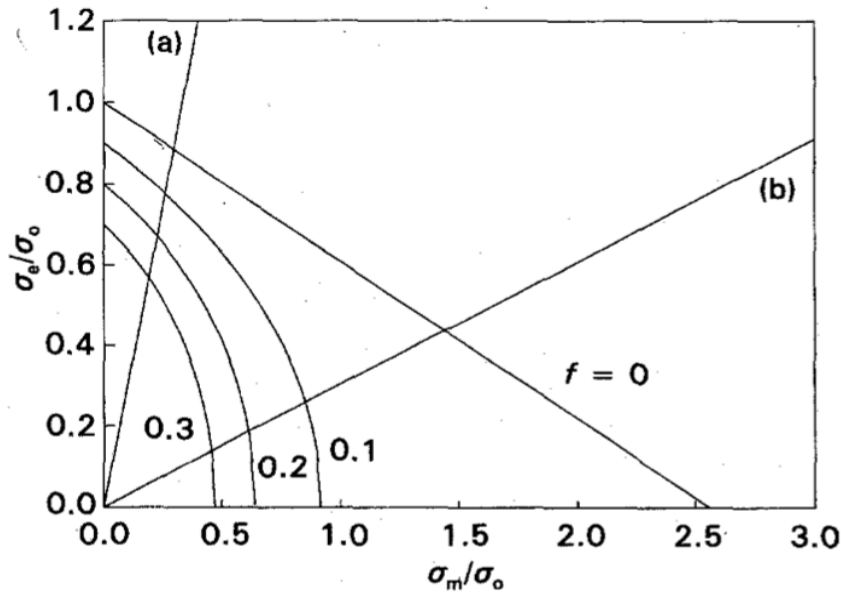


Figure 3.10 Effect of void volume fraction on the yield locus of pressure dependent material. (a) Uniaxial tension (b) crack tip plane strain tension<sup>8</sup>

Figure 3.10 shows different yield surfaces for materials with increasing voids volume fraction, using Equation 3.26. Variables on the abscissa and ordinate are both normalized with respect to  $\sigma_0$ . Considering that the abscissa lies along the stress-space diagonal defined by  $\sigma_{11} = \sigma_{22} = \sigma_{33}$  (3.27), the distance of any point from the space diagonal indicates the magnitude of the effective stress  $\sigma_e$ . The increase of void volume fraction provides an additional curvature of yield surface, indeed the tip of the original cone, used to describe the yielding of polymeric materials in absence of voids, becomes rounder in presence of voids.

When voids are present, the yield condition is reached earlier, in which the macroscopic equivalent stress becomes equal to the matrix flow stress, even in condition where the mean stress is low or zero. Moreover, in plane strain condition, usually present in case of crack tip (b), the mean stress is initially high with respect to the equivalent stress and the absolute value of yield stress is actually reduced when the polymer is able to develop voids inside.

Based on Equation (3.26), the following figure shows the effect of void volume fraction on the adimensional yield stress in uniaxial tension  $\sigma_{ty}(f)/\sigma_{ty}(0)$  and the adimensional effective stress at yield at a point immediately ahead of a sharp crack  $\sigma_{ey}(f)/\sigma_{ey}(0)$ .

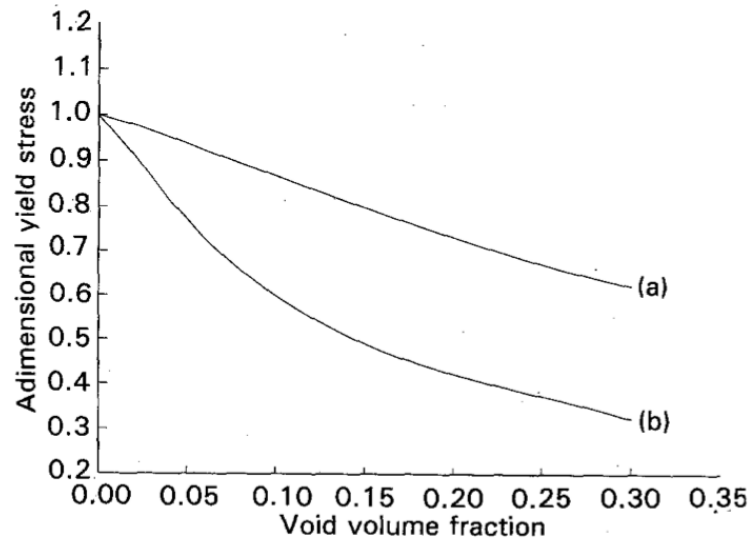


Figure 3.11 Effect of void volume fraction on the (a) adimensional tensile yield stress and (b) adimensional effective stress at yield according to the modified Gurson model<sup>8</sup>

Figure 3.11 gives significant evidence of the influence of cavitation on yielding; indeed, its effect is more remarkable in case of yielding at crack tip rather than in uniaxial tension. The main information to keep in mind is that cavitation of rubber particles is a phenomenon that precedes and actually is able to accelerate shear yielding in rubber toughened polymers.

This model proposed by Lazzeri and Bucknall determines a preferential direction for rubber particle cavitation which results into the reduction of yield stress and consequently in the concentration of shear deformation in the same direction.

### 3.5 Importance of cavitation on impact toughness

A brief analysis of the importance of cavitation on toughness is proposed here to emphasize the importance of this phenomenon in rubber toughened material.

Brittle polymers, such as PolyStyrene (PS) and PolyStyrene-co-acrylonitrile (PSAN), do not show secondary relaxation processes in the main chain, therefore they are quite brittle when tested below their glass transition temperature. To overcome this limitation,

rubber particles have been introduced in order to stabilize the craze formation in the stress field near the rubber particles, when deformed in plane strain condition.

This stable crazing is favoured by the relatively large particles, but when the rubber content is increased and the dimension is reduced, local plane stresses in the region between particles are favoured causing a transition from crazing to shear yielding and multiple crazing, as usually happens in ABS copolymers.

Ramsteiner F. et al<sup>11</sup> have shown in their studies that void formation substantially affects the impact toughness of the materials, indeed they carried out different experiments where allowing the crosslinking of the rubber phase in HIPS and ABS, they caused their embrittlement and consequently increased the resistance of rubber particles towards cavitation.

Other studies have been carried out by Bucknall and Paul in 2009<sup>12</sup>, they showed how the particle size and consequently the tendency to cavitation is fundamental in understanding the notched impact behaviour of polymer blends, indeed this study leads to the conclusion that maximum toughness is achieved when the particles are large enough to cavitate a long way ahead of a notch or crack tip, but not so large that they initiate unstable crazes and thus reduce fracture resistance.

Rubber modification for brittle polymers is based on the idea of enhancing crazing or shear yielding deformation mechanism, however these mechanisms are facilitated by cavitation of rubber particles, so it can be concluded that this peculiar phenomenon must be present in order to achieve a good level of toughness in rubber reinforced materials. Inspecting the effect of cavitation on toughness is surely fundamental when rubber toughened materials are considered, however this thesis will focus just on the monitoring and inspection of cavitation phenomenon through rheological instruments and consequently won't treat in detail its effect on mechanical properties.

## CHAPTER 4

### **How can cavitation phenomenon be studied ?**

As explained in the previous chapters, the deformation mechanisms responsible to some extent for the toughening mechanisms are of contrasting types:

- Cavitation and crazing, responsible for a change in volume
- Shear yielding, occurring at constant volume

Several theories of rubber toughening advanced in recent years suggested that these mechanisms operate simultaneously. So, understanding the toughening mechanisms involved in these materials cannot be possible without the study and inspection of the deformation processes involved, in this specific case the cavitation phenomenon. This effect, however, necessitates specific approaches to be investigated, different methods have been used over the years by researchers such as Differential Thermal Mechanical Analysis (DMTA), Transmission Electron Microscopy (TEM), thermal contractions tests, small-angle X-rays measurements and many others.

Among the different studies conducted on this subject through the help of these techniques, some can be mentioned. Transmission electron microscopy was a technique quite useful to study the energy absorption of one of the most important rubber-toughened polymers, high-impact polystyrene (HIPS). Cavitation was first reported in these materials that are able to absorb energy through multiple crazing of the polystyrene (PS) matrix, indeed TEM analysis provides a study of the fibrillation of the matrix to form crazes, that is usually coupled with coarser fibrillation of the rubber phase in the neighbouring particles. The latter effect is the main process enabling the rubber particles to match and resist the high strains generated in the surrounding matrix. X-rays measurements were proposed by Kramer et Al.<sup>13</sup> in 1991, they used real-time scans to show that cavitation of rubber particles in HIPS is a phenomenon that precedes craze formation in the matrix when the material is subjected to tensile impact conditions. The generated cavities act as nuclei for craze growth which occurs as a consequence of the meniscus instability mechanism.

Breuer et Al.<sup>7</sup> combined the TEM with low-angle light scattering analysis in order to inspect the importance of cavitation as a toughening mechanism able to increase the

resistance of the material towards crazing. Other possible techniques are the Dynamic Mechanical Thermal Analysis and thermal contraction tests, which were proposed by Bucknall et Al. in 1998<sup>14</sup> and 2000<sup>9</sup> to study the cavitation phenomenon.

Dilatometric analysis, DMTA, TEM and DSC were all used in the development of this thesis however, another important technique called Small-angle X-ray scattering has been proposed in the latest years to study the cavitation phenomenon, so it seems adequate to dedicate a small paragraph to it.

#### 4.1 Dilatometric technique

A dilatometer is a precision instrument able to provide measurements of dimensional changes in traditional or advanced materials, from ceramics and metals to polymers, as a function of temperature. The substance is subjected to a controlled temperature program in a specified atmosphere, in order to provide different test conditions.

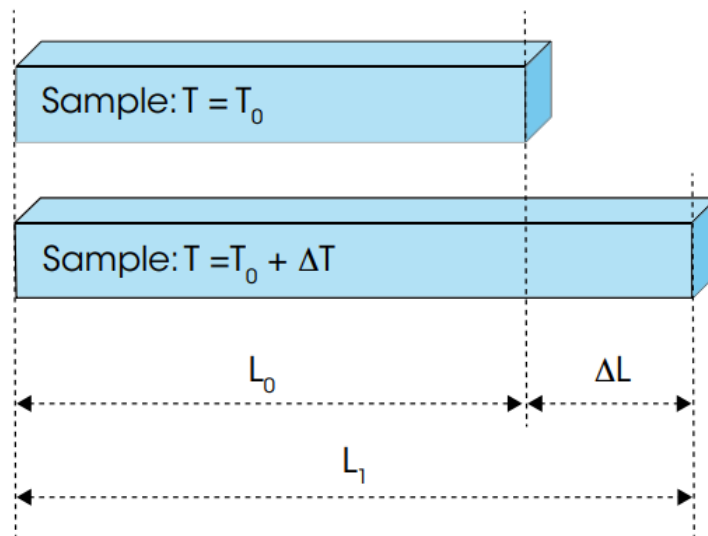


Figure 4. 1 Thermal expansion scheme of a sample<sup>33</sup>

Through dilatometry a lot of information can be retrieved:

- Determination of thermal expansion coefficient
- Glass transition temperature
- Volume changes
- Density changes
- Decomposition

Measurements can be carried out in contact or non-contact geometry, in the first case a sample is placed into a holder with one end brought into contact with a pushrod, in the

other case optical sensors provide the measurements. As output, linear dimensional changes monitored with respect to the temperature are provided.

Linear expansion means that the change is just in one dimension, as shown in *Figure 4.1*, in the direction of the length of the sample. This fractional change in length per degree of temperature change can be expressed, assuming a negligible effect of the pressure, in the following way:

$$\alpha = \frac{1}{L} \frac{dL}{dT} \quad (4.1)$$

In which  $L$  is the length measurement and its derivative with respect to the temperature represents the rate of change of that linear dimension per unit change in temperature. When the fractional change in length is small  $\Delta L/L \ll 1$  (4.2), the linear expansion coefficient does not change to a high extent over the change in temperature  $\Delta T$  and can be estimated as:

$$\frac{\Delta L}{L} = \alpha \Delta T \quad (4.3)$$

Furthermore, this technique can represent a good ally in monitoring the cavitation phenomenon, detecting, and quantifying the extent of rubber particle cavitation while the experiments are carried out, and providing useful insights about the void initiation mechanism. As already explained, rubber-reinforced polymers are composed of two materials the glassy matrix and the rubber particles, whose coefficient of thermal expansion are quite different. It is clear that the introduction of rubber particles into the matrix produces several changes in the thermal contraction of the reinforced polymer raising its coefficient even with a small quantity of rubber added. However, it must be considered that this effect, introduced by the rubber, is present just if the particles remain intact and well-bonded to the matrix. Taking into account these conditions, the thermal expansion behaviour of toughened materials and the relative changes resulting from the cavitation phenomenon can be quantified using the slightly modified version of Boyce's equation provided by Bucknall et al.<sup>9</sup>

The volumetric thermal expansion coefficient of the reinforced rubber polymer can be indeed expressed in the following way:

$$\beta_{RT} = \beta_m + (\beta_r - \beta_m) \phi \left[ \frac{4G_m K_r + 3K_m K_r}{4G_m K_m (1 - \phi) + K_r (4G_m \phi + 3K_m)} \right] \quad (4.4)$$

In which  $\beta_{RT}, \beta_m, \beta_r$  represent respectively the volumetric expansion coefficient of the rubber toughened material, matrix, and rubber,  $G_m$  is the shear modulus of the matrix while  $K_r, K_m$  represent the bulk modulus of the rubber and matrix,  $\phi$  is the volume fraction of the intact and well-bonded rubber particles.

Considering the relative insensitivity of the term in the square bracket to the volume fraction of rubber particles a simplification of *Equation (4.4)* can be provided:

$$\beta_{RT} = \beta_m + 0.81 \phi (\beta_r - \beta_m) \quad (4.5)$$

In particular, considering  $G_m, K_m$  and  $K_r$  typical values of 1.2, 4.0 and 2.0 *GPa*, the term in square brackets varies from 0.80 at  $\phi = 0.10$  to 0.82 at  $\phi = 0.25$ , explaining the 0.81 present in *Equation (4.5)*.

When the material undergoes a cooling process the triaxial stresses to which rubber particles are subjected can increase enough to cause either cavitation or debonding, consequently affecting the thermal expansion behaviour of the material. Indeed, cohesive, or adhesive failures of the rubber may reduce  $K_r$  to zero reducing *Equation (4.4)* to  $\beta_{RT} = \beta_m$  (4.6), expansion coefficient of the matrix. The model proposed by Bucknall and Lazzeri in the previous chapter provides some necessary criteria for the cavitation of rubber particles in particular, the driving force of this phenomenon is not the absolute value of triaxial stress acting on the particle, but the amount of energy available for the formation of a void. Furthermore, this will depend on the volume strain energy density in the rubbery phase, rubber particle size, shear modulus and surface energy of the rubber and the stored energy in the surrounding shell of rigid matrix phase. Considering the calculations done from this model, enough energy for cavitation in some or all rubber particles should be retrieved in many toughened polymers just by cooling

the material from the glass transition temperature of the matrix to the glass transition temperature of the rubber<sup>9</sup>.

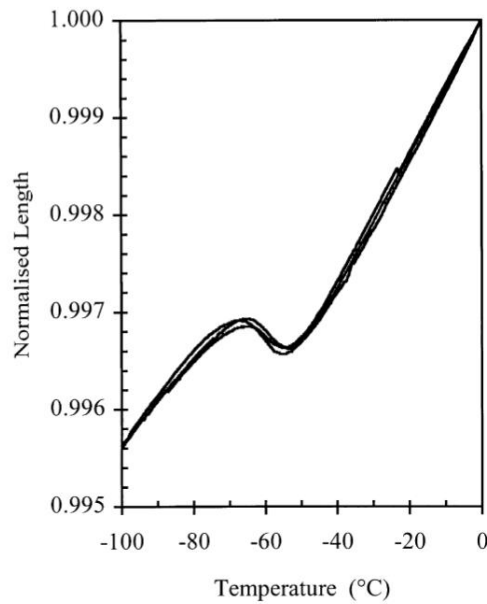


*Figure 4. 2 Thermal contraction behaviour of three fresh specimens of ABS with 16% of rubber particles, data are normalized with respect to the initial length at 0°C*

In *Figure 4.2* the normalized length is plotted against the temperature, in case of a rubber-toughened material. It is possible to notice a first linear zone corresponding to the matrix filled with intact and well-bonded rubber particles and a nonlinear S-shaped section between -45°C and -75°C which goes back to a linear course with a reduced slope below 75°C. The deviation from the straight line represents the expansion of the material with respect to the baseline, shown in the interval going from -45°C to -75°C. This expansion is possible only as a result of cavitation in the rubber particles or debonding at the particle-matrix boundary. A further indication of cavitation is the reduced slope, corresponding to a decrease in the thermal expansion coefficient, in the second linear zone after the S-shaped deviation.

This point is shown also in the following figure, in which the thermal contraction of the matrix, in this case PSAN, is compared with the contraction of ABS with different rubber content. The line defining the contraction of the matrix is the same one corresponding to 0% of rubber, while in the case of ABS, it is important to emphasize the fact that a line labelled as 8% of rubber content does not apply just to an ABS with

8% of intact particles, but also to an ABS containing 16% of rubber particles, whose half of which have cavitated.

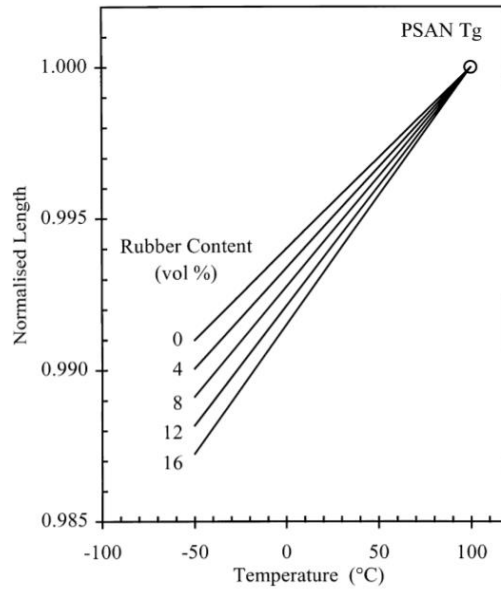


Figure 4. 3 Experimental expansion-contraction curve for PSAN (0% of rubber) compared with calculated curve for ABS containing different rubber content using Equation 4.4.

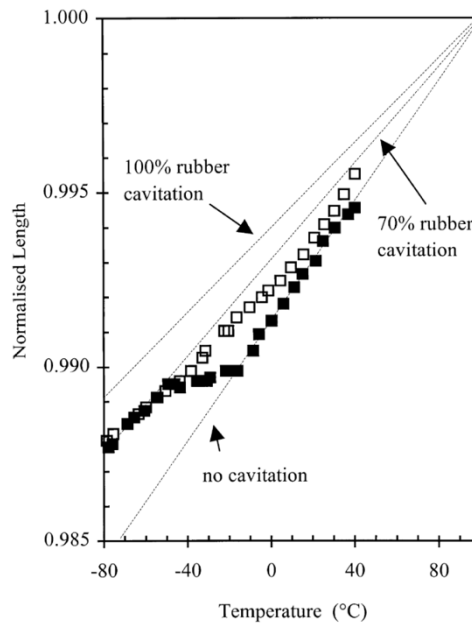


Figure 4. 4 Thermal contraction and expansion behavior of an ABS specimen, cooling represented with black squares and heating with white squares. Reference length taken as the initial length at 100°C

From this approach, it is possible to calculate an *effective degree of cavitation* coming from a simplified approach that does not consider the possibility that particles might not

be fully relaxed and consequently the fraction of cavitated particles may be higher than the one calculated in this way.

Indeed, by treating the ABS as a three-component composite, with a PSAN matrix containing a volume fraction  $x\phi_r$  of particles that are fully cavitated and a volume fraction  $(1 - x)\phi_r$  of intact and well-bonded rubber particles,  $\phi_r$  represents the total volume fraction of rubber particles. So, it can be defined that the fraction of cavitated particles corresponds to  $x$ .

*Figure 4.3* provides information about the current state of cavitation, points lying on the upper construction line correspond to 100% of cavitation, consequently the linear expansion coefficient will be approximately equal to the one of the matrix, while from the location of intermediates points the effective degree of cavitation can be calculated using *Equation (4.4)*.

For the sake of completeness, it must be said that multiple crazing and cavitation can provide similar changes in volume and consequently they can be mistaken during a dilatometric experiment. However, rubber particles cavitation can be induced simply by a cooling, due to the thermal expansion coefficient mismatch between rubber and matrix, while crazing is a phenomenon of plastic deformation that can arise just when the tensile force overcomes the elastic limit. Furthermore, it is clear that the introduction of rubber particles in a rigid matrix modifies the stress concentration giving rise to a local stress higher than the stress applied, close to the particles, but an external force is necessary to induce craze formation. The experiments carried out in this thesis will monitor the length variation with respect to the temperature by applying a negligible tensional force of 10 grams. It can be concluded that the thermal expansions, that will be presented in the results, are a genuine effect of the cavitation phenomenon.

## **4.2 Dynamic Mechanical Thermal Analysis (DMTA)**

Dynamic Mechanical Thermal Analysis often abbreviated as DMTA is a technique used to characterize materials, specifically it is useful to study the viscoelastic behaviour of polymers. Materials' properties can be measured as function of controlled frequency, amplitude, and temperature, in different stress conditions such as: compression, tension, bending and many other geometries. Elastic and viscous response of a sample subjected

to an oscillation load are monitored, indeed by changing temperature, frequency, or time and by imposing a controlled environment. This technique works by applying a sinusoidal deformation to a sample of known geometry. The measured parameters are stiffness and damping, reported as modulus and  $\tan\delta$ , since the applied force is sinusoidal, the modulus can be expressed as an out of phase component, the loss modulus, and a in phase component, the storage modulus. As explained in the viscoelasticity paragraph, the storage modulus expressed as  $E'$  or  $G'$  is a measure of the elastic behaviour of the sample while the loss modulus, defined as  $E''$  or  $G''$  is a measure of the viscous response. The energy dissipation of the material is represented by the damping.

Dynamic mechanical analysis facilitates the detection of a wide range of materials due to the solid-state rheological properties that can be analysed and provides information about relaxation processes and phase transitions. Different information can be retrieved by this simple analysis such as:

- Approximate glass transition temperatures and the intensity of the glass transitions
- Temperature and intensity of many types of secondary transitions
- Melting point of crystalline polymers
- Degree of crystallinity from the value of the modulus above  $T_g$
- Compatibility of mixtures of polymers
- Exact predictions of creep and stress relaxation behaviour for systems in the linear range
- Phase inversion in two phase systems
- Information on adhesion and on particle-particle friction in filled polymers
- Vibration damping and acoustic damping capability
- Heterogeneity of crosslinks and the presence of a second microgel phase in highly crosslinked polymers

These are just few of the information that can be useful to characterize polymeric materials. In this study of the cavitation phenomenon, attention will be restricted to the analysis of the peak of  $\tan\delta$  and loss modulus, but in some cases also to the curve of the storage modulus.

In order to have a visual idea of the typical plot generated by a DMTA experiment *Figure 4.5* is reported.

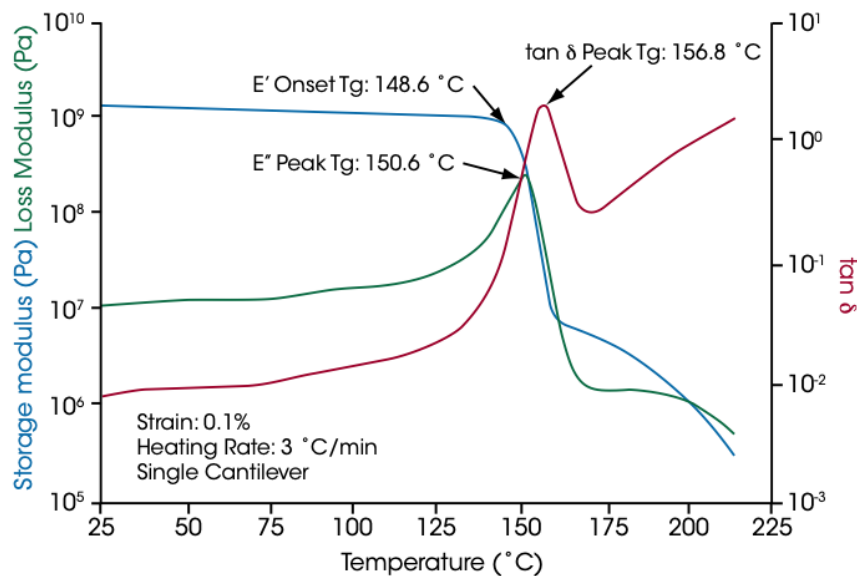


*Figure 4.5* Temperature Ramp on a Polycarbonate specimen<sup>31</sup>

As already anticipated, considering the energy balance model the energy required to form a void inside the rubber comes from two sources:

- Mechanical loading
- Differential thermal contraction due to coefficients' mismatch

In particular mechanical loading, such as tensile ones, are able to produce volume strains in the particle and its surroundings, which are released when the rubber is able to form a void inside itself, giving rise to cavitation. Additional volume strains of similar magnitude are generated by cooling the material from the glass transition temperature of its matrix to the glass transition temperature of the rubber phase. These volume strains on the rubber particles produce an increase of its free volume and shift the secondary loss peak, as well as the damping peak, to lower temperatures with respect to the  $T_g$  of the rubber alone. When cavitation occurs, a relaxation of the rubber particles to their equilibrium density is induced, providing a shift of the damping and loss peak to temperatures closer to the glass transition temperature of the unconstrained elastomer. By performing a DMTA experiment on a rubber toughened polymer it must be known that, according to the range of temperature chosen to be inspected, two different peaks

of  $\tan \delta$ , as well as loss modulus, can be found. Examples will be reported in terms of damping peak, but the following considerations will be true also for the loss modulus. In *Figure 4.6* two peaks are visible, at high temperature the glass transition temperature of the matrix is present, while at low temperature the one of the rubber phase.

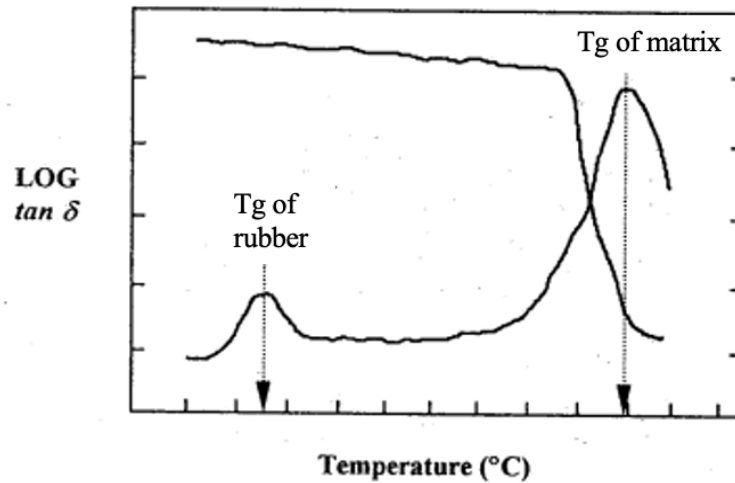


*Figure 4.6 Schematic representation of a Temperature Ramp conducted on a RT-plastic<sup>10</sup>*

In order to show the effect of cavitation two plots can be reported, in *Figure 4.7* the formation of the void relaxes the volume strain generated into the rubber particles splitting the damping peak.

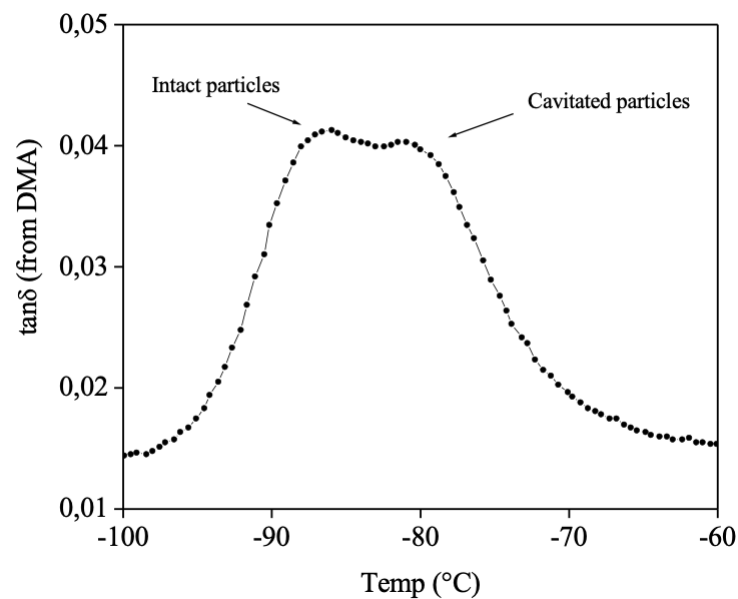


*Figure 4.7 Temperature Ramp on a specimen showing partial cavitation with splitting of damping peak*

These kinds of phenomena have been reported in several studies conducted over the years, as in the case of Morbitzer et Al.<sup>15</sup>, in which splitting and shifting of peaks were attributed to the different levels of grafting. In *Figure 4.7*, the left peak at lower temperatures refers to a fraction of intact and well-bonded particles still subjected to hydrostatic tension, while the peak on the right is due to a fraction of cavitated particles whose glass transition temperature is shifted closer to the  $T_g$  of the rubber in its unconstrained condition.

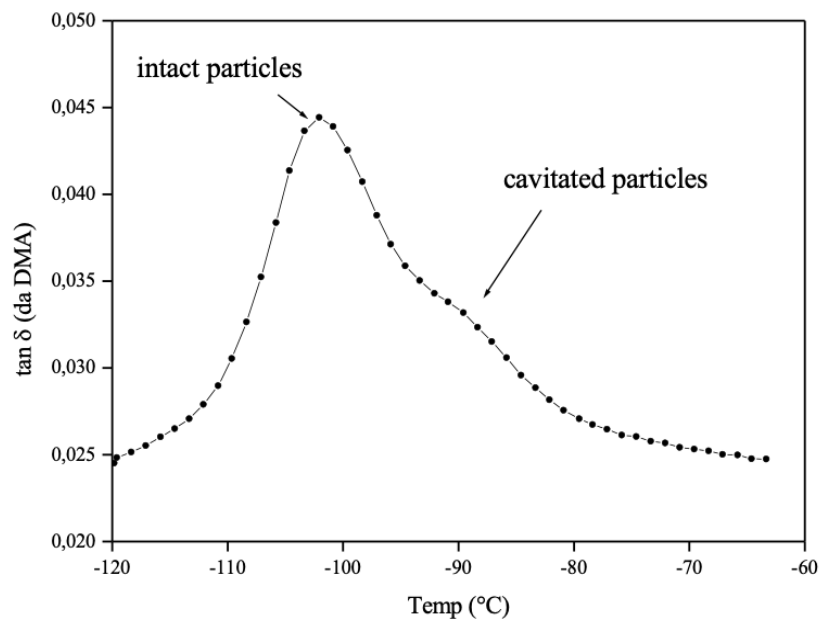


*Figure 4. 8 Temperature Ramp on a specimen showing partial cavitation, with small shoulder on the righten side of the peak*

Also, in *Figure 4.8* cavitation phenomenon is not fully complete, this means that since not all the rubber particles might be able to cavitate, the damping peak can split in two as in the previous case or can give rise to the formation of an asymmetric peak with a small shoulder. In this case the small shoulder on the right-hand side of the peak is related to a small fraction of particles that were able to release the hydrostatic tension to which they were subjected by forming micro voids inside.

These figures represent just some examples of what can be registered experimentally, in some cases damping and loss peaks are not splitted and can be shifted to lower or higher temperature according to the cavitation phenomenon. Indeed, if all the particles are not able to cavitate the peak will be shifted to the left, at lower temperature due to the hydrostatic tension, while if rubber particles are able to cavitate and release the tension,

the peak will be shifted to the right at higher temperatures, closer to the  $T_g$  of the unconstrained rubber.

### 4.3 Transmission Electron Microscope (TEM)

Transmission Electron Microscope is an instrument in which a beam of highly focused electrons is directed towards an ultra-thin specimen, with thickness lower than 200 nm. Thanks to the interaction of the electrons with the specimen and through the help of lenses a magnified image is generated.

The electron beam is generated in an electron gun, in which the heating of a tungsten filament allows the release of the electrons, that are later accelerated through the application of a voltage. According to the voltage applied, the resolution of the image will change, in particular the higher the voltage the better will be the resolution, that in case of very advanced TEM techniques can go below 0.5 Å. The images generated show different coloured areas according to the ability of the sample components to absorb or transmit the electrons. Indeed, areas of the sample that can absorb or scatter electrons will appear darker than those that are able to transmit electrons, whose colour will be brighter.

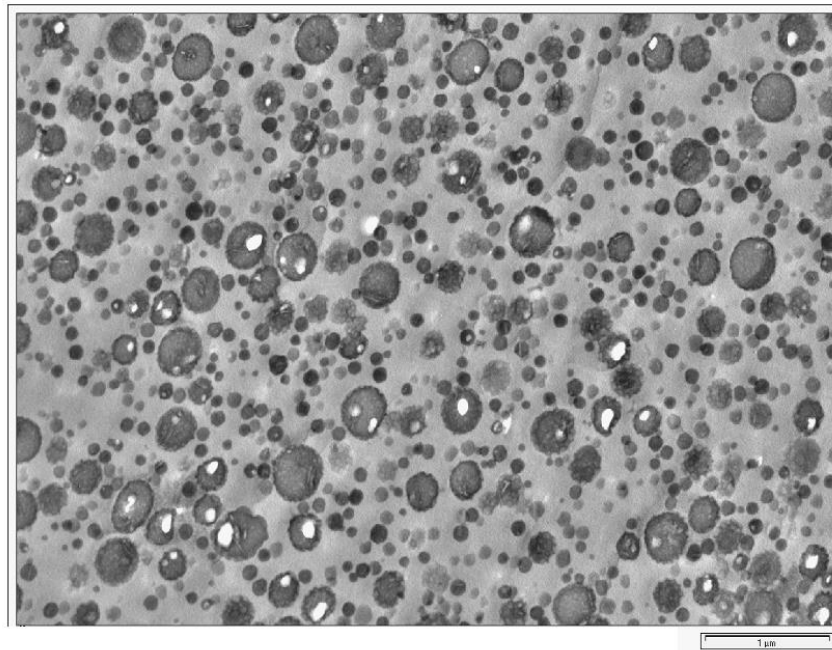
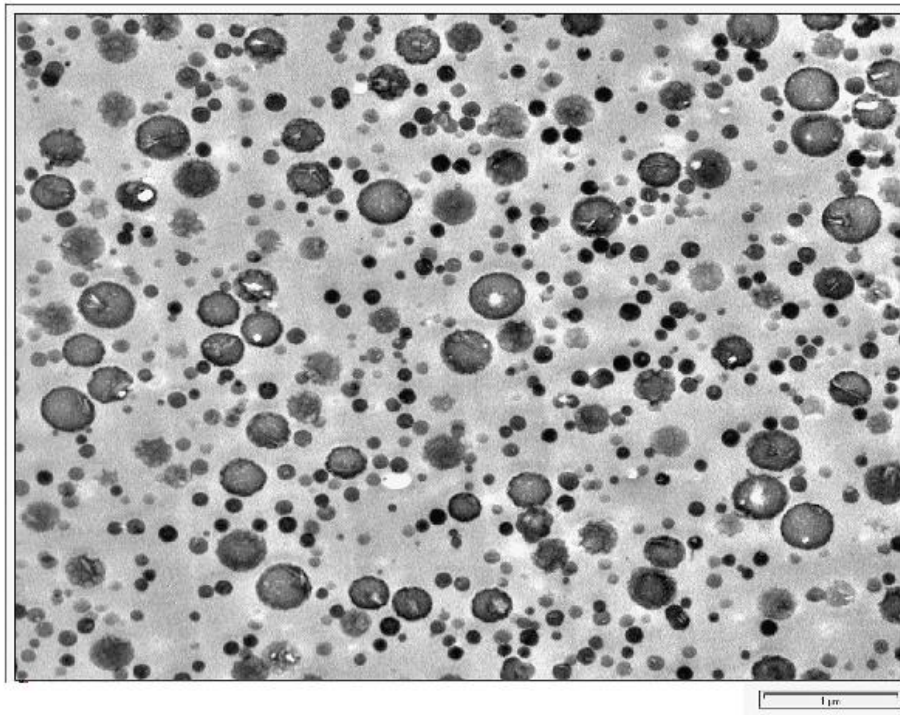


Figure 4. 9 TEM viewing of an ABS with voids in rubber particles

Sample preparation is required, in case of solid specimen very thin slices are cut using an ultramicrotome. When necessary samples are embedded in a polymeric resin that after its solidification will allow a clean cut.

Transmission Electron Microscope could be an ally when dealing with the study of rubber particle cavitation. In particular, before cutting thin slices of specimens are placed in a 4% aqueous solution of osmium tetroxide ( $\text{OsO}_4$ ) for 2 days in order to stain the polybutadiene phase, this is done according to the procedure developed by Kato in 1966<sup>16</sup>. Staining is required because osmium atoms attach to the unsaturated rubber of the sample making it more electron-absorbent. This will provide a strong contrast between the dark rubbery phase and the lighter matrix phase when images are generated. This microscope represents a useful ally because thanks to its high resolution allows to identify the morphology present in the specimens treated, but also shows in a strictly qualitative way the presence of voids inside the rubber particle, along with any kind of modification that could be present in the matrix. Furthermore, if necessary, it could also provide an analysis of the average dimensions of rubber particle present. Two TEM viewing are reported as examples, in which voids in rubber particles appear brighter.



*Figure 4. 10 TEM image of an ABS*

However, one important limitation is present, voids present in rubber particles are not just the product of rubber particle cavitation, but all or some of them may be artefacts created by the cutting blade of the ultramicrotome during sample preparation. Indeed, the analysis conditions invariably produce a substantial amount of shear yielding and/or crazing in the surrounding rigid matrix. The effectiveness of microscopy as technique to inspect cavitation phenomenon is limited in two important ways:

- Cavities will result bigger than their original equilibrium dimensions because the increasing local strains produced in the matrix will induce their expansion
- It is difficult to determine whether yielding takes place before or after cavitation in rubber particles

To conclude TEM technique allows direct observation and characterization of morphology of the cavities formed in the rubber particles, but it is not able to detect and monitor the early stages of the cavitation phenomenon.

#### **4.4 Differential Scanning Calorimeter (DSC)**

Differential scanning calorimetry is a thermal technique used to retrieve information about phase transitions, glass transitions and chemical reactions. This thermal analysis measures the physical properties of a material with respect to temperature, time, and controlled atmosphere. DSC measures endothermic and exothermic processes and is widely used to characterize a vast range of materials including polymers, foods, biologicals, and many others.

In this technique a heat flow is directed to two pans, one containing the sample while the other one is used as reference material. The sample is encapsulated in a pan, made typically of aluminium, and together with an empty reference pan, is positioned on a thermoelectric disk surrounded by the furnace. Both sample and reference are subjected to the same programmed thermal cycle, but when a chemical or physical change results in the emission or absorption of heat in the sample, a thermal energy is added to or removed from the sample in order to maintain the same temperature of the reference pan.

Two different loops are present to control the temperature:

- The first loop maintains the sample and the reference pan at the same temperature

- The second loop compensates the energy difference generated by transitions, by varying the heat supplied to keep both pans at the same temperature

A material's response in a DSC is defined by the equation below:

$$q = C_p \left( \frac{dT}{dt} \right) + f(T, t) \quad (4.7)$$

In which  $q$  is the sample heat flow,  $C_p$  is the sample specific heat capacity,  $dT/dt$  represents the heating rate and  $f(T, t)$  is a function that represents the kinetic response at a specific temperature and time. The first term of the equation expresses the specific heat capacity and changes in the heat capacity, including the glass transitions observed in polymers. Curing, evaporation, decomposition, and many other processes are considered in the kinetic function, whereas melting is an endothermic process that can be expressed as sum of both terms: heat capacity and kinetic components. One big advantage is that very small amount of sample is required, but it is a destructive technique because after the analysis the sample must be discharged. As output a thermogram is obtained, in which on the y-axis it is present the normalized heat flow and on the x-axis the temperature. When transitions are exothermic or endothermic such as melting and crystallization, they are displayed by positive or negative peaks. Furthermore, glass transitions are observed as inflections points and chemical reactions such as decomposition, curing, oxidation are observed as peaks.

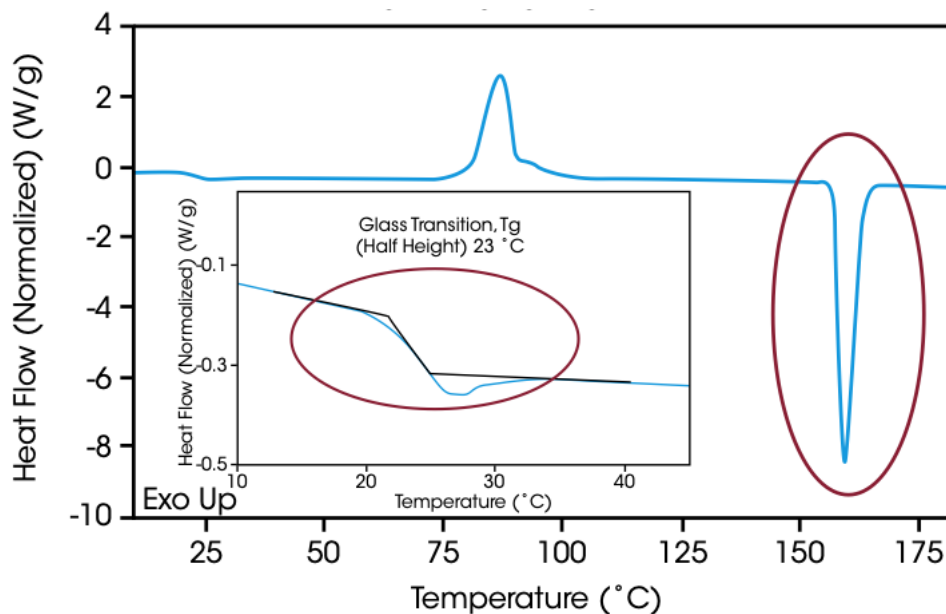
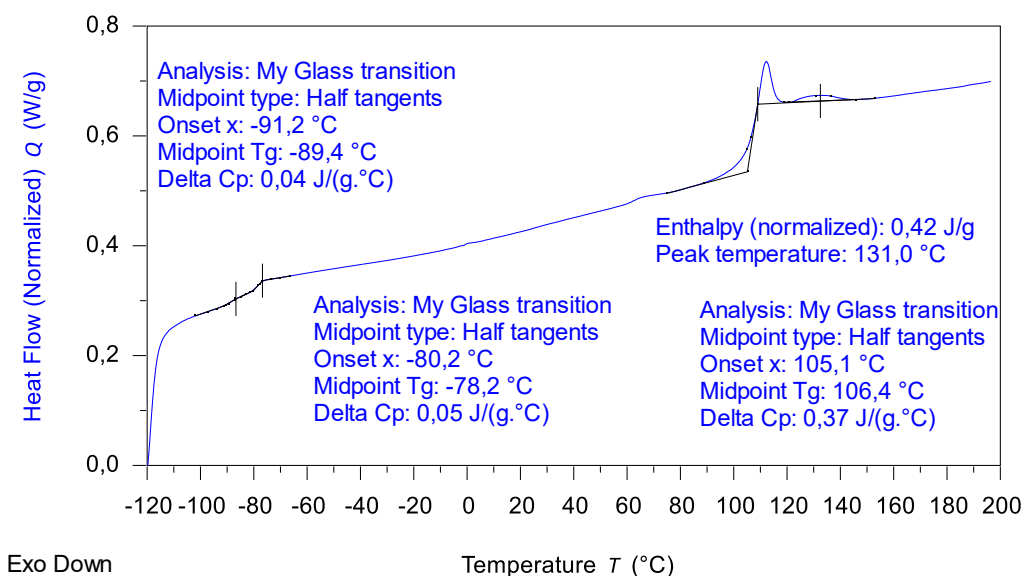


Figure 4. 11 Example of DSC thermogram, highlighting endothermic events

Different information can be retrieved from this analysis, for instance glass transition and melting temperature can be determined, as well as the degree of crystallinity, the effect of plasticizers and many others. It becomes useful even in case of cavitation phenomenon because evidence of splitting of glass transition temperature in the range of  $T_g$  of the rubber or moving of its  $T_g$ , even in this analysis can be present. This technique has a big advantage because it has a very good control of temperature, moreover external forces are not required to carry out the analysis, consequently the splitting of glass transition temperature is given by a partial cavitation. However, a disadvantage is also present, and it is related to the limited amount of sample required that will produce a small signal.

An example of DSC thermogram in case of partial cavitation is shown in *Figure 4.12*, in which two inflection points are registered referring to the glass transition temperatures of intact and cavitated particles. So, it can be concluded that rubber particles cavitation occurs and can be studied also using this instrument.



*Figure 4. 12 DSC thermogram of an ABS showing partial cavitation*

## 4.5 Small-angle X-ray Scattering (SAXS)

Small-angle X-ray scattering is a technique able to quantify the nanoscale density differences in the sample. This means that it can be useful in determining nanoparticle size distributions, size and shape of macromolecules, pore sizes and much more. These variables are obtained by analysing the elastic scattering behaviour of X-rays when they

pass through the material. According to the angular range in which their scattering at small angles can be recorded, SAXS is capable of determine structural information of dimension between 1 and 100 *nm*. This instrument uses a monochromatic beam of X-rays that interacts with the sample, some of the X-rays will scatter, while most of them simply pass through the sample without interacting.

One big advantage of this instrument is the possibility in some models to simultaneously apply a force to the specimen while performing the experiment. This technique was also used to inspect rubber particle cavitation, one example of this work was the one carried out by Declet-Perez et Al<sup>17</sup>. In which using established analytical models, they found efficient and coherent cavitation of the spherical rubbery cores, in block copolymer modified epoxy resins, coincident with yielding and absence of cavitation in the glassy nanodomains. To conclude SAXS technique can be quite useful in the inspection of this micro phenomenon, but it will not be considered in this thesis that will be dedicated just to the rheological approach.

## CHAPTER 5

### Materials and Instruments

This chapter will be dedicated to the presentation of samples and instruments used during the experimental work. In particular, properties and morphology will be presented, as well as a brief description of the instruments' characteristics.

#### 5.1 Samples

Three different type of ABS specimens have been analysed in term of rubber particles cavitation for purpose of comparison. One sample is produced by a competitor while the other two are Versalis products.

##### Sample A

*Sample A* is an ABS produced through an emulsion technology by a competitor, particularly indicated for those applications in which high esthetical and mechanical properties are required. The main advantage of an ABS produced with this technology is the dispersion of the rubbery phase obtained, whose morphology will influence in a huge way the final fractural resistance because it provides a synergistic combination of all three deformation mechanisms: rubber particle cavitation, shear yielding and crazing.

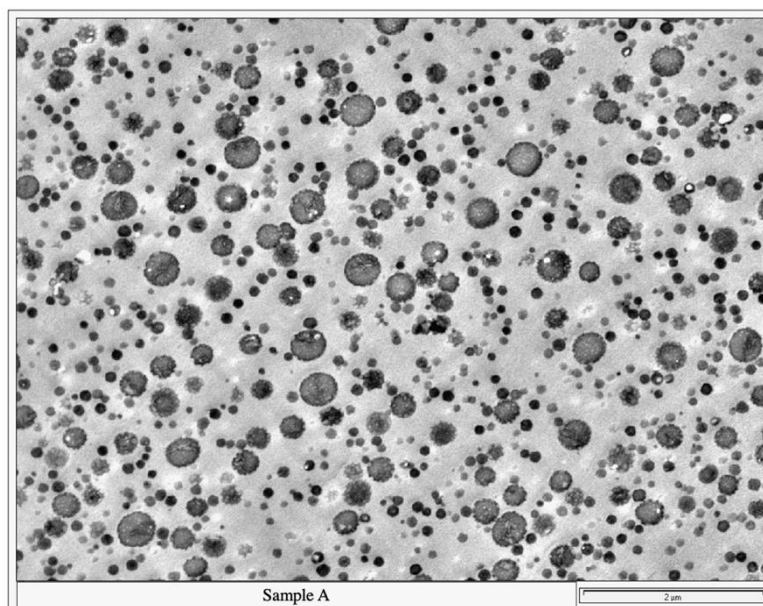


Figure 5. 1 TEM image of Sample A

This sample, as shown in *Figure 5.1*, has a bimodal distribution of spherical rubber particles, without matrix inclusions inside. From transmission electron microscopy it is possible to derive information about the particles' dimensions, that will be coupled with the other properties in the table below.

<i>Sample A</i>	
Numeric diameter	132.8 nm
Volumetric diameter	291.5 nm
Polybutadiene	14.9 %
Vicat (5 Kg – 50°C/h)	93.4
Izod ISO	17.6 KJ/m <sup>2</sup>
MFI (220°C – 10Kg)	31.9 g/10min
GPC Mw (matrix)	101451 Dalton
GPC Mn (matrix)	40521 Dalton

*Figure 5. 2 Table of properties of Sample A*

### *Sample B*

*Sample B* is an ABS sample produced by Versalis and it is obtained by using an alternative technology. This innovative patented technique has the great advantage of producing ABS with small particle dimensions, eliminating the last step involved in the rubber process and increasing the grafted copolymer in order to avoid agglomeration.

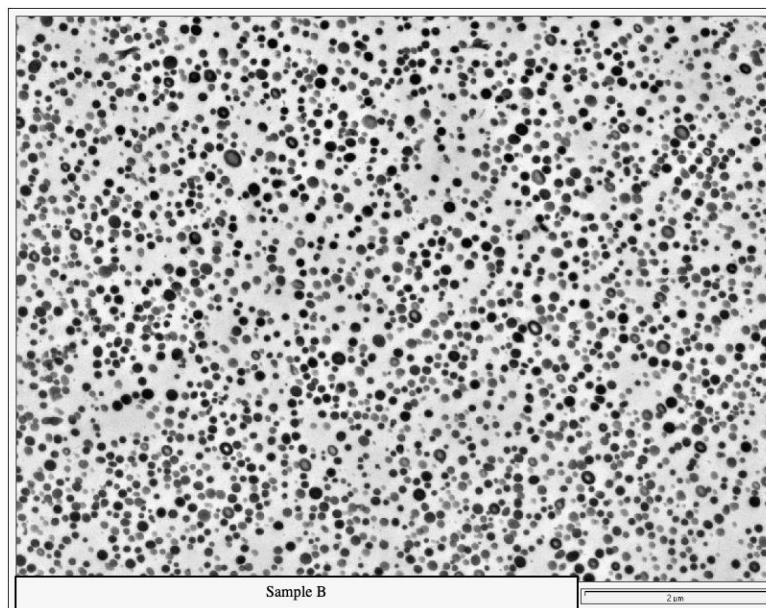


*Figure 5. 3 TEM image of Sample B*

The goal of this production technique is to provide final products with “emulsion-like” properties. From *Figure 5.3*, it is possible to see the morphology of the sample, it shows a less evident bimodal distribution of full and spherical rubber particles with smaller dimensions than rubber particles of Sample A.

<i>Sample B</i>	
Numeric diameter	79.2 nm
Volumetric diameter	98.6 nm
Polybutadiene	12.1 %
Izod ISO	2.7 KJ/m <sup>2</sup>
MFI (220°C – 10Kg)	12.9 g/10min
GPC Mw (matrix)	110542 Dalton
GPC Mn (matrix)	46572 Dalton

*Figure 5. 4 Table of properties of Sample B*

### *Sample C*

*Sample C* is an ABS produced with the same alternative technology of *Sample B*, but it is characterized by a different morphology. It shows a bimodal distribution with small rubber particles and big salami particles with inclusion of matrix inside.

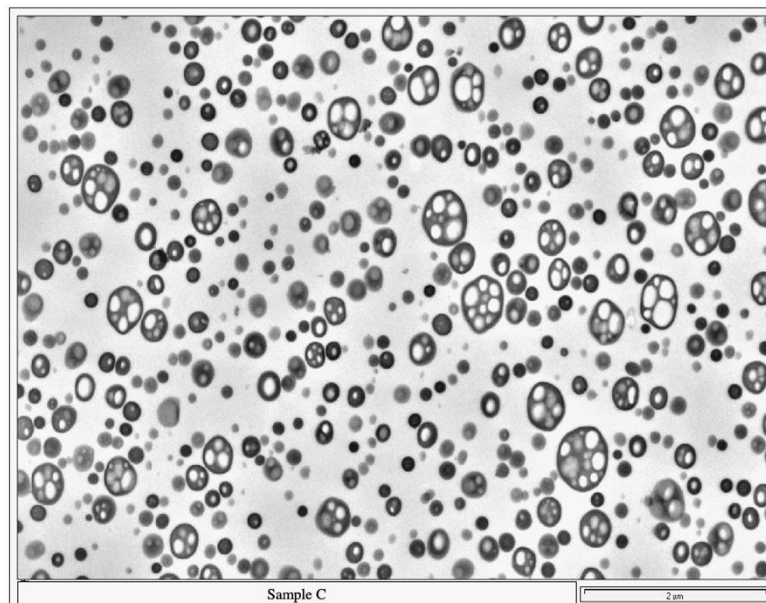


*Figure 5. 5 TEM image of Sample C*

*Sample C* has a wider distribution of particle dimensions that is comparable to that of *Sample A*, however part of this increased distribution is due to presence of big rubber particles full of matrix inclusions.

<i>Sample C</i>	
Numeric diameter	168.3 nm
Volumetric diameter	331.6 nm
Polybutadiene	15.6 %
Izod ISO	18.9 KJ/m <sup>2</sup>
MFI (220°C – 10Kg)	14.2 g/10min
GPC Mw (matrix)	118392 Dalton
GPC Mn (matrix)	48721 Dalton

Figure 5. 6 Table of properties for *Sample C*

### *Samples' distribution of particles dimensions*

In order to provide a visual and clear evidence of the difference in distributions of particle dimensions of the three different specimens analysed, the bar chart along with the best fit of the curves are reported.

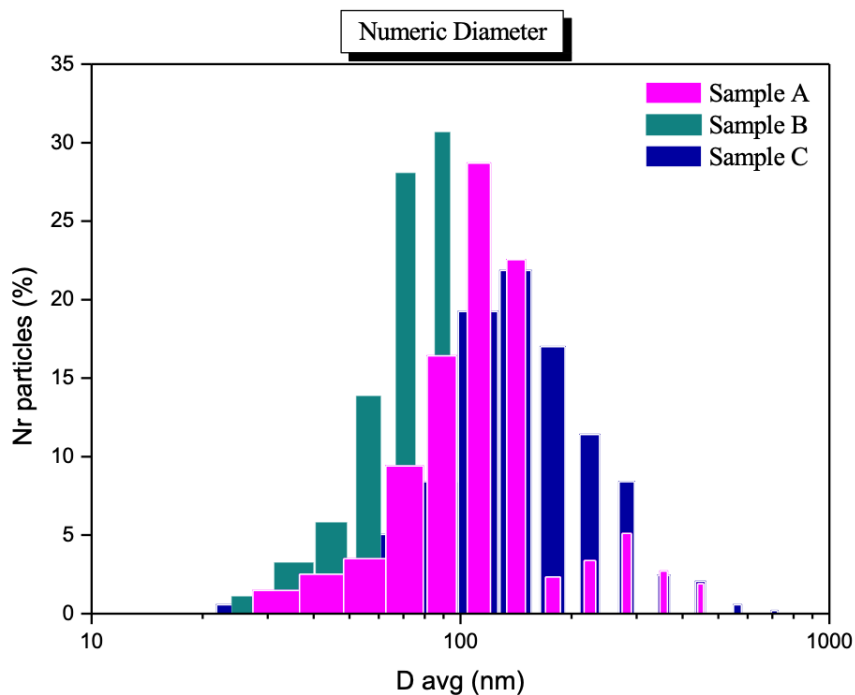


Figure 5. 7 Distribution of particles dimensions

Figure 5.7 shows the number of particles as percentage with respect to the logarithmic average diameter. The three samples A, B and C are represented respectively in magenta, dark cyan and blue. To easily compare these distributions a fit of data curves is provided in Figure 5.8.

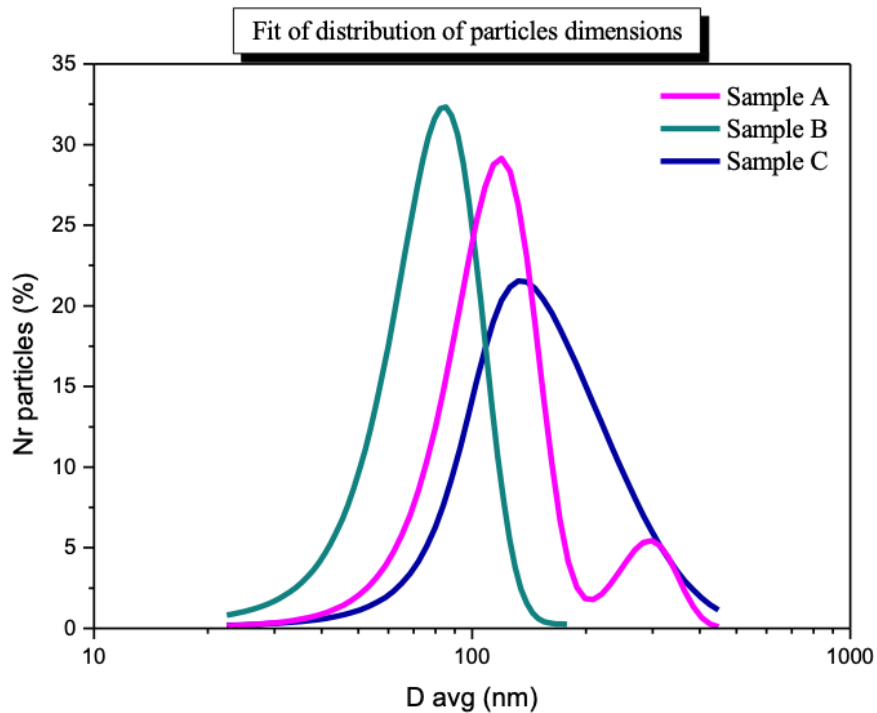


Figure 5. 8 Fit of particles dimensions distribution

Sample A has a wide distribution of diameters, whose bimodality is represented by the presence of a double peak. Sample B is fitted with narrow single peak shifted to the left, at values of average diameters definitely smaller than Sample A and C. Sample C is represented by a wider asymmetric bell curve, whose right shoulder is due to the presence of big salami particles.

## 5.2 RSA-G2 and accessories

*RSA-G2 Solids Analyzer* is one of the most advanced platforms developed by TA Instruments for mechanical analysis of solids. It presents a separated motor and transducer to ensure the purest mechanical data through independent control of deformation and measurement of stress. Since solid and soft solid materials are subjected to a wide range of mechanical deformations over a large range of

environmental conditions, RSA-G2 allows a fully characterization and understanding of the complex mechanical behaviour of solids.

The instrument imposes a mechanical deformation on a specimen and measures the resulting stress response, in order to provide information about the material analysed, RSA-G2 and rheology theory come to help.



*Figure 5. 9 RSA-G2 instrument<sup>31</sup>*

Rigid and soft solids, but also highly viscous liquid materials are studied in terms of numerous materials parameters such as modulus, compliance, and elasticity. Modulus is a measure of the overall material's resistance to deformation; compliance measures the ability of the material to respond to a mechanical deformation and elasticity is a measure related to the material's ability to store deformational energy.

The RSA-G2 is capable of applying a variety of deformation types over a wide range of temperatures and timescales and it calculates these material parameters providing a wealth of information about material's structure-property relationships and its performance characteristics. Indeed, the environment is simulated thanks to the presence of a forced convection oven, designed to optimize temperature response time,

uniformity, and stability. Gases, in this specific case nitrogen (N<sub>2</sub>), passes between two resistive gun heaters and into a specifically shaped oven cavity that allows and improve gas mixing. Five thermocouples are present to continuously measure the temperature, this oven is designed to perform extremely rapid heating and cooling over a range that goes from  $-150\text{ }^{\circ}\text{C}$  to  $600\text{ }^{\circ}\text{C}$ . Furthermore, the heating and cooling rate can be controlled up to  $60\text{ }^{\circ}\text{C}/\text{min}$ .

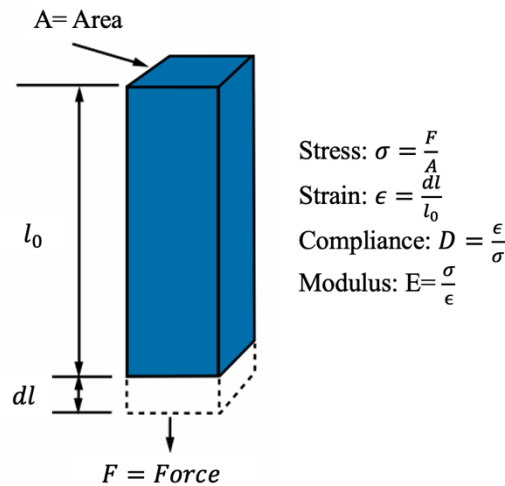


Figure 5. 10 Schematic representation of a specimen deformation<sup>31</sup>

This instrument is arranged with different clamping system that provide multiple modes of deformation to accommodate a wide range of sample stiffness. In this thesis, most of the experiments are conducted on rectangular bar samples, exception made for some tests conducted on rubbers. The most used geometries are:

- Three-point bending
- Tension

Three-point bending is a conformation geometry in which the sample is deformed around three-point contacts at both ends and in the middle of the specimen. This is a “pure mode of deformation”, since the sample is not constrained at the ends, but just positioned onto the clamps. This is ideal to test stiff materials such as ABS, HIPS, but also composites, ceramics, and many others.

Tension mode uses the same rectangular bar of the previous geometry, but here the sample is clamped at the top and bottom and a tensional force is applied. This geometry can become useful also in testing fiber bundles and thin films.

In case of parallel plates, the sample is positioned between an upper and lower round plate and a deformation under various conditions of compression is applied. Here materials with low to moderate modulus can be tested such as: elastomers, gels, and soft solids.

Shear sandwich is a particular geometry in which two equal-size pieces of a material are “sandwiched” between two ends and a central plate. A parallel deformation is applied in order to give rise to a simple shear experiment, usually samples like elastomers, gels, polymer melts are tested.



Figure 5. 11 RSA-G2 geometries<sup>31</sup>

RSA-G2 has been used in this thesis to carry out temperature ramp tests on ABS specimen in order to monitor and study the cavitation phenomenon, but more important for dilatometric analysis. As already explained in the previous chapter, cavitation can be studied through monitoring of expansion and contraction curves. Since a dilatometer was not available, RSA-G2 has been used as a good replacement, indeed it is able to follow the length variation of the specimen with respect to the temperature by using the tension geometry and applying a negligible axial force. It has a very good control of the temperature coupled with a displacement resolution of one nanometre.

### 5.3 Rheometrics Mechanical Spectrometer Model 800 (RMS-800)

Rheometrics Mechanical Spectrometer Model 800 is another instrument able to evaluate viscoelastic properties of materials, in the solid, melt or liquid state in either dynamic or steady mode. RMS-800 is an instrument similar to the RSA-G2 Solid Analyzer because

motor and transducer are separated, but it is older and has a different sensitivity. However, the main difference between the two instruments is the kind of deformation applied. Indeed, in the RSA-G2 specimens are subjected to tensile or compressive forces, while specimens tested in the RMS-800 are deformed through the application of a shear force. In this thesis, tests were carried out in dynamic mode during which the instrument applies a precise sinusoidal shearing to the sample and measures the sample's response. Analysis of the applied strain and the resulting response yields the sample's elastic modulus  $G'$ , viscous modulus  $G''$ , and loss tangent  $\tan\delta$  along with other factors such as complex modulus  $G^*$ , complex viscosity  $\eta^*$ , shear storage and loss compliance,  $J'$  and  $J''$ .

Torsion measurements are performed extensively on rotational rheometers to characterize the low temperature behavior of polymers, composites, blends, and other materials. Different geometries are available, but the typical one, that has been used in the experimental work, is the torsional geometry reported in the following figure.

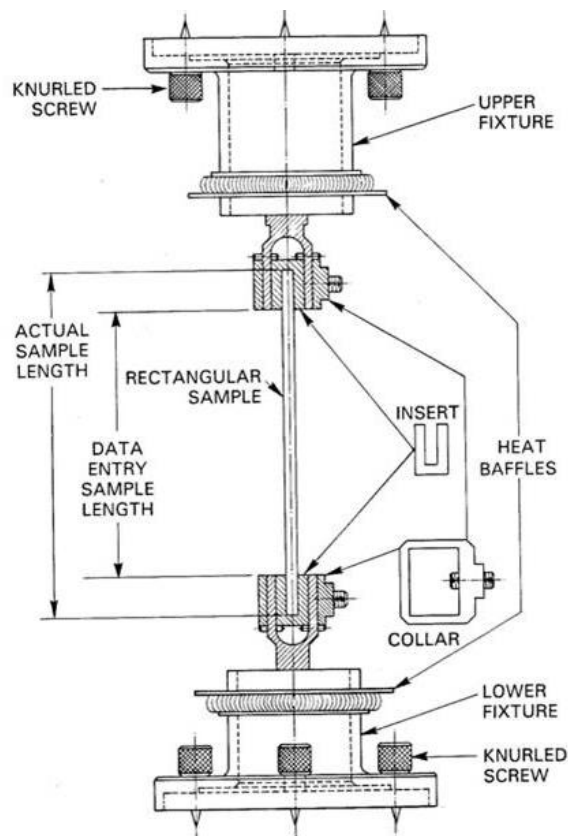


Figure 5. 12 Scheme of torsional geometry in the RMS-800

The specimen, molded as a rectangular bar, is positioned in the insert, and clamped with the collars. The upper fixture is blocked, while the lower one is able to move, giving the possibility to apply a shear deformation.

The sample can be cooled or heated with different rate, going from  $1^{\circ}\text{C}/\text{min}$  to  $15^{\circ}\text{C}/\text{min}$ . Cooling and heating rate must be chosen according to the sample thickness. Indeed, by choosing the correct value of rate and due to the flat aspect ratio of the specimen, no gradients of temperature are generated inside, and a uniform temperature distribution is ensured. The instrument is able to simulate a specific environment thanks to the presence of forced gas convection oven. Nitrogen is usually used, and a wide range of temperature is guaranteed, indeed the instrument is able to go from  $-150^{\circ}\text{C}$  to  $600^{\circ}\text{C}$ .

To conclude, the main advantage of using this old instrument is the possibility of monitoring the length variation of the specimens and the linear viscoelastic properties simultaneously. This represented a huge advantage in studying the cavitation phenomenon. However, the displacement resolution is not comparable to the one of RSA-G2, consequently just the preliminary tests were conducted with this rheometer and all the other experiments were carried out with the newest instrument available.

#### **5.4 Other instruments (DSC, TEM, NMR)**

During the experimental work, other techniques have been used in combination with all the rheological instruments available. Specifically, Differential Scanning Calorimetry has been very helpful in terms of detection of glass transition temperatures as well as evaluation of other transitions such as melting temperatures. The instrument used is *Discovery DSC 2500* of TA Instruments equipped with a cooling system able to reach  $-120^{\circ}\text{C}$ .

Transmission electron microscopy was used to provide a qualitative comparison between specimens subjected to different thermal history, but also to give information about the particle size distributions. The TEM available was a *Philips CM120* operating at a voltage of  $80\text{ KV}$ . Ultrathin sections of  $100\text{ nm}$  were prepared using *Leica EMUC7* ultramicrotome at room temperature and analysis of the particle dimensions of the dispersed phase was performed using *AnalySIS* software.

Another technique, called Nuclear Magnetic Resonance (NMR), has been useful in the determination of the breakdown of comonomers and the isomerism of the polybutadiene fraction present in the ABS specimen treated. Spectra are determined by a *Bruker magnet* (14.1 T) having a protonic resonance *Larmor* frequency of 600 MHz, coupled with a *Cryoplatform Prodigy Unit* for the internal cooling of the probe.

### Experimental work and results

The cavitation phenomenon represents a key issue in understanding the toughening mechanisms involved in rubber-reinforced polymers. The goal of this thesis is to provide a rheological study to inspect rubber particle cavitation in ABS copolymers. This rheological approach finds its basis in the extensive literature available concerning this fundamental aspect of rubber-toughened plastics. All tests required for this analysis were conducted on *RSA-G2 Solid Analyzer*, while some preliminary tests were carried out on *RMS-800* rotational rheometer. In order to investigate the cavitation phenomenon, linear viscoelasticity tests were performed in shear and three-point bending geometry, on the other hand, dilatometric studies were carried out through a tensile geometry. Experimental conditions have been defined and improved by testing different specimen dimensions, heating, and cooling rate. After defining the procedure for the preparation of the specimen, experimental results and data elaboration will be provided.

#### 6.1 Optimization of tests conditions

A preliminary study has been conducted on an ABS specimen which was not affected by the cavitation phenomenon. The goal of these preliminary tests was to optimize the experimental conditions in order to measure the most reliable data. Attention was given to the way the specimen has to be introduced and clamped inside the instrument, to its dimensions, and also to the cooling and heating rate imposed during the tests. As concerns the introduction into the machine, the only care to keep in mind is to insert and clamp the specimen just at the end of the filling phase of nitrogen into the dewar of the rheometer. Indeed, during the nitrogen filling, it is not possible to control the temperature inside the oven which can even reach  $-140^{\circ}\text{C}$ . Just at the end of the filling procedure, the temperature starts to be controlled and can reach the imposed value. As regards specimens' dimensions, two rectangular moulds for compression were suitable for the experimental work done on the instruments. One has a width of about 8 mm and 2 mm of thickness that will be called "thick specimen", while the other one has a width

of 12 mm, but a thickness of 1 mm, referred to as “thin specimen”. Length is not an influent parameter to consider, because the maximum actual sample length that can be introduced in the oven is 45 mm.

Several tests were conducted at different heating and cooling rates on the two types of specimen dimensions, and by determining the position of the damping peak related to the glass transition temperature of the polybutadiene thermostating differences were analysed. Comparisons of the damping peaks are reported below for both specimens and different rates.

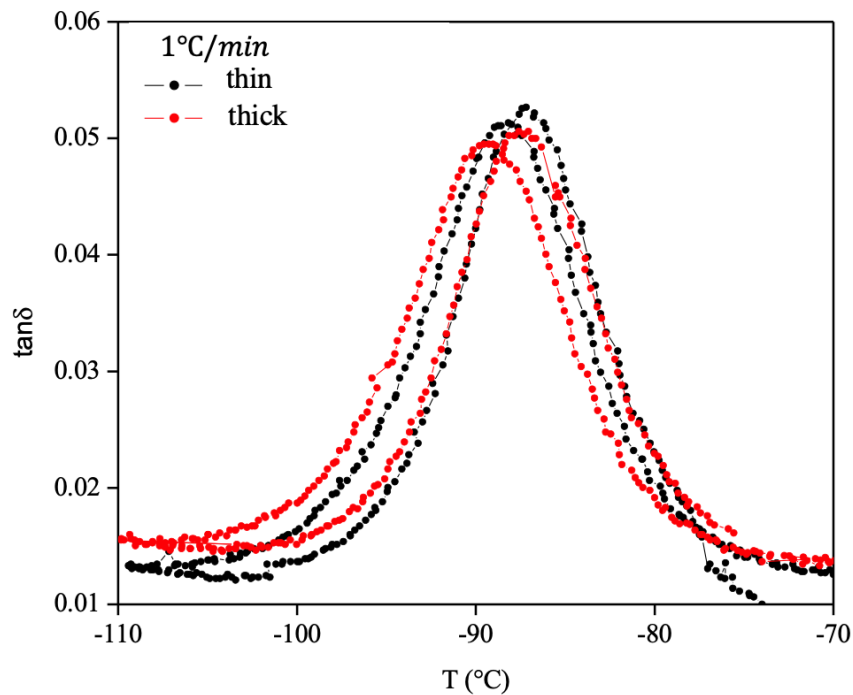


Figure 6.1 Dynamic Temperature Ramp on ABS samples, cooling and heating scans measured at 1°C/min

Figure 6.1 shows on the abscissa the temperature, while on the ordinate the values of the damping peaks. Specimens are reported with two different colours, the thin sample is reported in black, while the thicker one is shown in red. Heating and cooling scans are measured, in this case at 1°C/min, and are reported in the graph. The other tests are reported in the figures below, colours remain the same, while different will be the cooling and heating rate.

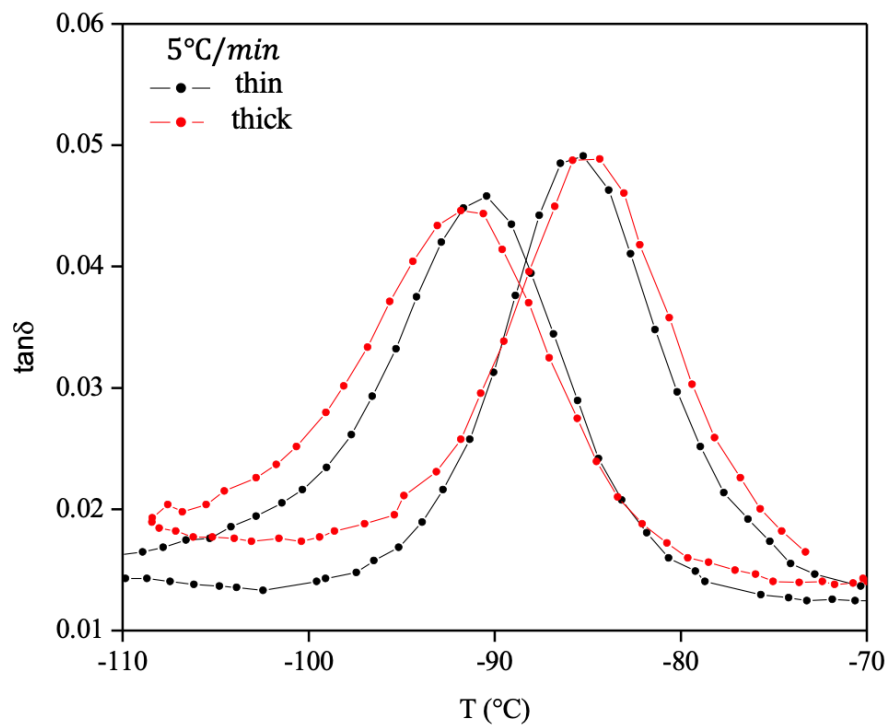
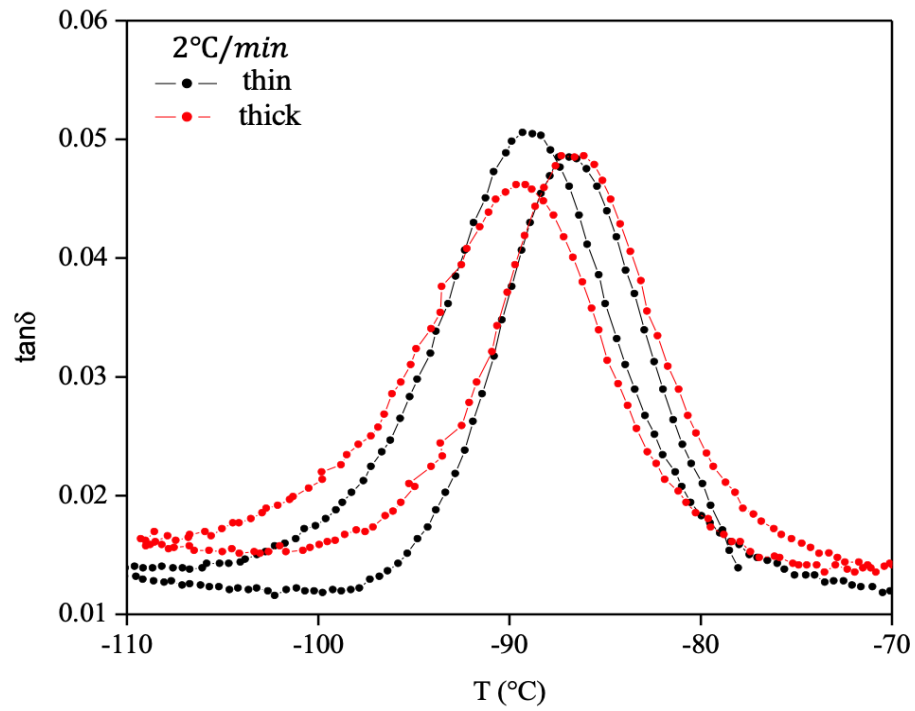


Figure 6. 2 Dynamic Temperature Ramp on ABS samples, cooling and heating scans measured at 2°C/min and 5°C/min

In the previous figures, it was evident that the glass transition temperatures measured during cooling and heating are different for both specimens. This evidence is shown in the plot reported below:

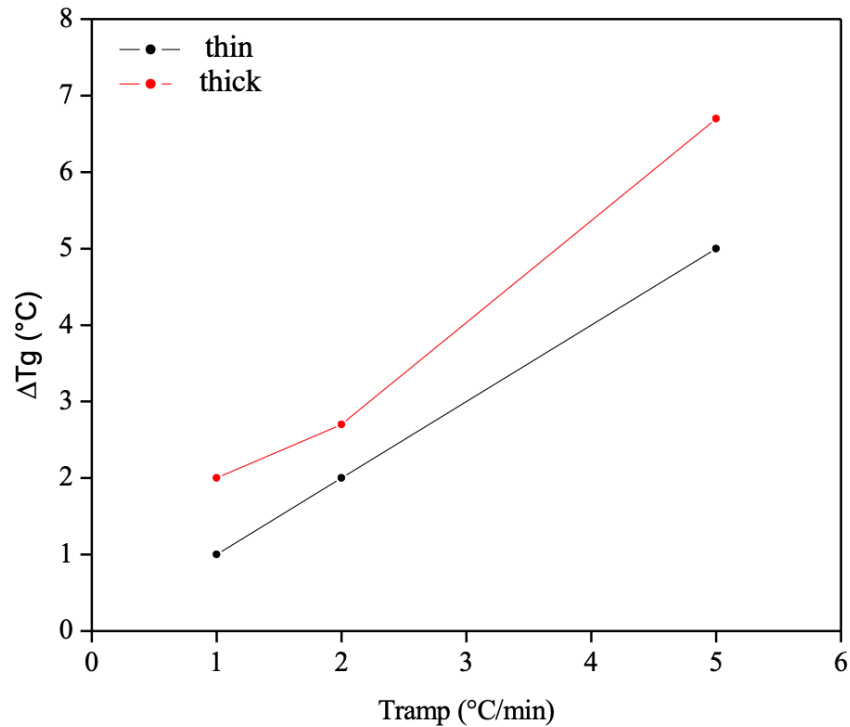


Figure 6. 3 Variation of  $\Delta T_g$  with respect to the cooling or heating rate

In an ideal case, the differences between the glass transition temperatures measured with different thicknesses should be zero but, as predictable, the thin specimen shows smaller values of  $\Delta T_g$  with respect to the thick one. Indeed, the thin sample is able to thermostat rapidly, following the temperature control of the oven. Furthermore, decreasing the cooling rate, lower will be the distance between peaks. Considering the high amount of nitrogen required to run dynamic temperature ramp tests and taking into account that tests conducted at  $1^\circ\text{C}/\text{min}$  will necessitate a longer time, it has been decided that the cooling and/or heating rate more adequate to decrease the difference in glass transition temperature and avoid a long time of analysis is of  $2^\circ\text{C}/\text{min}$ , exception made for a few tests conducted at  $5^\circ\text{C}/\text{min}$ .

## 6.2 Specimen preparation

In this study, specimens were prepared through compression moulding technique. A Carver compression moulding machine was used to prepare them. In case of tests conducted on the matrix alone, Styrene Acrylonitrile (SAN) pellets were dried in an oven at 60 °C for at least 4 hours under vacuum conditions, before moulding. This procedure is required because the hydrophilic behaviour of the matrix can be responsible for the presence of residual humidity inside the pellets and consequently could give rise to the formation of air bubbles during the compression moulding.

Materials were moulded in a mould set composed of two polished metal plates and moulding chase of the desired geometry. For all the viscoelasticity and dilatometric tests the rectangular bar geometry was used. The approximate dimensions are reported in the following image.

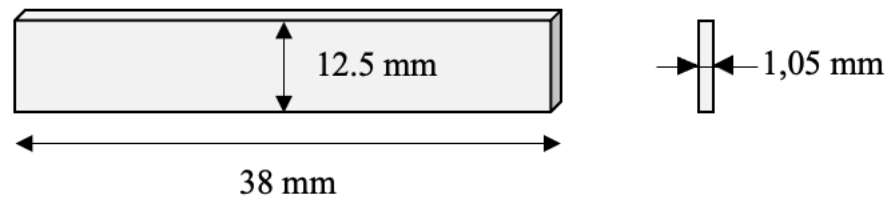


Figure 6. 4 Shape and dimensions of the specimens used

Specimens were moulded at a temperature of 200 °C and with the application of approximately 480 *bar* for 5 minutes. Then the metal plates containing the chase and the material were removed from the press and were cooled at ambient temperature. In order to maintain the geometry during cooling, a load of 5 *Kg* was positioned onto the plates. Once the plates reached the ambient temperature, the specimens were removed from the mould and the excess of material was eliminated.

## 6.3 Dynamic Temperature Ramp Results

Preliminary tests were conducted on Sample A using *RMS-800* instrument with torsion rectangular geometry. The specimen was compression moulded in the Carver press and then subjected to a specific thermal cycle, in which it was first cooled and then heated

at the same rate. A dynamic temperature ramp test was performed with a cooling and heating rate of  $2^{\circ}\text{C}/\text{min}$  from  $0^{\circ}\text{C}$  to  $-120^{\circ}\text{C}$  and imposing a frequency of  $1\text{ Hz}$ . The applied strain was  $1\%$  to ensure the measurement of properties in the linear regime. The loss modulus and the damping peak during the heating scan are reported below.

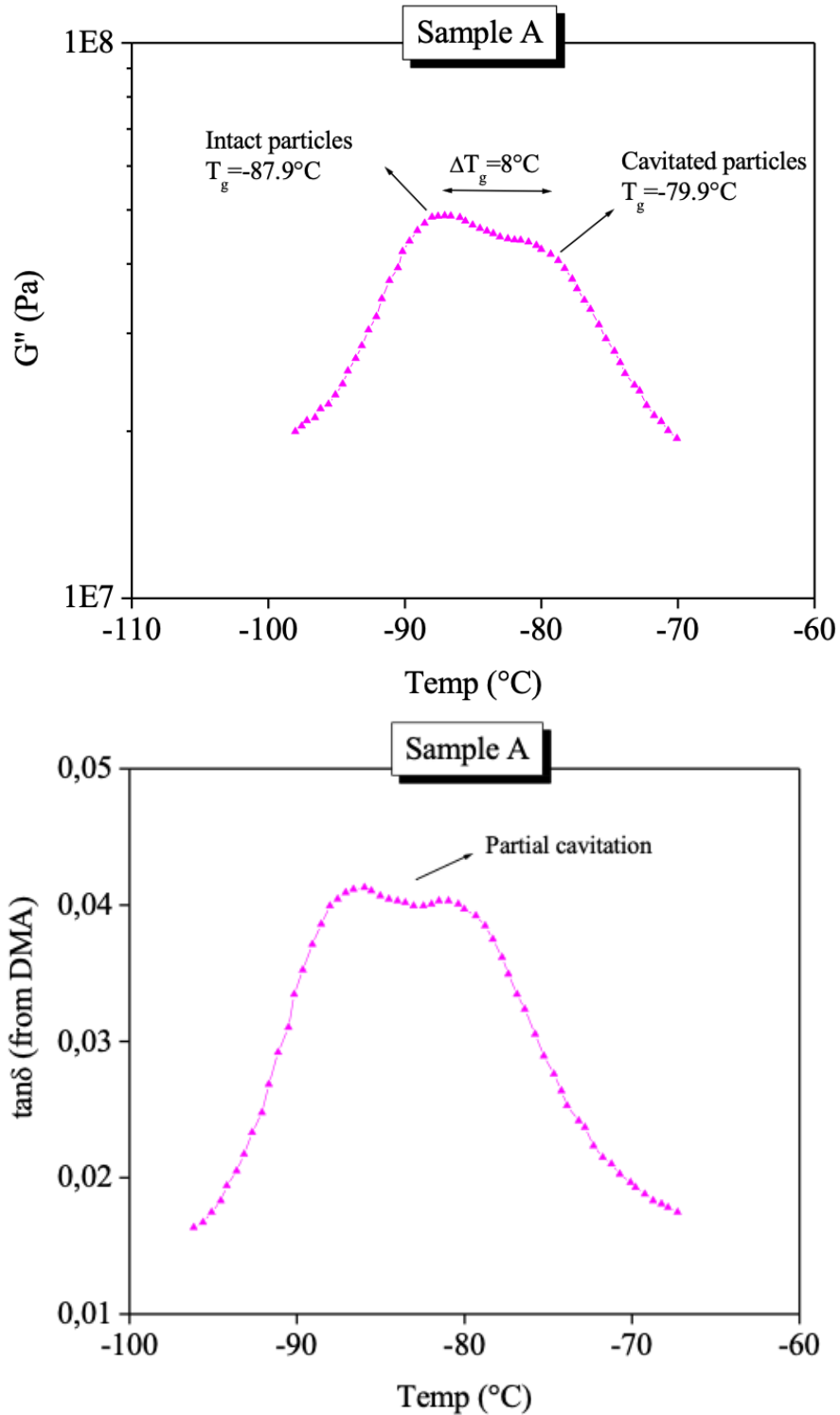


Figure 6. 5 Loss and damping peaks for Sample A, registered during the heating scan in RMS800

Figure 6.5 reports loss and damping peaks as a function of temperature for Sample A, measured during the heating scan performed at  $2^{\circ}\text{C}/\text{min}$  in *RMS-800*. The most important evidence is their splitting originated from a partial cavitation phenomenon. Both  $\tan\delta$  and  $G''$  peaks are shown in a reduced range of points, with respect to those actually collected, in order to clearly show the peaks. As previously explained, DMTA analysis provides information about the cavitation phenomenon, in particular by analysing the damping and loss modulus peaks at low temperatures, where the glass transition temperature of the rubber phase is present. Here, both viscoelastic functions clearly report a splitting of the peak, the left peak refers to a fraction of particles still intact and well bonded to the matrix, while the peak on the right is due to a fraction of particles that were able to release the hydrostatic tension by forming micro-voids inside and consequently moved their glass transition temperature at higher value, closer to the  $T_g$  of the rubber in its unconstrained conditions. In order to have information about the values of glass transition temperatures of intact and cavitated particles, it is necessary to know the values of temperature corresponding to the peaks of the viscoelastic functions.

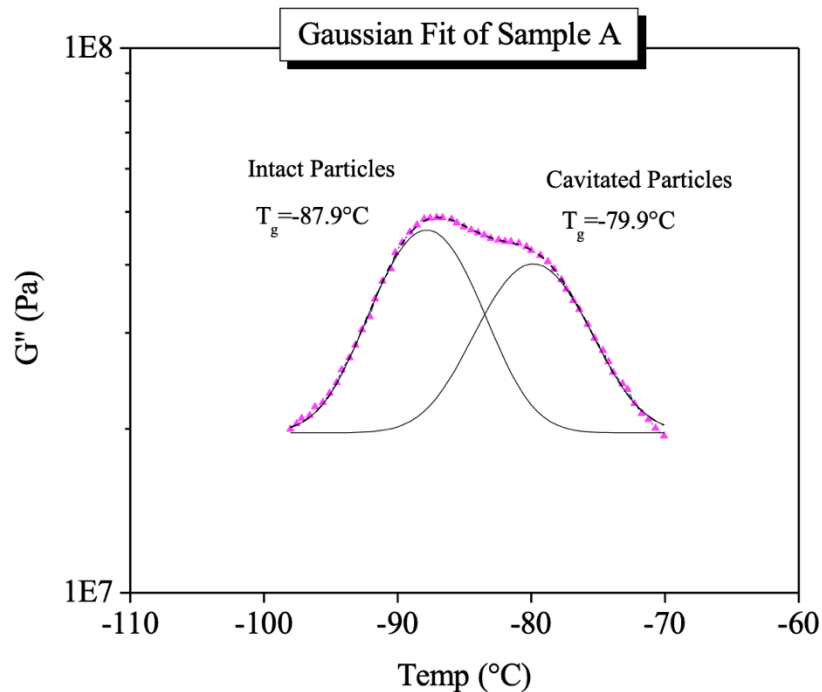


Figure 6. 6 Multi peaks Gaussian fit for loss modulus of Sample A

In this case, the splitting is so evident that the position can be simply retrieved, but sometimes could be not clear and when possible a deconvolution of the double peak by

using a Gaussian curve can be useful. For the sake of completeness, a gaussian fit of the loss modulus is reported, but the same analysis can be done even for the damping peak. After the preliminary tests conducted on Sample A with RMS-800 instrument, the experimental work was performed on the newer instrument, the RSA-G2. This choice has been made for reasons related to the displacement resolution and the temperature control of the machine. The displacement resolution of one nanometre was fundamental in the dilatometric studies to inspect the rubber particles cavitation by monitoring the change in length of the specimen and consequently the change in thermal expansion coefficient. The better resolution of the displacement along with the improved temperature control allow to surely define the RSA-G2 as the most suitable instrument to study the cavitation phenomenon. However, it must be said that one of the great advantages of the RMS-800 was the possibility of simultaneously monitoring the length variation and the linear viscoelasticity.

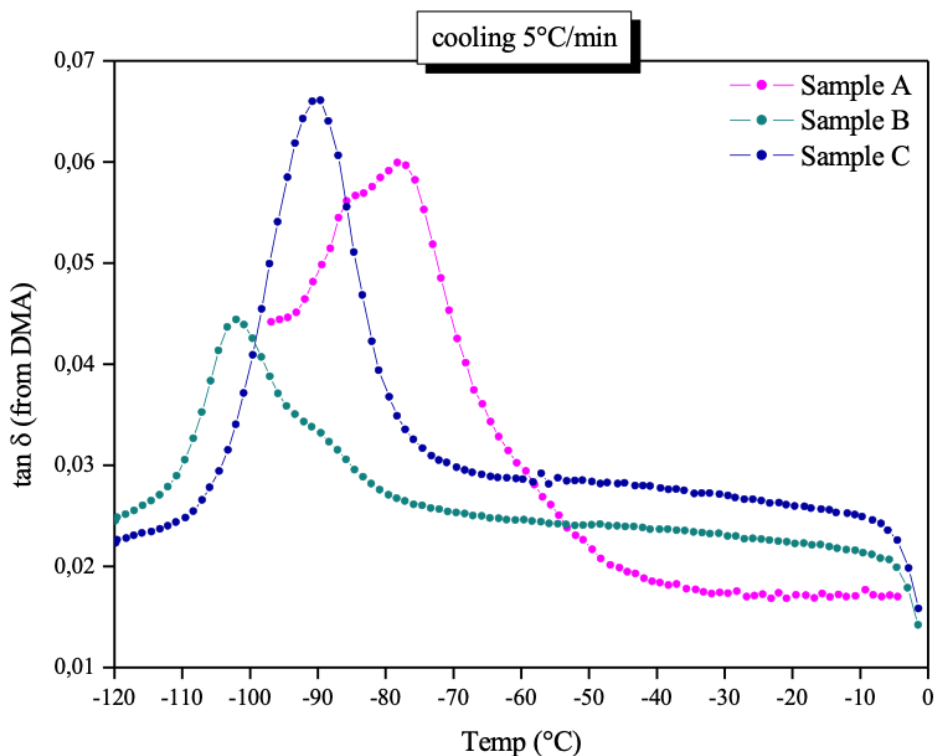


Figure 6. 7 Damping curve of Sample A-B-C measured with three-points bending geometry in RSA-G2

In order to compare the viscoelastic behaviour of all samples, temperature ramp tests have been conducted at  $5^{\circ}\text{C}/\text{min}$  using the three-point bending geometry in the RSA-G2.

A cooling rate of  $5^{\circ}\text{C}/\text{min}$  has been chosen in order to reduce the time requested to carry out the experiments. The figure reported shows the damping peaks of the three samples as a function of the temperature. As already shown in the previous results, Sample A is subjected to a partial cavitation phenomenon that results in a splitting of the loss and damping peaks. One difference to keep in mind is the position of the glass transition temperature, Sample A is the specimen with the highest  $T_g$  while Sample B and C show clearly lower glass transition temperatures. Surprising is the difference in  $T_g$  present between Sample B and C. Indeed, these samples are produced with the same bulk rubber. Consequently, in absolute terms, their glass transition temperature should be in the same position. However, this is not verified in the experimental data. The same consideration can be done also in terms of loss curves. In order to explain the difference shown by Sample B and C, a detailed analysis of the possible parameters influencing the absolute position of the glass transition temperature is provided in the next paragraph.

#### **6.4 Parameters affecting $T_g$**

The transition from the glass to a rubber-like state is an important feature of polymer behaviour, marking the region where a dramatic change of physical properties such as hardness and elasticity occurs. This transition is reversible and is a function of the molecular cooperative motion of only a few monomers. In the rubber-like state, polymeric chains are able to rapidly move, but when the temperature is lowered, the movement progressively reduces until, eventually, the available thermal energy is insufficient to overcome the rotational energy barriers in the chain. In the case of elastomers like the polybutadiene used in ABS copolymer, the glass transition temperature is quite low reaching a value of about  $-90^{\circ}\text{C}$ .

Several parameters influence the position of  $T_g$  of the polybutadiene phase present in the matrix of Sample B and C:

- Molecular weight
- Isomeric composition of the rubber (microstructure)
- Degree of crosslinking

- Hydrostatic tension

Each of them will be analysed in detail.

### Molecular Weight

The glass transition temperature is affected by the molecular weight. In particular in polymer physics, a simple empirical formula relates this variable to the glass transition temperature. This relation was proposed by Paul J. Flory and Thomas G. Fox and takes the name of “Flory-Fox Equation”. The equation relates the number average molecular weight  $M_n$  to the glass transition temperature as shown in the following expression.

$$T_g = T_{g,\infty} - \frac{K}{M_n}$$

(6. 1)

In which  $T_{g,\infty}$  is the maximum glass transition temperature that can be achieved at a theoretical infinite molecular weight and  $K$  is an empirical parameter that is related to the free volume present in the polymer sample.

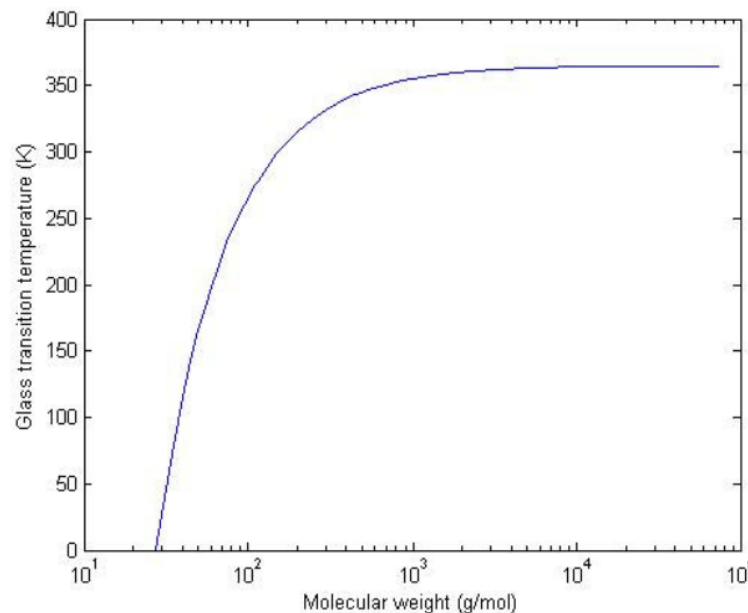


Figure 6. 8 Glass transition Temperature vs number average molecular weight<sup>34</sup>

Figure 6.8 shows that the glass transition temperature increases with increasing molecular weight and reaches a plateau for a value of molecular weight higher than  $10^3 \text{ g/mol}$ . Since the rubber used in ABS production usually has a high value of

molecular weight, such as 65 – 75 *KDa*, this parameter does not influence the different positions of the glass transition temperature of Sample B and C.

Isomeric composition of the rubber

The glass transition temperature of polybutadiene is affected by its microstructure. In particular polybutadiene is a random terpolymer composed of *cis* 1,4, *trans* 1,4 and 1,2 isomers. This terpolymer is characterized by a glass transition temperature that can be retrieved by using the general equation proposed by DiMarzio and Gibbs<sup>18</sup>. The equation reported below relates the glass transition temperature of a copolymer to the microstructure and the  $T_g$  of its three homopolymers.

$$C[T_g - T_g(cis)] + T[T_g - T_g(trans)] + V[T_g - T_g(vinyl)] = 0 \tag{6.2}$$

In which  $C$ ,  $T$  and  $V$  denote the weight fractions of *cis* 1,4, *trans* 1,4 and 1,2 (*vinyl*) groups, respectively.  $T_g(cis)$ ,  $T_g(trans)$  and  $T_g(vinyl)$  represent the glass transition temperatures of the homopolymers. The reported values of these temperatures have been measured by differential thermal analysis in the work of W. S. Bahary et al.<sup>18</sup>

$T_g(cis)$	-106°C
$T_g(trans)$	-107°C
$T_g(vinyl)$	-15°C

Figure 6. 9  $T_g$  of the homopolymers of polybutadiene

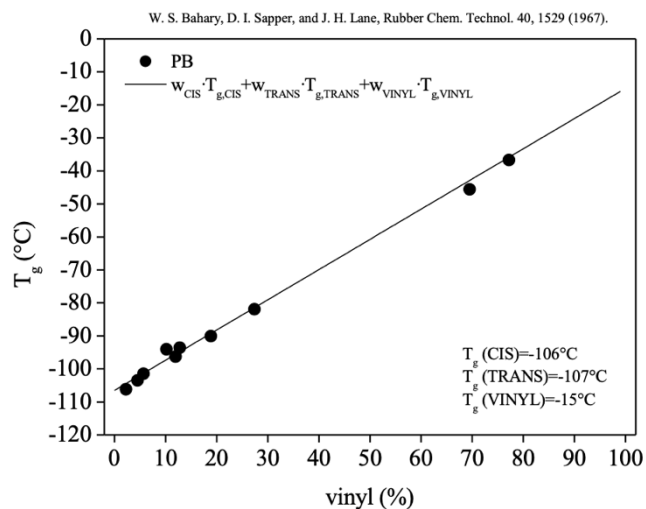


Figure 6. 10 Glass transition temperature versus vinyl percentage

Since  $T_g(cis)$  is equal to  $T_g(trans)$  within experimental error, Equation (6.2) can be reduced to:

$$T_g = 91 V - 106 \quad (6.3)$$

It can be concluded that the  $T_g$  of polybutadiene is essentially determined by vinyl content, as it is shown in Figure 6.10.

One of the parameters that can actually explain the difference in glass transition temperatures of Sample B and C is actually the vinyl content. In order to have information about the isomeric composition of the rubber present in Sample B and C, the NMR technique can be a useful instrument. The spectra registered by the instrument give information about the ABS signals, in particular the styrene-aromatic component, those related to the unsaturated protons of the double bond of the polybutadiene component and the part relative to the aliphatic protons. The areas associated with the resonance of the component of ABS are then corrected by subtracting the area of the blank (reference) and at the end by transforming these areas into absolute molar concentration and multiplying by the molecular weight allow to obtain the distribution of weight in percentage.

	% SAN			% BUTADIENE		
	AN	STYRENE	1,2 Vinyl	1,4 Trans	1,4 Cis	Total PB
Sample B	21.3	68.7	0.9	4.4	4.7	10
Sample C	20.2	65.9	1.4	5.7	6.8	13.9

Figure 6. 11 Weight percentage distribution for Sample B and C

Keeping attention just to the polybutadiene phase it is possible to retrieve the vinyl percentage just for the rubber phase in both Sample B and C. Indeed, by considering the total amount of polybutadiene the percentage is retrieved and is almost equal for both samples to 10%.

% 1,2 Vinyl	
Sample B	9
Sample C	10.07

Figure 6. 12 Percentage of 1,2 Vinyl for Sample B and C

Consequently, it can be concluded that the difference in glass transition temperatures present between Sample B and C cannot be attributed to the difference in isomeric composition. Eliminating the molecular weight and the isomeric composition contributions, it is required now to consider the effect of the degree of crosslinking. This latter effect is extremely important in ABS production because it will influence the final properties of the materials.

### Degree of crosslinking

The glass transition temperature is also affected by the degree of crosslinking, in particular when a material starts to create ionic and/or covalent bonds its overall mobility decreases. Indeed, the presence of crosslinks between chains restricts rotational motion and hence, the greater the degree of crosslinking, the higher will be the glass transition temperature. In order to have information about the degree of crosslinking of the rubber present in ABS, an indirect method could be used, like the measure of the swelling index. This indirect way of retrieving information about the degree of crosslinking of rubber in ABS is one of the most used techniques by many industrial companies. The evaluation of the swelling index of a rubber gel in rubber-modified styrene polymers has been proposed by H. J Karam et al.<sup>19</sup> in 1985 and it is based on a modification of the Flory-Rehner equation. The procedure consists of dissolving 1 g of polymer into 20 g of a 50 – 50 mixture of toluene and methyl ethyl ketone that are used as solvents. The solution obtained is placed into a graduated glass centrifuge tube and after the centrifugation two phases will be obtained:

- Swollen gel
- Supernatant

Upon completion of the centrifugation step, the volume and concentration of the upper and lower phase are determined, and the swelling index can be determined as:

$$\text{swelling index} = \frac{\text{wet gel weight}}{\text{dry gel weight}}$$

(6. 4)

$$\%gel = 100 \cdot \frac{dry\ weight}{sample\ weight}$$

(6. 5)

Since in this thesis samples are ABS specimens solvents must be changed indeed, a mixture of toluene and tetrahydrofuran has been used. The swelling index is inversely proportional to the degree of crosslinking because the higher the swelling index, the lower will be the degree of crosslinking and the lower will be also the glass transition temperature. The value of the swelling index retrieved for Sample B and C are reported below:

Swelling index	
Sample B	21
Sample C	12.1

*Figure 6. 13 Swelling index of Sample B and C*

Once the swelling index is known a relation between glass transition temperature and swelling index must be found. A great amount of another ABS with similar morphology to Sample C was available at different values of swelling index and consequently different degrees of crosslinking. So, this material called Sample D has a bimodal distribution of particles, with small spherical rubber particles and big salami particles with inclusions of matrix inside as shown in *Figure 6.14*.

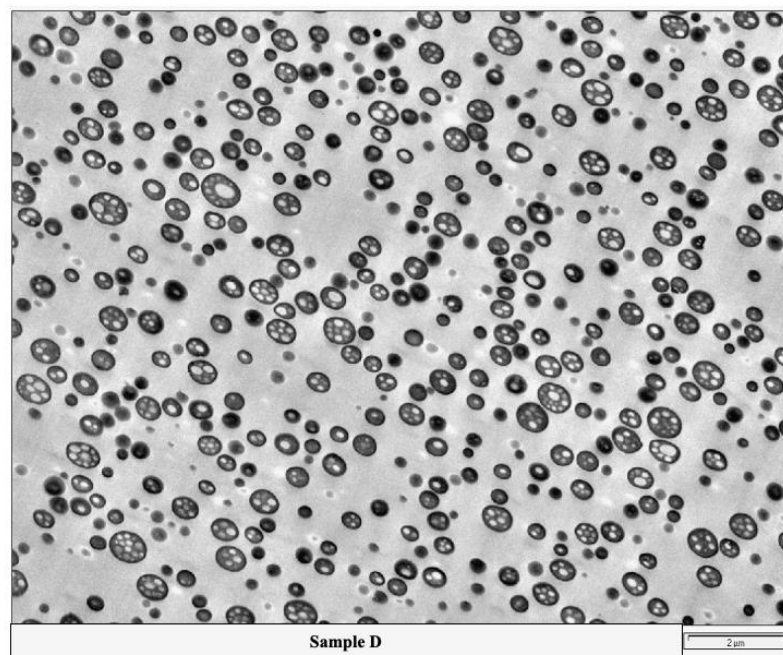


*Figure 6. 14 TEM image of Sample D*

By using the RMS-800 rheometer equipped with the torsional geometry and performing linear viscoelastic experiments at  $2^{\circ}\text{C}/\text{min}$ , the glass transition temperature of the rubber for Sample D at different swelling index were measured and their values are plotted with respect to the swelling index in *Figure 6.15*. Sample D provides a correlation between  $T_g$  and swelling index that can be used just for specimens with similar morphology, otherwise the correlation might change.

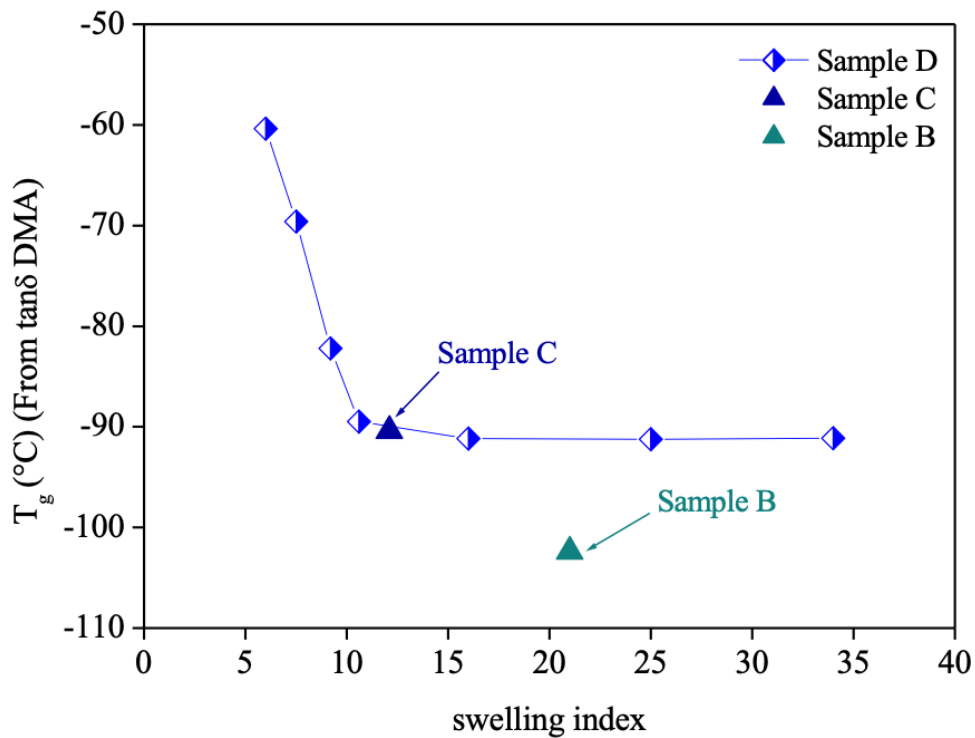


*Figure 6. 15  $T_g$  of Sample D versus Swelling index. Position of Sample B and C are also reported*

From this plot, it is possible to see how strongly the glass transition temperature depends on the swelling index. Specifically, the glass transition temperature is affected just at low values of swelling index going from 5 to 10, while at values higher than 10 reaches a plateau in which the  $T_g$  remains almost constant. Sample D has the same morphology as Sample C. Consequently, they can be directly compared. Indeed, Sample C has a value of glass transition temperature and swelling index that allow its positioning in the plateau area.

While for Sample B some considerations must be made. The relationship between  $T_g$  and swelling index holds true when the same morphology is compared, but as shown in *Chapter 5*, Sample B has a distribution of small and full spherical particles without any

inclusion of matrix inside. So, a comparison between Sample D and Sample B cannot be possible. However, attention must be given to an important limitation of the swelling index technique: the overestimation of the swelling index for salami particles. Indeed, when the material is swollen into the solvent, salami particles containing inclusions of matrix will swell more due to the fact that also the inclusions of matrix will be subjected to swelling. The swelling index measured for Sample D and C is overestimated. The value of the swelling index retrieved for Sample B is 21, supposing a morphology with salami particles the specimen will show an overestimation of the swelling index giving rise to a higher value. It can be concluded that with equal morphology Sample B will have a swelling index that allows its positioning into the zone of constant  $T_g$ . Consequently, the difference in glass transition temperature shown between Sample B and C cannot be attributed to a difference in the degree of crosslinking of the rubber. Now, it just remains the effect of the negative hydrostatic tension to consider.

### Hydrostatic tension in rubber particles

It is well known in the literature that the cavitation phenomenon can be generated by two sources: mechanical loading and differential thermal contraction. This mechanical loading gives rise to volume strains in the particles and the surrounding furthermore, additional volume strains of similar magnitude are generated even by subjecting the polymer to a cooling starting from the  $T_g$  of the matrix. Indeed, taking into account just the differential thermal contraction, according to *equation 8.1* proposed by Bucknall in the book “The physics of glassy polymers” by Young<sup>3</sup>, the volume strains are generated by a misfit of the thermal expansion coefficients and by the difference in temperature. The equation is reported below, while its derivation will be presented in the appendix.

$$\Delta V_r = \frac{\sigma_{mr}}{K_r} = \frac{(\beta_m - \beta_r)\Delta T}{1 + \frac{K_r}{K_m(1-c)} \left( 1 + \frac{v_m}{2(1-2v_m)} + c \right)}$$

(6. 6)

Assuming both rubber and matrix polymer fully relaxed at the  $T_g$  of the matrix, the volume strain and consequently the mean stress generated on cooling to temperature  $T$

are considered by expressing the temperature interval as  $\Delta T = T - T_{g,matrix}$ . In the equation,  $\beta_m$  and  $\beta_r$  are the volumetric thermal expansion coefficients of the matrix and the rubber,  $c$  represents the rubber concentration,  $K_r$  is the bulk modulus of the rubber,  $K_m$  and  $\nu_m$  represent the bulk modulus and Poisson's ratio of the matrix. Calculations are usually based on the following typical values:

- The glass transition temperature of the matrix that is SAN (styrene-acrylo-nitrile) is taken as 103°C
- Thermal expansion coefficients of the matrix and the polybutadiene rubber are taken from the value suggested by Bucknall in 2000<sup>9</sup> and are  $\beta_m = 1.8E-04 K^{-1}$  and  $\beta_r = 7.6E-04 K^{-1}$
- The bulk modulus of polybutadiene rubber is taken from the same article suggested in the previous point and it is  $K_r = 2000 MPa$
- As regards the bulk modulus of the matrix, it is taken as  $K_m = 3500 MPa$
- Poisson's ratio for most materials has a range that goes from 0 to 0.5. Usually, soft materials such as rubber where the bulk modulus is much higher than the shear modulus have a value close to 0.5. Many typical solids have Poisson's ratios in the range of 0.2 – 0.4. For the matrix, the value of Poisson's ratio has been measured using a video extensometer by the research group of Andrea Lazzeri<sup>20</sup> and has been found equal to 0.37
- The rubber content must be chosen according to the sample considered

As shown in the work of Morbitzer et al.<sup>15</sup> and Bucknall et al.<sup>21</sup> the presence of these thermally or mechanically induced volume strains has a great influence on the secondary loss peak of the polybutadiene. One effect of these volume strains on the rubber particles is the increase of their free volume and shift of the loss modulus peak to lower temperatures. This shifting is strictly related to the volume strain acting on the rubber particles which is inversely proportional to the rubber concentration. Specifically, in the work of Morbitzer et al., it is shown how changing the amount of rubber and grafting gives rise to significant changes in temperature shifting. In order to relate the temperature shifting to the volume strain or, more specifically, to the hydrostatic

pressure generated into the rubber particles, a relation between  $T_g$  and pressure must be considered.

Caillaux et al. in 2003<sup>22</sup> proposed a study to determine the glass transition temperature of polybutadiene under the application of very high pressure, keeping attention on the relative effects of temperature and density on the  $T_g$ , which depend on the pressure and temperature conditions. The local structure and slow dynamics have been studied by using neutron scattering and calorimetry. Coupling the results obtained for a polybutadiene rubber with 0% of 1,2 vinyl with the value obtained in previous work of Huang et al.<sup>23</sup> for a polybutadiene rubber with 55% of 1,2 vinyl, it is possible to retrieve, supposing a linear variation, the value of  $\frac{dT_g}{dP}$  ( $\frac{^\circ\text{C}}{100\text{bar}}$ ) for the rubber present in Sample B and C with 10 % of 1,2 vinyl. Assuming valid that this variation of  $T_g$  with respect to the pressure also at negative values of pressure applied, as in the case of hydrostatic tension, and considering adequate a linear behaviour, the following relation can be taken into account.

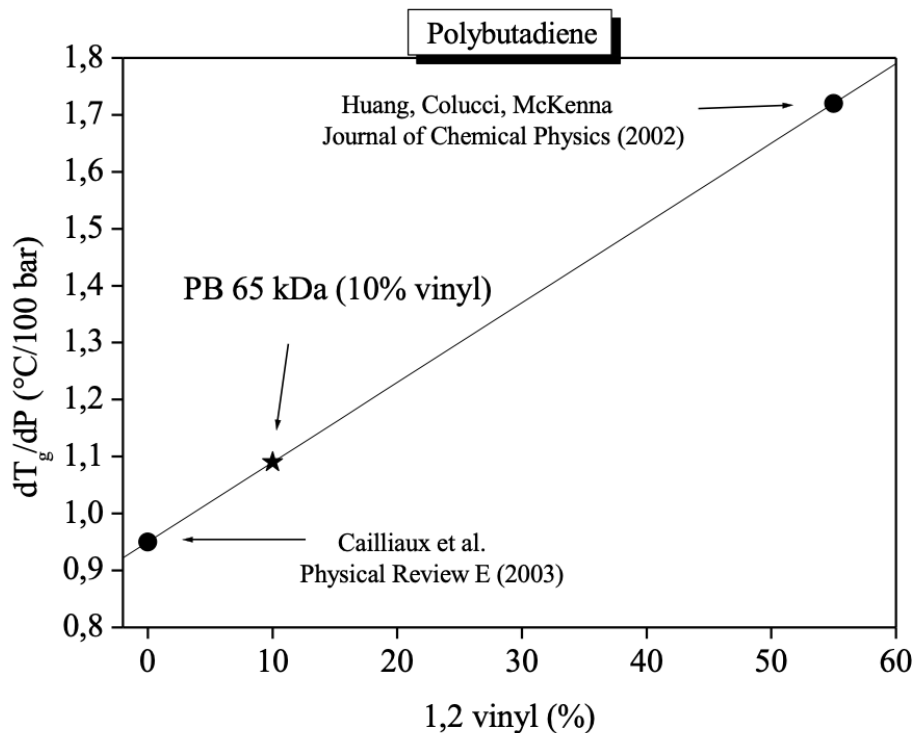


Figure 6. 16 Variation of  $T_g$  with respect to pressure, shown as function of 1,2 vinyl

The value indicated with a star corresponds to  $\frac{dT_g}{dP} = 1.09 \frac{^\circ\text{C}}{100\text{bar}}$  (6. 7) for a polybutadiene rubber with 65 KDa of molecular weight and 10% of 1,2 vinyl as in the case of Sample

B and C. In order to better analyse the effect of the hydrostatic tension on the position of  $T_g$  detailed calculations and results will be presented in the next paragraph.

*Sample B and C: Quantitative analysis of the position of  $T_g$*

The quantitative analysis of the position of  $T_g$  can be done only by knowing the actual position of the glass transition temperature of the polybutadiene rubber. This does not represent a problem in the case of Sample B and C because the rubber was available for testing.

$T_{g,r}$ (from $G''$ ) ( $^{\circ}C$ )	-92
$G_r$ (Pa)	8.50E+05

Figure 6. 17  $T_g$  and shear modulus of anionic rubber 75 KDa

The polybutadiene rubber used for the production of Sample B and C is an anionic rubber with 65 – 75 KDa of molecular weight. The rubber was tested in the *RSA-G2 Solid Analyzer* by using a shear sandwich geometry in which the deformation applied is parallel to the sample thickness and the resultant deformation is simple shear.

From this analysis the shear modulus of the rubber and glass transition temperature can be retrieved and are reported in *Figure 6.17*.

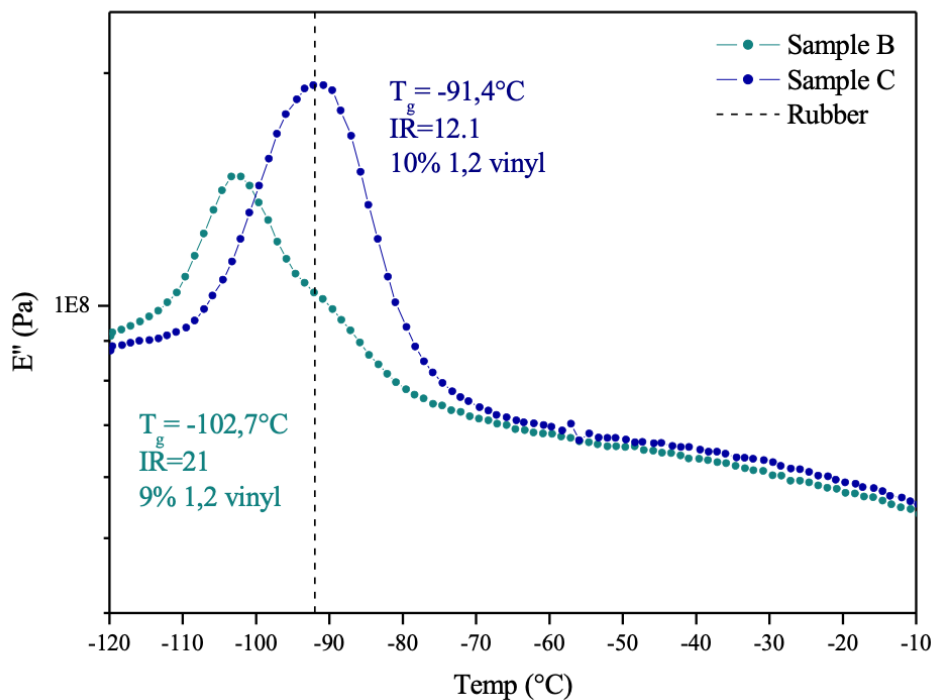


Figure 6. 18 Loss modulus of Sample B and C compared with the value of glass transition temperature of the rubber reported by the dashed line

Knowing the glass transition temperature of the rubber, it is possible to compare it with the loss peaks of Sample B and C. In *Figure 6.18* it is evident that Sample C represented in blue has a loss peak positioned approximately at the same temperature of the rubber  $T_g$ , while Sample B shown in dark cyan has a splitted peak. The peak shifted to the left indicates the intact particles with a glass transition temperature of  $-102.7\text{ }^\circ\text{C}$  on the other hand, the shoulder on the right, referring to the cavitated particles, has a position comparable to the unconstrained rubber. In terms of hydrostatic force, it is evident that Sample C, which actually presents salami particles with small spherical particles has an overall hydrostatic tension acting on the full spherical particles that can be considered negligible with respect to the hydrostatic tension acting on Sample B, that shows a difference in  $T_g$  with respect to the rubber of  $10.7\text{ }^\circ\text{C}$ . The analysis of the position of  $T_g$  will be consequently done just on Sample B. In order to perform a quantitative analysis, a comparison between the experimental difference in temperature and the one predicted by the variation of  $T_g$  with respect to the pressure applied, must be done. The comparison is done using the glass transition temperature retrieved by the loss peak because it is known that the  $T_g$  taken from  $G''$  is the most similar value to the  $T_g$  measured by DSC.

Sample B		
$\beta_m$	1.80E-04	1/K
$\beta_r$	7.60E-04	1/K
$K_r$	2000	MPa
$K_m$	3500	MPa
$c$	12.1	%
$\nu_m$	0.37	
$T_g$ rubber	-92	$^\circ\text{C}$
$T_g$ matrix	103	$^\circ\text{C}$
$\Delta V_r$	-4.05	%
$\sigma_m$	-799.8	bar
$\Delta T_g(\text{exp})$	10.7	$^\circ\text{C}$
$\Delta T_g(\text{calc})$	8.7	$^\circ\text{C}$

*Figure 6.19* Table of properties for Sample B with calculation of volume strain and  $\Delta T_g$

The predicted difference in glass transition temperature is calculated using the following approach:

- I. The volume strain is calculated using *Equation (6.6)*

- II. The calculated volume strain is transformed into a negative hydrostatic pressure using the bulk modulus of the rubber
- III. Once the hydrostatic pressure is known, the relation expressed in *Equation (6.7)* is used to predict the difference in glass transition temperature
- IV. The predicted difference will be compared with the experimental value for  $\Delta T_g$

Material properties, shown in *Figure 6.19*, are taken from the extensive literature provided during the years by Bucknall. For Sample B the rubber concentration was known and equal to 12.1%, while the glass transition temperature of its rubber was measured as shown before. By taking into account the variation of glass transition temperature with respect to the negative hydrostatic pressure  $\sigma_m$ , the values for the experimental and calculated difference are retrieved. It is possible to see that the experimental value is 10.7°C and the predicted one is 8.7 °C. The two values differ by two Celsius degrees corresponding to 18% of deviation. It can be concluded that the analysis shows a good agreement between experimental data and calculated ones, even if some deviation is present.

#### *Sample A: Quantitative analysis of the position of $T_g$*

Using the same approach proposed in Sample B analysis, also for Sample A the comparison between experimental and predicted data can be proposed. However, in this case, there was no possibility of testing the rubber alone or knowing its glass transition temperature, so another approach must be followed.

Sample A as already shown in *Figure 6.6* shows splitted loss and damping peaks due to a partial cavitation phenomenon. Moreover, the exact value of the glass transition temperatures of both peaks have been fitted using Gaussian curves. As already explained, the splitting of the peak gives information about the intact and well-bonded particles, on the left, and the cavitated particles, on the right. The cavitated ones represent those rubber particles that were subjected to the negative hydrostatic tension, as the intact ones, but were able to release this tension, shifting their  $T_g$  closer to that of the unconstrained rubber. Consequently, the temperature value closer to the  $T_g$  of the

rubber in unconstrained conditions was the glass transition temperature of the cavitated particles, that will be used in the analysis.

Even in this case, the same material's properties suggested for Sample B are used. Of course, the rubber concentration is different for Sample A and equal to 14.9% , while the 1,2 *vinyl* percentage is equal to 11%, so  $\frac{dT_g}{dP} \left( \frac{^{\circ}\text{C}}{100\text{bar}} \right)$  can be taken equal to Sample B. The volume strain and consequently the negative hydrostatic pressure are lower than Sample B. Indeed, lower is the experimental difference registered between cavitated and intact rubber particles. In this case, it is evident that experimental and predicted values of  $T_g$  are essentially equal, so extreme agreement is present.

Sample A		
$\beta_m$	1.80E-04	1/K
$\beta_r$	7.60E-04	1/K
$K_r$	2000	MPa
$K_m$	3500	MPa
$c$	14.9	%
$\nu_m$	0.37	
$T_g$ rubber	-79.9	$^{\circ}\text{C}$
$T_g$ matrix	103	$^{\circ}\text{C}$
$\Delta V_r$	-3.7	%
$\sigma_m$	-729.8	bar
$\Delta T_g(\text{exp})$	8	$^{\circ}\text{C}$
$\Delta T_g(\text{calc})$	8	$^{\circ}\text{C}$

Figure 6. 20 Table of properties for Sample A along with volume strain and experimental and calculated difference in glass transition

It is true that the 18% of difference between experimental and predicted  $\Delta T_g$  in the case of Sample B is not enormous, but it must be said that the bulk modulus of the rubber suggested by Bucknall as 2000 MPa is adequate for a rubber used in the emulsion production as in the case of Sample A because it requires a higher degree of crosslinking. While for Sample B, the value of  $K_r$  seems a bit too low, due to the different production technique and the value of the swelling index retrieved. Indeed, choosing the right and adequate value of bulk modulus for the rubber has always represented a challenge. In the next paragraph, a possible method to choose the correct value for the rubber bulk modulus is presented.

### The problematic nature of the rubber bulk modulus

The difference between the experimental data and the predicted values of  $\Delta T_g$  in the case of Sample B are strictly related to the importance of choosing a realistic value for the rubber bulk modulus. Rubbers are characterized by low shear moduli and high bulk moduli, the usual procedure to calculate the bulk modulus requires the value of the Young's modulus  $E_r$  but also another parameter that is the Poisson's ratio  $\nu_r$ .

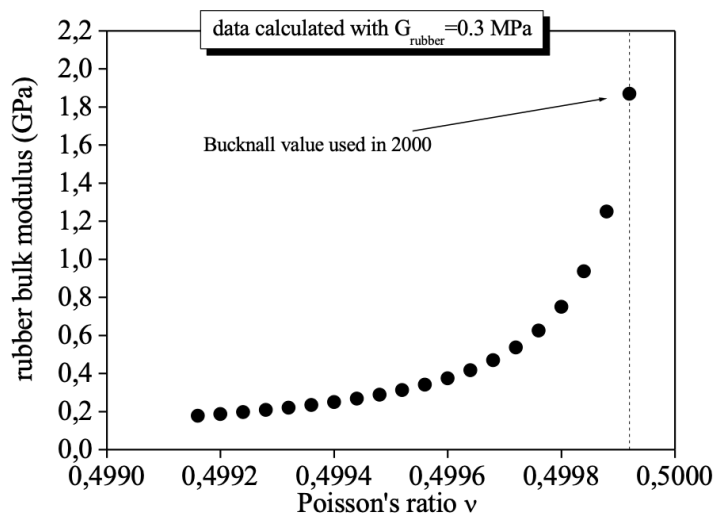


Figure 6.21 Bulk modulus of a rubber with 0.3 MPa of shear modulus as function of the Poisson's ratio

This calculation can give widely erroneous results when dealing with rubbers, unless  $\nu_r$  is chosen with care. This problematic nature can be explained by showing the bulk modulus as a function of the Poisson's ratio. Indeed  $K_r$  shows an asymptote that tends to infinite when the Poisson's ratio tends to 0.5. So, it is extremely important to choose a good value of Poisson's ratio in order to obtain realistic results for the bulk modulus of the rubber. As explained before, the rubber present in Sample B was tested and the value of shear modulus has been measured. Consequently, calculation of the rubber bulk modulus can be provided using the following equation:

$$K_r = \frac{2G_r(1 - \nu_r)}{3(1 - 2\nu_r)}$$

(6.8)

in which  $G_r$  is equal to 0.85 MPa as measured and reported in *Figure 6.17*, the Poisson's ratio will be chosen according to the deviation of the experimental and the predicted  $\Delta T_g$ . The approach followed is presented below:

- I. Compare  $\Delta T_{g,exp}$  and  $\Delta T_{g,calc}$
- II. Minimize the difference between  $\Delta T_g$  by changing the bulk modulus of the rubber
- III. The final value of the rubber will be used to calculate an appropriate value for the Poisson's ratio

Sample B		
$\beta_m$	1.80E-04	1/K
$\beta_r$	7.60E-04	1/K
$K_r$	4200	MPa
$K_m$	3500	MPa
$c$	12.1	%
$\nu_m$	0.37	
$T_g$ rubber	-92	°C
$T_g$ matrix	103	°C
$\Delta V_r$	-2.38	%
$\sigma_m$	-984.5	bar
$\Delta T_g(\text{exp})$	10.7	°C
$\Delta T_g(\text{calc})$	10.7	°C

*Figure 6. 22 Table of properties for Sample B,  $K_r$  changed according to the difference in glass transition temperature*

Using this procedure, the rubber bulk modulus changes from 2000 MPa with Poisson's ratio of 0.4999 to 4200 MPa with calculated Poisson's ratio of 0.499899.

## 6.5 Dilatometric curves

Dilatometric analysis was suggested in 2000 by Bucknall et Al.<sup>9</sup> as a method to initiate rubber particle cavitation under conditions that do not simultaneously produce shear yielding in the matrix. Thermal expansion-contraction measurements allow to detect and quantify the extent of rubber particles cavitation while it is taking place. Two important limits to keep in mind during this analysis of thermally induced cavitation in ABS are the glass transition temperature of the matrix and the rubber. Indeed above  $T_{g,m}$  there aren't thermal contraction stresses at the particle-matrix boundary and in the region of

$T_{g,r}$  the shear modulus of the rubber phase strongly increases causing an increase in rigidity that brings the cavitation phenomenon to a stop.

The materials tested are Sample A, B and C, but in order to have information about the thermal contraction of the matrix alone, also a rectangular bar of SAN has been tested, for simplicity, this will be called just Sample S. Thermal contraction and expansion experiments were carried out on these samples at a cooling rate of  $2^{\circ}\text{C}/\text{min}$  in a nitrogen atmosphere, using *RSA-G2 Solid Analyzer*. The specimens were tested in a tensile geometry, and during each test 10 g of tensile load was applied. As output the length variation of the specimens is monitored with respect to the temperature.

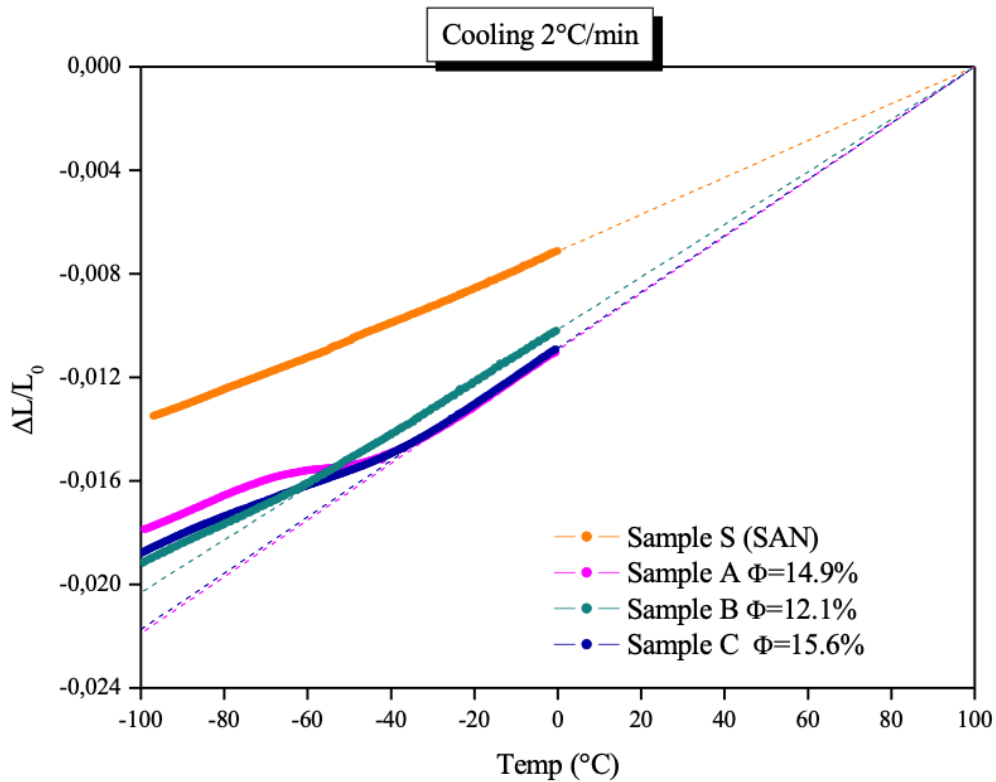


Figure 6. 23 Dilatometric curves obtained at  $2^{\circ}\text{C}/\text{min}$

The experimental curves, reported in *Figure 6.23*, have been elaborated in order to extrapolate their values at the  $T_g$  of the matrix, by using linear fitting. The data are normalised with respect to the extrapolated reference length of the sample at  $100^{\circ}\text{C}$ , which corresponds to the  $T_g$  of the matrix. For Sample A, B and C, the linear fit has been calculated taking into account the linear zone pre-cavitation. Considering Sample S, which is just the matrix alone, it is evident that the contraction is linear while all the other samples show a non-linear S-shaped section. In particular, Sample A and C present

a linear thermal contraction curve between 0 and  $-40^{\circ}\text{C}$ , then they pass through a non-linear S-shaped section between  $-40^{\circ}\text{C}$  and  $-70^{\circ}\text{C}$ , resuming at the end a linear course with reduced slope after  $-70^{\circ}\text{C}$ . On the other hand, Sample B shows a linear trend till  $-60^{\circ}\text{C}$  and a not so evident S-shaped section. Four dashed straight lines are represented, the orange one is related to Sample S and represents just an extrapolation of its behaviour at high temperature, while for Sample A, B and C these lines represent the ideal contraction of the ABS specimen when cavitation does not occur.

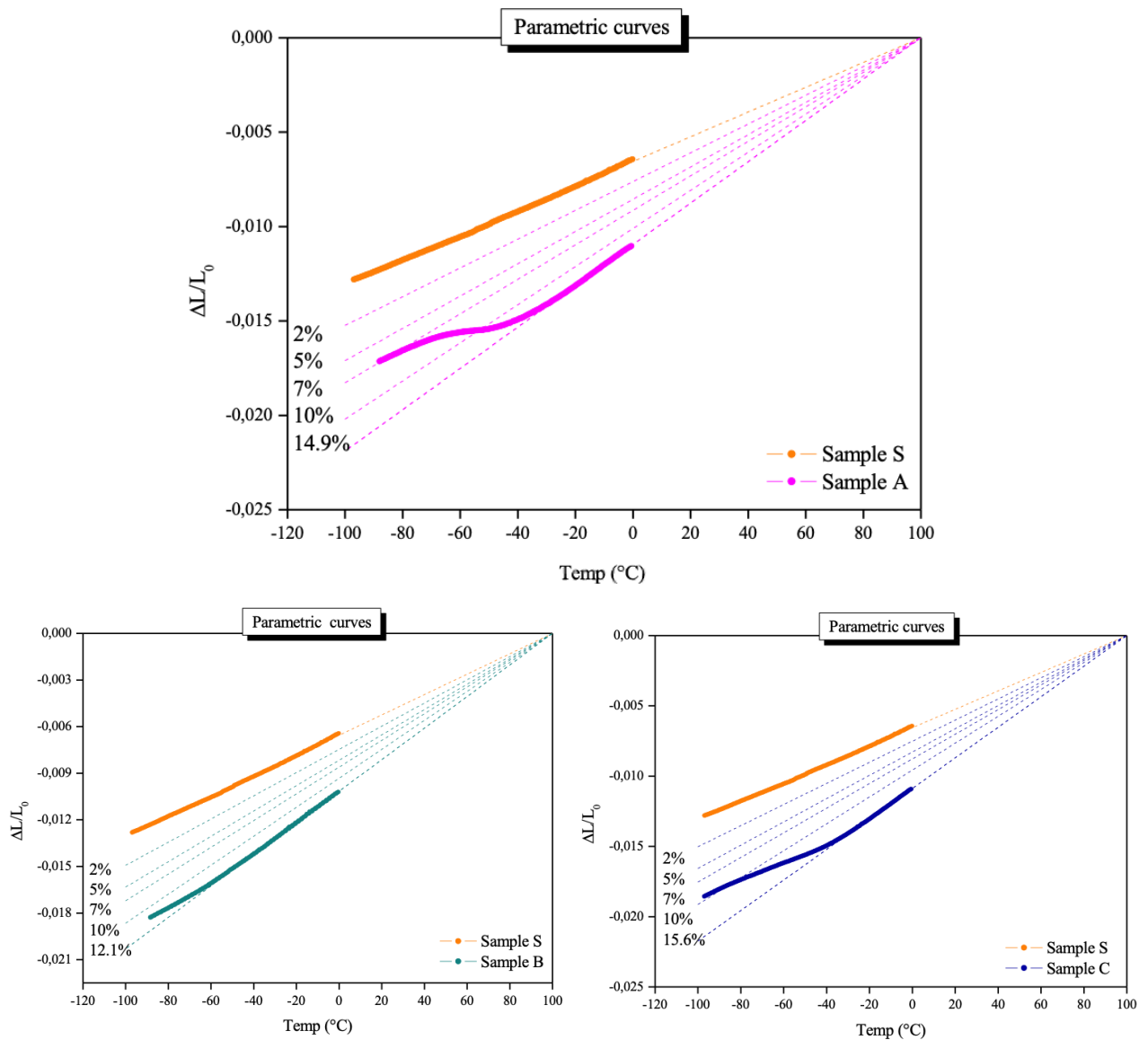


Figure 6. 24 Parametric curves shown separately for each sample

Indeed, the cavitation phenomenon is observable through the dilatometric technique because the release of the hydrostatic stresses to which the rubber particles are subjected is represented experimentally by the S-shaped deviation from the dashed straight line

and corresponds to an expansion of the ABS with respect to the baseline. Another indication of the cavitation phenomenon studied is the reduction in the thermal expansion coefficient. Furthermore, it must be mentioned the irreversibility of the phenomenon because the expansion curve of a specimen reheated to ambient temperature does not show an S-shaped curve, but rather an approximate linear trend, an indication that cavitation below  $T_{g,m}$  is irreversible and just partly recoverable.

As already explained in *Chapter 4*, the position of the elaborated experimental curves depends on the rubber content, in particular, parametric curves can be constructed in order to have a qualitative idea about the amount of cavitated particles. The theory behind is related to the fact that cavitated ABS will show after an S-shaped deviation a linear trend with a reduced thermal expansion coefficient. This linear trend after cavitation can be associated with an ABS with a lower rubber content. Indeed, points lying on the lower construction line indicate that no cavitation has taken place, while points lying on the upper line for SAN (Sample S) correspond to 100% of cavitation, involving the full relaxation of the internal stresses. Parametric curves together with experimental cooling curves are reported, for each ABS, in *Figure 6.24*.

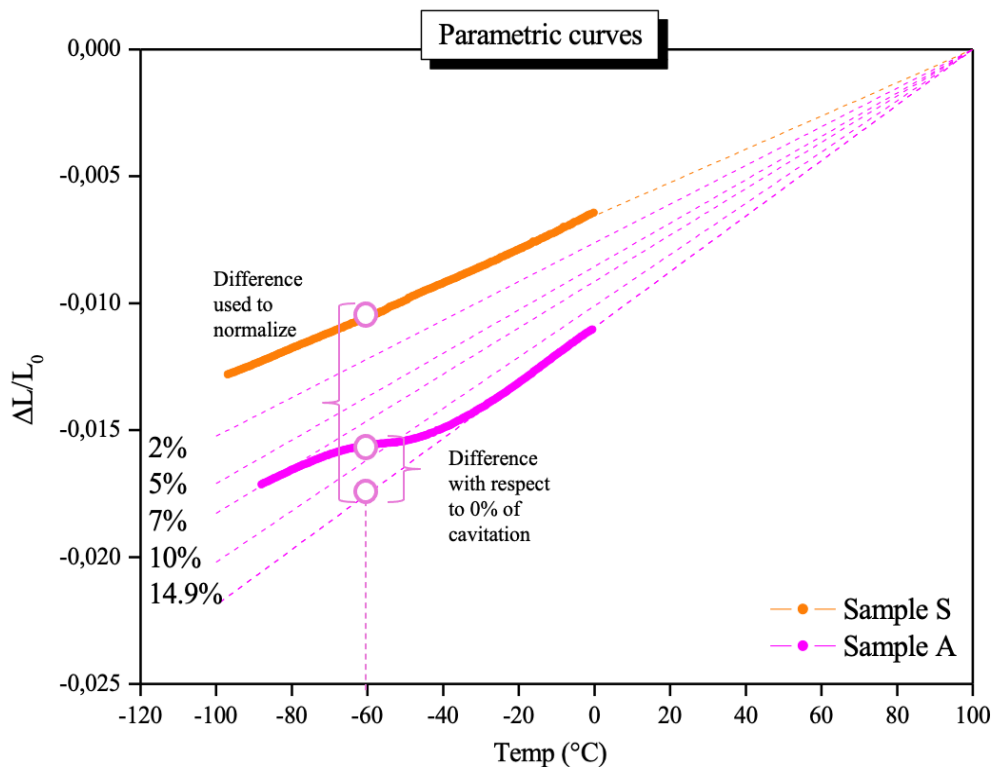


Figure 6. 25 Schematic representation of the approach used to calculate the percentage of cavitation.

A percentage of cavitated particles can be retrieved by subtracting the ideal contraction of the non-cavitated specimen from the experimental data, then at each temperature, this difference will be normalized with respect to the difference between the ideal contraction curve of the ABS and the contraction line of Sample S that represents an ABS with 100% of cavitated particles. This procedure is schematically represented in *Figure 6.25* for Sample A and at one temperature, the same approach will be used also for Sample B and C and must be done at each temperature. Mathematically, this approach can be expressed in the following way.

$$\% \text{ of cavitated particles} = \frac{\left(\frac{\Delta L}{L_0}(T)\right)_{exp,A} - \left(\frac{\Delta L}{L_0}(T)\right)_{nocav,A}}{\left(\frac{\Delta L}{L_0}(T)\right)_{exp,S} - \left(\frac{\Delta L}{L_0}(T)\right)_{nocav,A}}$$

(6.9)

In which  $T$  represents the temperature, the suffix  $exp,A$  and  $exp,S$  correspond respectively to the experimental data of Sample A and S. The suffix  $nocav,A$  refers to the ideal contraction value of Sample A in absence of cavitation.

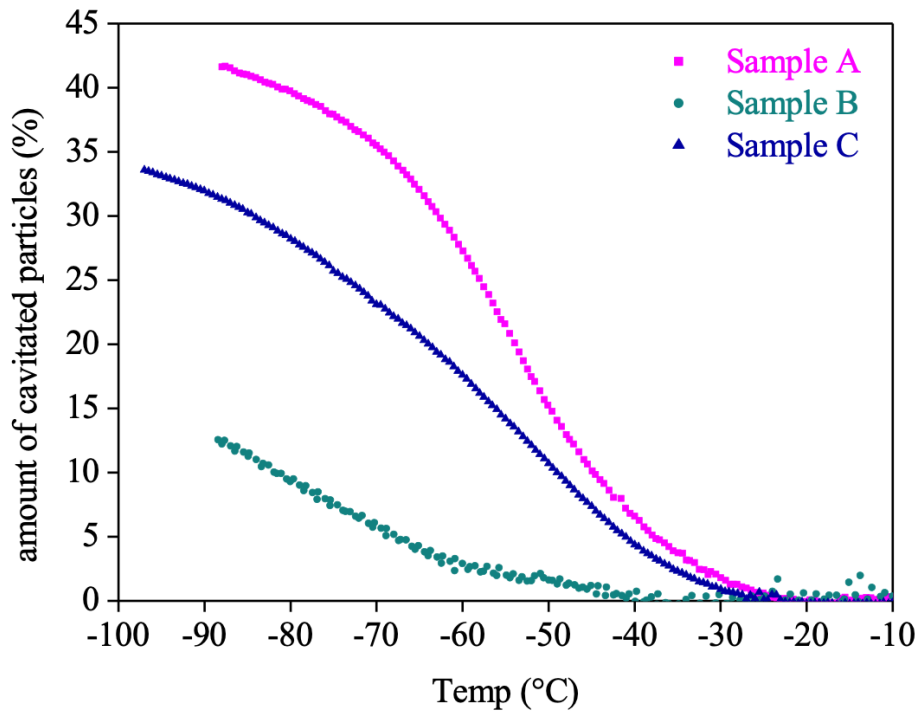


Figure 6. 26 Amount of cavitated particles versus Temperature for Sample A, B and C

The percentage of cavitation with respect to temperature is represented in *Figure 6.26* from which some important information can be retrieved. In particular, it is more evident the temperature at which the cavitation starts, and it is clearer which sample has a higher extent of cavitation. Indeed, Sample A and C show a similar behaviour with a cavitation phenomenon that starts at around  $-30^{\circ}\text{C}$ . Moreover, the amount of cavitated particles is comparable. Sample A starts with an initial value of rubber content of 14.9% and it reaches almost 42% of cavitated particles. On the other hand, Sample C which presents initially 15.6% of rubber content, is able to reach almost 35% of cavitated particles. Sample B, instead, reveals that its particles start to cavitate at a lower temperature with respect to the other two samples, at around  $-40^{\circ}\text{C}$ . Moreover, it is able to cavitate just 12% of particles.

## **6.6 Isothermal cavitation**

As anticipated in the previous chapters, the energy of the rubber particles is given by the sum of three different contributions: the residual volumetric strain energy, the surface energy of the void and the local rubber membrane stretching around the void. Considering the rubber particle dimension fixed, as the cavity radius increases the volumetric strain energy is gradually released till the rubber particle reaches its equilibrium unstressed density and the energy falls to zero. After this point, further growth of the void generates compressive stresses that will provide a rapid increase in the volumetric strain energy. Due to the presence of the surface and rubber stretching term the minimum of the overall energy will occur earlier than the minimum in volumetric strain energy. In 1998 Bucknall and Ayre<sup>24</sup> showed that rubber particles are much more resistant to cavitation than what is predicted by the thermodynamic criterion. Indeed, in their work, experimental results have shown that this criterion in which the overall energy at the minimum has to be lower than the initial value of energy is a necessary but not sufficient condition for void formation in rubber particles. In order to explain this higher resistance to cavitation a further analysis of the energy of the particle-matrix system is required. At small voids dimensions, the energy balance predicts an energy maximum due to the disproportionate effect of the surface energy term on the energy necessary to form the void. This energy barrier introduces a further condition to

the cavitation phenomenon and suggests a “kinetic” criterion. Similar activation energies are present in other processes in which, however, the energy barrier is fixed, and rates increase with increasing temperature. On the other hand, the height of the energy barrier of the cavitation phenomenon depends on the temperature and also on the surface energy. In particular, the energy barrier decreases by decreasing the temperature in contrast with almost all the other physical and chemical processes where an increase in temperature produces an increase of the thermal energy available to surmount the barrier. The kinetic aspect and consequently the presence of an activation barrier are essential to properly describe the cavitation phenomenon. Some preliminary results conducted in RMS-800 on Sample A provide insight about cavitation kinetics. Sample A has been tested by using the torsional geometry and has been subjected to a defined thermal cycle. Cooling and heating were performed at  $2^{\circ}\text{C}/\text{min}$  applying a strain of 0.1%.

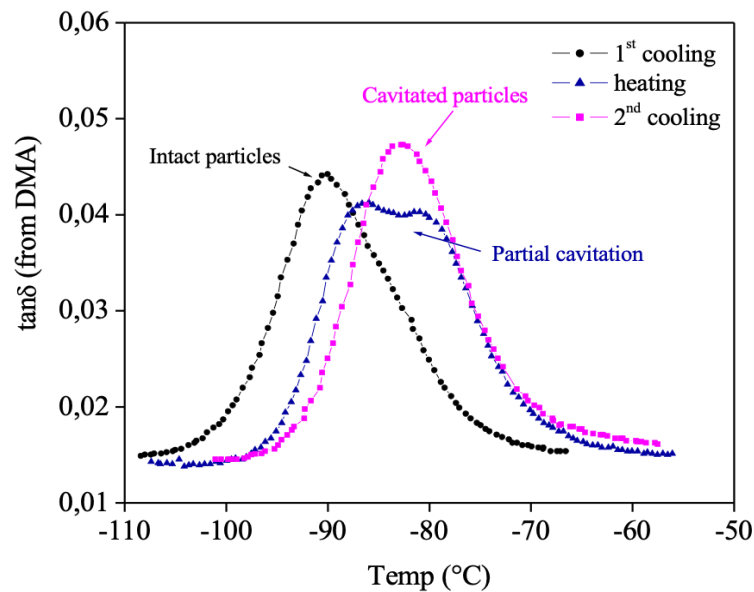


Figure 6. 27 Evidence of cavitation kinetics in Sample A

From the plot reported, in *Figure 6.27*, it is evident that during the first cooling, Sample A shows a damping peak shifted at lower temperatures, due to the hydrostatic tension acting on the intact and bonded particles, then heating is performed in which the cavitation phenomenon seems activated and gives rise to partial cavitation of rubber particles with splitting of the damping peak. In the last step, further cooling produces a single peak shifted at higher temperatures suggesting an almost complete rubber particle

cavitation. These results surely suggest the presence of a cavitation kinetics that has been further analysed by performing some isothermal experiments.

When a specimen is subjected to a cooling experiment, it reaches very low temperatures at which the volume strains are quite high but by monitoring the length variation as a function of temperature it is possible to notice that after the S-shaped deviation, a linear behaviour is recovered suggesting the end of the cavitation phenomenon. However, not all the rubber particles have been able to cavitate, despite the favourable conditions in terms of thermodynamic and activation energy barrier. Consequently, the question was: how can the cavitation time-dependency be inspected?

To answer this question isothermal curves have been carried out on Sample A in RSA-G2 with tensile geometry and the same conditions as the dilatometric curves. The difference is related to the presence of a further step, Sample A is cooled at  $2^{\circ}\text{C}/\text{min}$  till the desired temperature and then the length is monitored as a function of time till a constant value is reached. The length variation registered as function of time can be transformed with the same approach, explained in the previous paragraph, into a percentage of cavitation, as indicated in *Figure 6.25*.

The amount of cavitated particles reached keeping the temperature constant will also consider the extent of particles already cavitated before the isothermal step.

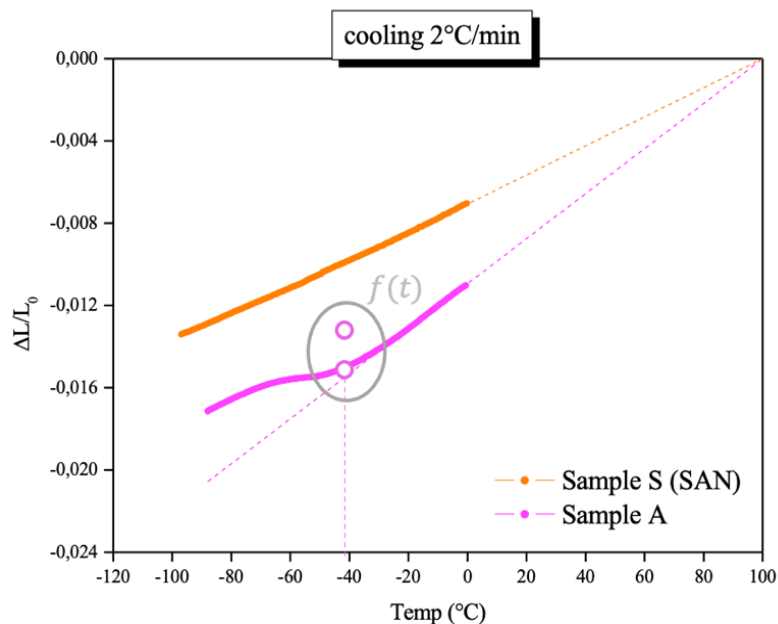


*Figure 6. 28 Scheme representing how the cavitation will be monitored*

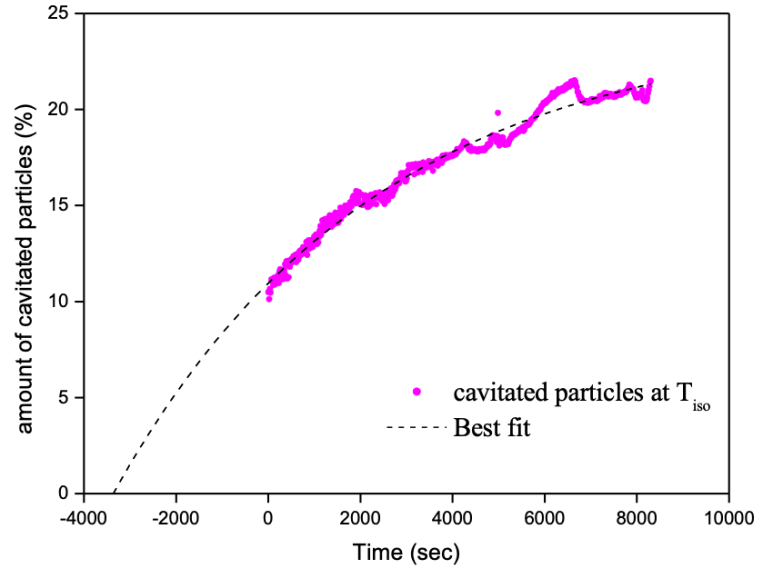


Figure 6. 29 Best fit of the amount of cavitated particles versus time at  $T_{iso} = -42.5^\circ\text{C}$

These experimental data were well fitted with a single exponential mathematical function:

$$\%cavitated\ particles(t) = (\%cav)_0 + ((\%cav)_\infty - (\%cav)_0) \left( 1 - \exp\left(-\frac{t - t_0}{\tau}\right) \right)$$

(6. 10)

In which  $\%cav_0$  is the percentage of cavitated particles at  $t_0$ ,  $\%cav_\infty$  is the percentage when time tends to infinite and  $\tau$  represents the time scale of the recovery process (approximately the time required to reach a plateau of the percentage of cavitation).

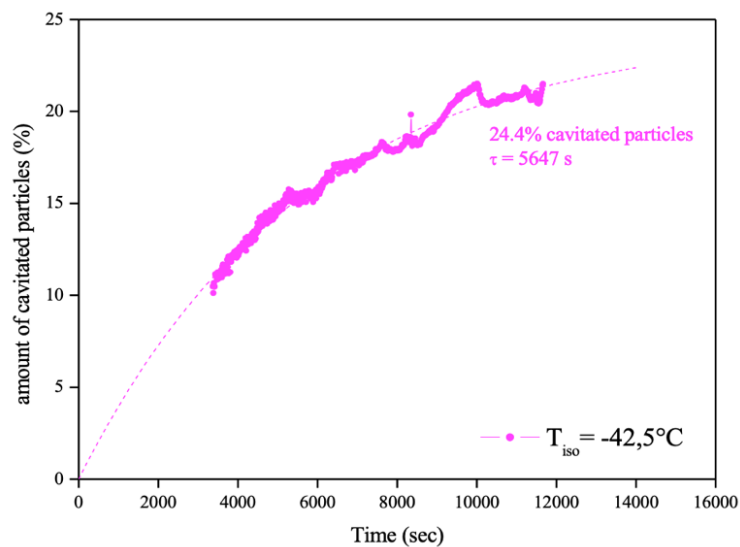


Figure 6. 30 Percentage of cavitation shifted of  $t_0$

In order to have a percentage of cavitation that is null at  $t_0$  equal to zero, the experimental times are shifted by summing the value of  $t_0$ , as reported, as a typical example, in *Figure 6.30*. In this way the final elaborated curve will be described by the following function:

$$\%cavitated\ particles(t) = (\%cav)_0 + ((\%cav)_\infty - (\%cav)_0) \left(1 - \exp\left(-\frac{t}{\tau}\right)\right) \quad (6.11)$$

All the elaborated isothermal curves obtained for Sample A are reported in the figure below.

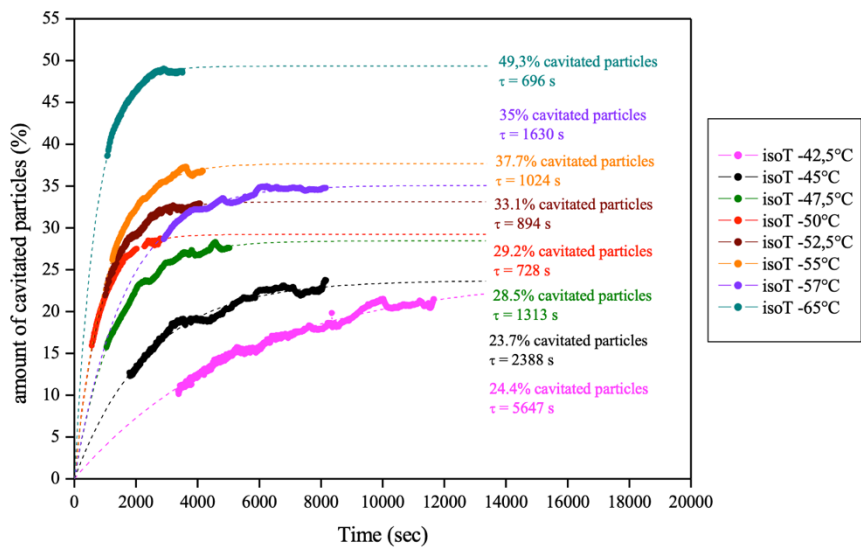


Figure 6.31 Isothermal curves fitted. Percentage of cavitation and time to reach a plateau shown.

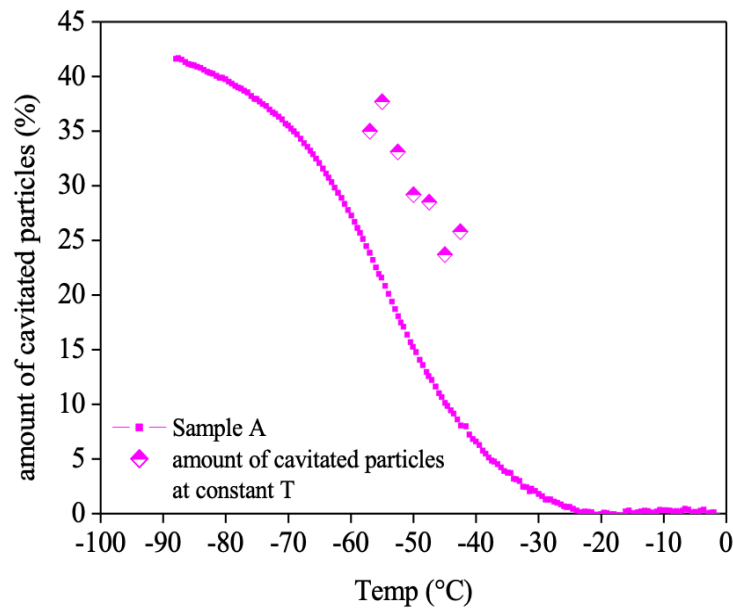


Figure 6.32 Amount of cavitated particles during cooling and isothermal curve for Sample A

When a material is subjected to a cooling experiment it gives rise to a contraction. In the case of rubber particle cavitation at a certain point the contraction stops and an expansion due to the formation of voids inside the rubber occurs. By keeping the temperature constant and consequently the volume strain, ideally the expansion should stop, however this does not occur experimentally and an increase in the percentage of cavitation with respect to time is registered. This interesting phenomenon is not an immediate process but requires time to complete all the possible cavitation at a specified temperature.

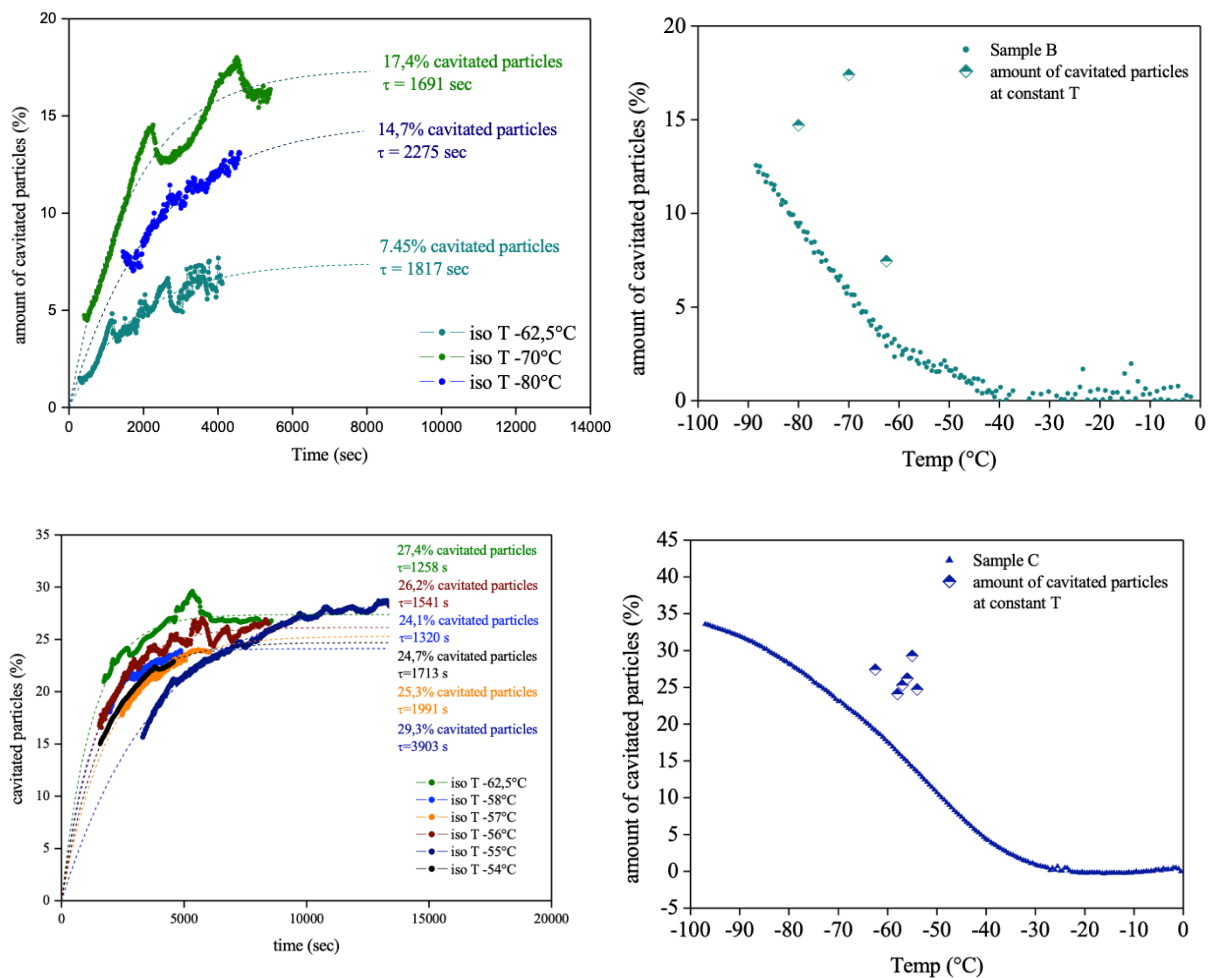


Figure 6.33 Isothermal curves and percentage of cavitation during cooling and isothermal curves for Sample B and C

Plotting the amount of cavitated particles from 0 to  $-100^{\circ}\text{C}$  at  $2^{\circ}\text{C}/\text{min}$  and the percentage of cavitation at the plateau in Figure 6.32, it is evident that the amount of cavitation at constant temperature is sharply higher than the percentage of cavitation obtained during the cooling. For instance, at  $-45^{\circ}\text{C}$  the percentage of cavitation passes from almost 8% during cooling to 24% reached by keeping the temperature constant.

The same considerations can be done also for Sample B and C. However, for Sample B only few experimental data are available due to the high request of nitrogen and time required to carry out the analysis.

From all the figures reported it is quite evident that the cavitation phenomenon is not the same for all the specimens, especially in terms of percentage of cavitation and time required to reach a plateau. To conclude the great advantage of this experimental technique is not just the measure of a cavitation percentage, but also the monitoring of the activation step in this rate-controlling process of cavitation. All the experimental times and percentages of cavitated particles obtained from the isothermal tests and data elaborations are included in the following table.

Sample A			Sample B			Sample C		
Temp (°C)	cavitated particles %	$\tau$ (sec)	Temp (°C)	cavitated particles %	$\tau$ (sec)	Temp (°C)	cavitated particles %	$\tau$ (sec)
-65	49.3	696	-80	14.7	2275	-62.5	27.4	1258
-57	35	1630	-70	17.4	1691	-58	24.1	1320
-55	37.7	1024	-62.5	7.45	1817	-57	25.3	1991
-52.5	33.1	894				-56	26.2	1541
-50	29.2	728				-55	29.3	3903
-47.5	28.5	1313				-54	24.7	1713
-45	23.7	2388						
-42.5	24.4	5647						

Figure 6. 34 Time, percentage of cavitation and temperature of the isothermal curves for Sample A, B and C

It must be noticed that at lower temperature a great scattering is present in the experimental data as well as a low excursion of values of percentage of cavitation. Consequently, further analysis and proof are required in order to inspect the goodness of the results obtained.

## 6.7 Double isothermal curves

Further proof of the kinetic aspects of the cavitation phenomenon is provided in this paragraph. Indeed, further isothermal curves are provided, but with some differences in the experimental conditions. Rectangular bars are tested by cooling the specimens at 2 °C/min till the desired temperature at which the length is monitored against time. Once this isothermal curve reaches the cavitation plateau, the specimen is subjected again to the cooling step till the desired temperature for the second isothermal curve.

The important aspect to notice in these peculiar experiments, one of which is reported as a typical example for Sample A in *Figure 6.35*, is the fact that the cavitation phenomenon strongly depends on temperature and consequently on volume strain, but it also exhibits a quite important time-controlled aspect.

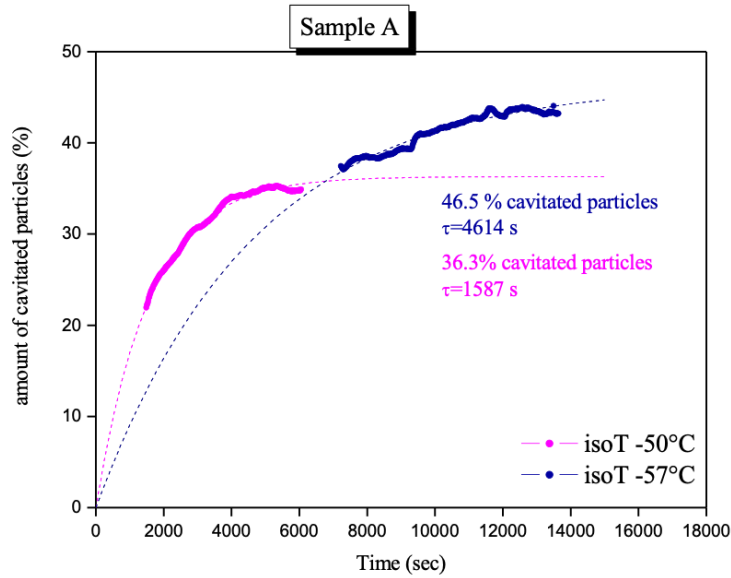


*Figure 6. 35 Double isothermal curve conducted on Sample A, first at -50 and then at -57 °C*

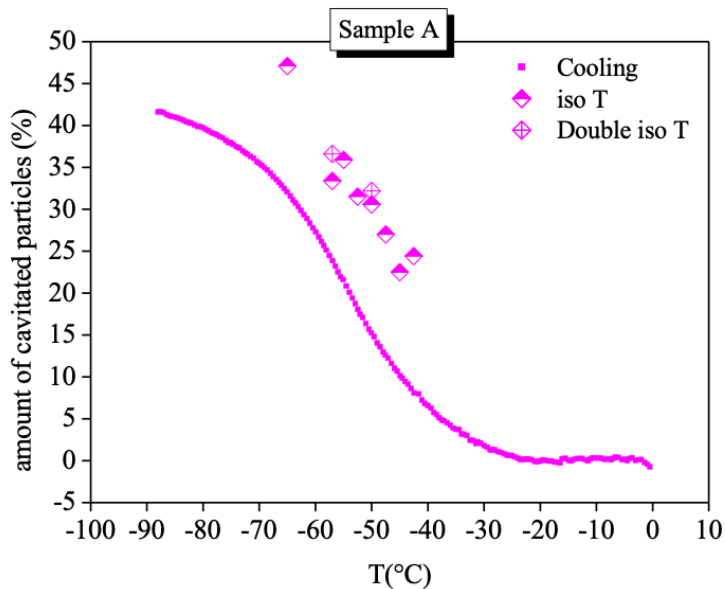


*Figure 6. 36 Percentage of cavitated particles for Sample A for all the isothermal curves*

Indeed, as it is evident from the plot reported, during the first isothermal curve, the specimen starts to expand till a plateau is reached representing the symptom of an

exhausted driving force. When the specimen is subjected to a further cooling step, even of few degrees, a certain amount of driving force is restored and by fixing the temperature, expansion is monitored again.

The percentage of cavitation obtained with this experimental condition of double isothermal curves shows good agreement with the values obtained in the case of single isothermal curves. The same analysis can be carried out even for Sample B and C, but due to the lack of time, attention was not given to this further aspect of the cavitation phenomenon that will surely become object of future studies.

## Analysis of the kinetic barrier

### 7.1 Critical volume strain

In 2000 Lazzeri and Bucknall<sup>25</sup> proposed a review and introduced some developments for their quantitative model of cavitation according to some experimental data. Rubber particles are able to cavitate, under the application of hydrostatic stresses, when the stored volumetric strain energy density  $W_0$  overcomes a critical value.  $W_0$  is defined by the following expression:

$$W_0 = \frac{K_r \Delta V_r^2}{2} \quad (7.1)$$

in which, as already explained,  $K_r$  is the bulk modulus of the rubber and  $\Delta V_r$  is the volume strain of the particle. After the formation of a void of diameter  $d$  the energy density stored in the rubber particles is given by:

$$W(d) = \frac{K_r}{2} \left( \Delta V_r - \frac{d^3}{D^3} \right)^2 + \frac{6\Gamma}{D} \frac{d^2}{D^2} + \frac{3G_r F(\lambda_f)}{2} \frac{d^3}{D^3} \quad (7.2)$$

the variables used in this expression were mentioned before,  $\Gamma$  is the surface energy of the rubber particles,  $G_r$  is the shear modulus of the rubber,  $D$  is the diameter of rubber particles and  $F(\lambda_f)$  is a function of the elongation at break of the rubber in a biaxial state of stress. At low volume strains  $W(d)$  is a monotonic function that increases with  $d$ , in this way  $W(d)$  is always greater than  $W_0$ . However, at high volume strains the stored energy density is no longer monotonic. Indeed, the energy density increases till a maximum is reached, corresponding to an energy barrier and then decreases towards a minimum. If the volume strain is high enough, the energy density at the minimum is smaller than the initial energy,  $W(d) < W_0$  (7.3).

To denote the critical condition over which the cavitated particle is more energetically stable than an intact particle, the authors proposed to look for the critical condition by imposing simultaneously the first and second derivative of *Equation (7.2)* equal to zero. Setting the second derivative equal to zero, it is possible to identify the inflection point, but if the first derivative becomes simultaneously null, it means that the function is parallel to the abscissa at the inflection point. The first and second derivatives are reported:

$$\frac{\partial}{\partial d} \left( \frac{K_r}{2} \left( \Delta V_r - \frac{d^3}{D^3} \right)^2 + \frac{6\Gamma d^2}{D D^2} + \frac{3G_r F(\lambda_f) d^3}{2 D^3} \right) = \frac{d(-6K_r \Delta V_r D^3 d + 6K_r d^4 + 24\Gamma D^3 + 9G_r F(\lambda_f) D^3 d)}{2D^6} \quad (7.4)$$

$$\frac{\partial^2}{\partial d^2} \left( \frac{K_r}{2} \left( \Delta V_r - \frac{d^3}{D^3} \right)^2 + \frac{6\Gamma d^2}{D D^2} + \frac{3G_r F(\lambda_f) d^3}{2 D^3} \right) = \frac{-6K_r \Delta V_r D^3 d + 15K_r d^4 + 12\Gamma D^3 + 9G_r F(\lambda_f) D^3 d}{D^6} \quad (7.5)$$

The system of the derivatives imposed equal to zero, gives rise to the following solutions.

$$d_1 = -\frac{\sqrt[4]{2^4 \sqrt{6\Gamma} D^{\frac{3}{4}}}}{\sqrt{3^4 \sqrt{K_r}}} \quad (7.6)$$

$$d_2 = \frac{\sqrt[4]{2^4 \sqrt{6\Gamma} D^{\frac{3}{4}}}}{\sqrt{3^4 \sqrt{K_r}}} \quad (7.7)$$

$$d_3 = 0 \quad (7.8)$$

Solutions  $d_1$  and  $d_3$  are not possible because the void diameter assumes negative and zero values, so  $d_2$  remains the possible solution with the following condition.

$$G_r F = \frac{2 \left( 9K_r \Delta V_r D^{\frac{3}{4}} + 4 * 2^{\frac{3}{4}} \sqrt{3^4 \sqrt{K_r}} (6\Gamma)^{\frac{3}{4}} \right)}{27D^{\frac{3}{4}}} \quad (7.9)$$

Rearranging the critical volume deformation is retrieved.

$$\Delta V_r = 4 \left( \frac{4\Gamma}{3D} \right)^{\frac{3}{4}} + \frac{3G_r F}{2K_r}$$

(7.10)

This critical value is shown graphically by the continuous green line, in *Figure 7.1*, and represents the critical volume strain or the value of particle diameter below which the cavitated particle is not stable.

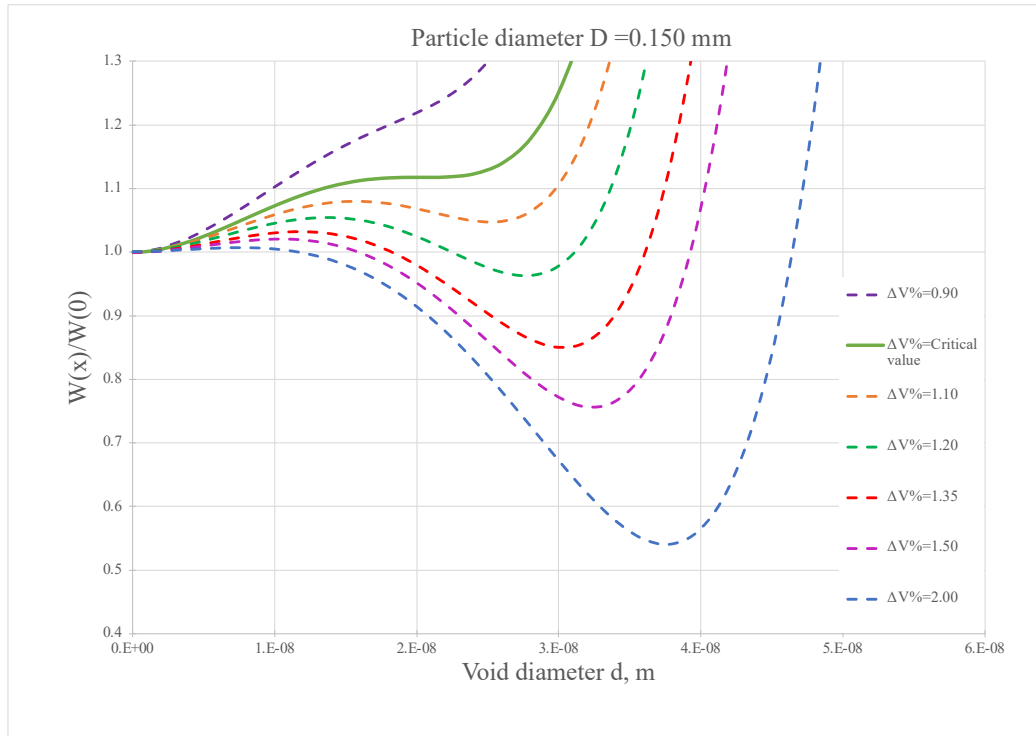


Figure 7.1 Normalized energy density as function of the void diameter. Values calculated using  $\Gamma = 0.03 \frac{J}{m^2}$ ,  $G_r = 0.4 \text{ MPa}$ ,  $K_r = 2000 \text{ MPa}$ ,  $F(\lambda(f)) = 1$ .

However, this approach of imposing both derivatives equal to zero presents a limitation. The formation and growth of voids inside the particles, at some volume strains even higher than the critical one, do not produce an energy decrease below the initial value, condition that represents a necessary requirement for cavitation as expressed in *Equation 7.3*. This fundamental aspect is evident also in *Figure 7.1*, in which both the continuous line denoting the critical volume strain and the dashed line corresponding to a volume strain of 1.10% do not produce a situation in which the energy of the cavitated particle is lower than the initial energy of the particle before cavitation. Indeed, the necessary critical condition for cavitation, as explained by Bucknall et al. in 1994<sup>26</sup>, is strictly dependent on the ability of the rubber particle to reach lower energy by forming a void.

This condition is denoted by imposing the first derivative equal to zero and  $W(d)/W(0) = 1$  (7.11).

## 7.2 Analytical expressions of maximum and minimum

Two interesting results, achieved during this thesis, are the analytical determination of the void's diameters at which the energy density shows a maximum and a minimum. Mathematically the maximum and minimum of a function can be found by imposing the first derivative equal to zero and the second derivative higher or lower than zero.

$$\begin{aligned}
 a \neq 0, \quad x = & \\
 & \frac{1}{2} \sqrt{\left( (16 \sqrt[3]{2} c d^3) / \left( \left( \sqrt{2125764 a^2 (3 e d^3 - 2 a b d^3)^4 - 95551488 a^3 c^3 d^9 +} \right. \right. \right. \\
 & \left. \left. \left. 1458 a (3 e d^3 - 2 a b d^3)^2 \right)^{1/3} \right) + \frac{1}{18 \sqrt[3]{2} a} \right. \\
 & \left. \left( \left( \sqrt{2125764 a^2 (3 e d^3 - 2 a b d^3)^4 - 95551488 a^3 c^3 d^9 +} \right. \right. \right. \\
 & \left. \left. \left. 1458 a (3 e d^3 - 2 a b d^3)^2 \right)^{1/3} \right) \right) - \frac{1}{2} \sqrt{\left( - \left( (16 \sqrt[3]{2} c d^3) / \right. \right. \right. \\
 & \left. \left. \left. \left( \left( \sqrt{2125764 a^2 (3 e d^3 - 2 a b d^3)^4 - 95551488 a^3 c^3 d^9 +} \right. \right. \right. \right. \\
 & \left. \left. \left. \left. 1458 a (3 e d^3 - 2 a b d^3)^2 \right)^{1/3} \right) \right) - \frac{1}{18 \sqrt[3]{2} a} \right. \\
 & \left. \left( \left( \sqrt{2125764 a^2 (3 e d^3 - 2 a b d^3)^4 - 95551488 a^3 c^3 d^9 +} \right. \right. \right. \\
 & \left. \left. \left. 1458 a (3 e d^3 - 2 a b d^3)^2 \right)^{1/3} \right) \right) - \\
 & (3 e d^3 - 2 a b d^3) / \left( a \sqrt{\left( (16 \sqrt[3]{2} c d^3) / \right. \right. \right. \\
 & \left. \left. \left. \left( \left( \sqrt{2125764 a^2 (3 e d^3 - 2 a b d^3)^4 - 95551488 a^3 c^3} \right. \right. \right. \right. \\
 & \left. \left. \left. \left. d^9 + 1458 a (3 e d^3 - 2 a b d^3)^2 \right)^{1/3} \right) \right) + \right. \\
 & \left. \frac{1}{18 \sqrt[3]{2} a} \left( \left( \sqrt{2125764 a^2 (3 e d^3 - 2 a b d^3)^4 -} \right. \right. \right. \\
 & \left. \left. \left. 95551488 a^3 c^3 d^9 + 1458 a \right. \right. \right. \\
 & \left. \left. \left. \left. (3 e d^3 - 2 a b d^3)^2 \right)^{1/3} \right) \right) \right) \right), \quad d \neq 0
 \end{aligned}$$

Figure 7. 2 Value of diameter of the void  $d$  at which the energy becomes maximum, solution of Wolfram Alpha

The computation was carried out by using a website, *Wolfram Alpha*<sup>27</sup> and the resulting expressions for the maximum and the minimum are reported in *Figure 7.2* and *7.3*.

$$\begin{aligned}
 a \neq 0, \quad x = & \\
 & \frac{1}{2} \sqrt{\left( (16 \sqrt[3]{2} c d^3) / \left( \left( \sqrt{2125764 a^2 (3 e d^3 - 2 a b d^3)^4 - 95551488 a^3 c^3 d^9 +} \right. \right. \right. \\
 & \left. \left. \left. 1458 a (3 e d^3 - 2 a b d^3)^2 \right)^{\wedge (1/3)} + \frac{1}{18 \sqrt[3]{2} a} \right. \right. \\
 & \left. \left( \left( \sqrt{2125764 a^2 (3 e d^3 - 2 a b d^3)^4 - 95551488 a^3 c^3 d^9 +} \right. \right. \right. \\
 & \left. \left. \left. 1458 a (3 e d^3 - 2 a b d^3)^2 \right)^{\wedge (1/3)} \right) + \frac{1}{2} \sqrt{\left( - \left( (16 \sqrt[3]{2} c d^3) / \right. \right. \right. \\
 & \left. \left( \left( \sqrt{2125764 a^2 (3 e d^3 - 2 a b d^3)^4 - 95551488 a^3 c^3 d^9 +} \right. \right. \right. \\
 & \left. \left. \left. 1458 a (3 e d^3 - 2 a b d^3)^2 \right)^{\wedge (1/3)} \right) \right) - \frac{1}{18 \sqrt[3]{2} a} \\
 & \left( \left( \sqrt{2125764 a^2 (3 e d^3 - 2 a b d^3)^4 - 95551488 a^3 c^3 d^9 +} \right. \right. \\
 & \left. \left. \left. 1458 a (3 e d^3 - 2 a b d^3)^2 \right)^{\wedge (1/3)} \right) - \\
 & (3 e d^3 - 2 a b d^3) / \left( a \sqrt{\left( (16 \sqrt[3]{2} c d^3) / \right. \right. \\
 & \left. \left( \left( \sqrt{2125764 a^2 (3 e d^3 - 2 a b d^3)^4 - 95551488 a^3 c^3} \right. \right. \right. \\
 & \left. \left. \left. d^9 + 1458 a (3 e d^3 - 2 a b d^3)^2 \right)^{\wedge (1/3)} \right) + \right. \\
 & \left. \frac{1}{18 \sqrt[3]{2} a} \left( \left( \sqrt{2125764 a^2 (3 e d^3 - 2 a b d^3)^4 -} \right. \right. \right. \\
 & \left. \left. \left. 95551488 a^3 c^3 d^9 + 1458 a \right. \right. \right. \\
 & \left. \left. \left. (3 e d^3 - 2 a b d^3)^2 \right)^{\wedge (1/3)} \right) \right) \right), \quad d \neq 0
 \end{aligned}$$

*Figure 7. 3 Expression of the void diameter d at which the energy density is minimum, solution from Wolfram Alpha*

In *Figures 7.2-7.3*, letters are used to express the following parameters:

- $x = d$
- $a = K_r$
- $b = \Delta V_r$
- $c = 6\Gamma$

- $e = G_r F(\lambda_f)$
- $d = D$

To conclude it is possible to determine the value of the void diameters at which the energy density  $W(d)$  or also the particle energy  $U(d)$  are maximum and minimum.

In the plot below the value of diameters at which the energy density is maximum, for the curves shown in *Figure 7.1*, are reported. Same plot can be done also for the minimum in the energy.

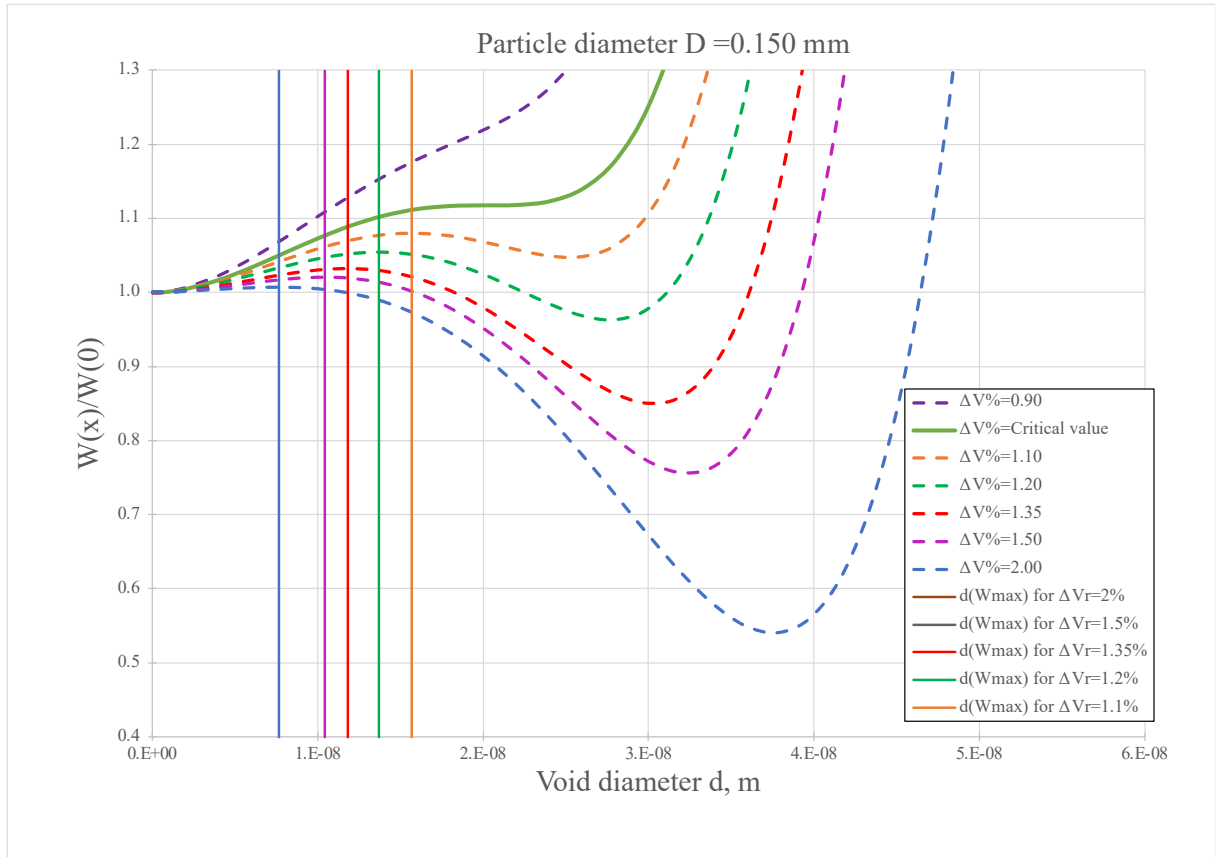


Figure 7. 4 Normalized energy density as function of the void diameter at different volume strain. Continuous lines parallel to the y-axis represent the value of void diameter at which the density energy is maximum. Values calculated using  $\Gamma = 0.03 \frac{J}{m^2}$ ,  $G_r = 0.4 MPa$ ,  $K_r = 2000 MPa$ ,  $F(\lambda_f) = 1$ .

Thanks to the analytical determination of the maximum, the height of the kinetic barrier can be retrieved and calculated considering the difference between the energy at the maximum and its initial value.

$$\Delta U = W_{max} - W_0 \quad (7. 12)$$

As suggested by Bucknall et al. in 2000<sup>28</sup>, the presence of this small barrier, denoted as  $\Delta U$ , at low values of voids diameter, gives rise to a rate-controlling step in the cavitation

process. It has to be noted that, in cavitation initiated by cooling, the height of the energy barrier  $\Delta U$  is not fixed (as in standard thermally activated chemical processes) but changes with the temperature.

By means of the now available analytical solution for the void diameter  $d$  at which  $W(d) = W_{max}$  (Figure 7.2), a quantitative description of the void formation kinetics can now be proposed.

### 7.3 Cavitation Kinetics

#### Arrhenius equation

As already introduced in the paragraph dedicated to the isothermal curves, an activation time for cavitation can be calculated by performing the best fit of the experimental data measured as a variation of length with respect to time. This rate-controlling step of activation is strictly related to the height of the kinetic barrier which has a strong temperature and surface energy dependency. Our first approach to a quantitative description of cavitation kinetics was by the application of the Arrhenius equation which is usually able to explain the kinetics of conversion from one state to another, limited by the presence of a barrier.

The general form of the Arrhenius equation in terms of frequency is:

$$k = A \exp\left(-\frac{\Delta H}{k_B T}\right) \quad (7.13)$$

where  $A$  is a pre-exponential factor,  $\Delta H$  represents the activation energy of the process and it is divided by the product of the Boltzmann constant equal to  $1,3806E-23$  J/K and the temperature expressed in Kelvin.

Using the Arrhenius form, the cavitation kinetics for a given particle diameter  $D$  can be expressed considering the inverse of time retrieved from the data elaboration.

$$\frac{1}{\tau} = A \exp\left[\frac{-((W_{max} - W_0)V_p)}{k_B T}\right] \quad (7.14)$$

In which  $\tau$  is the time constant, expressed in seconds, for the cavitation process during the isothermal curve,  $W_{max}$  is the energy density  $W(d)$  calculated at the value of  $d$  given

by the expression in *Figure 7.2* and  $W_0$  is the energy density of intact rubber particles.  $V_p$  represents the volume of the rubber particle,  $k_b$  is the Boltzmann constant and  $T$  is the temperature. The Arrhenius equation can be expressed in different forms according to the process considered, usually the gas constant  $R$  is used in chemistry when dealing with moles of material, while the Boltzmann constant is used in physics when kinetic units at a molecular level are considered. In case of the cavitation phenomenon, nanometric voids are present and thus  $k_B$  will be used in the Arrhenius equation, since the voids' dimension is comparable to the dimension of molecules.

The activation energy of the cavitation phenomenon is expressed as the energy density difference in Joules per unit of volume. Indeed, the volume of the rubber particles is required to transform this energy density into energy expressed in Joules. So, the term expressed as  $(W_{max} - W_0) * V_p$  represents the energetic barrier that the rubber particle must overcome in order to cavitate and form a stable cavity inside.

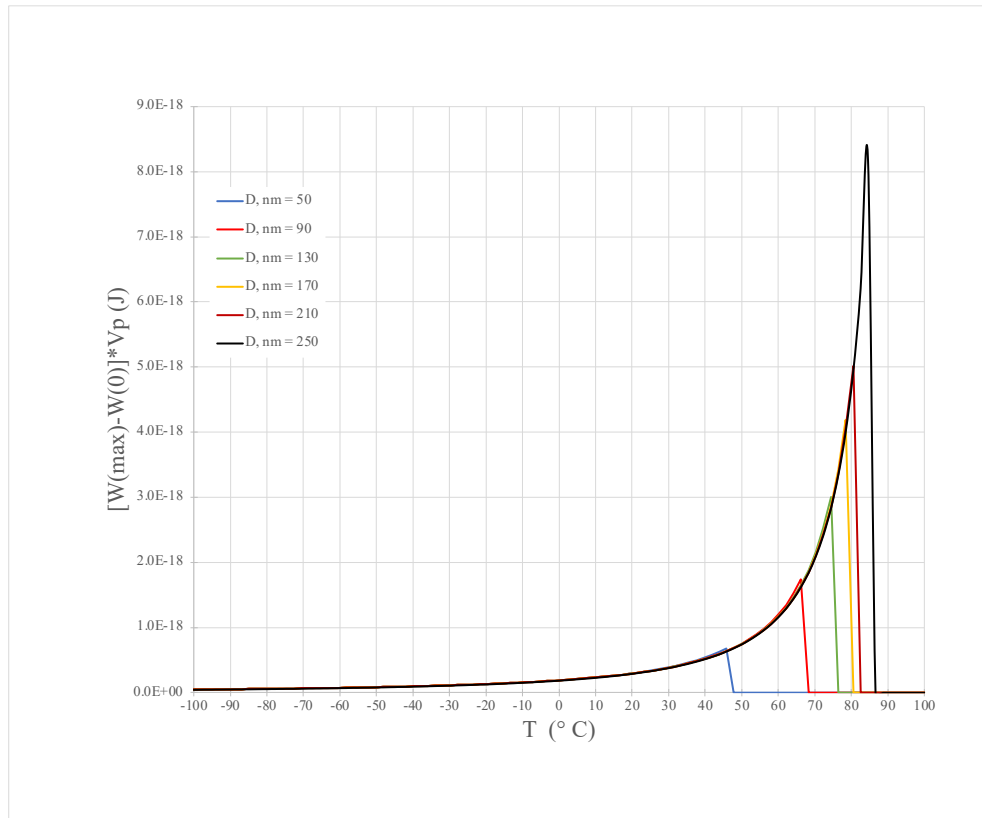


*Figure 7. 5 Height of the energetic barrier with respect to the temperature, for diameters of rubber particles shown in the legend.*

An important difference with respect to the traditional Arrhenius is the strong temperature dependency of this energetic barrier that is not fixed as in most common rate processes. This temperature dependency is shown in *Figure 7.5* for different rubber

particle diameters, from which it can be observed that the height of the energetic barrier does not depend on the rubber particle diameter, exception made for the low limiting value of the volume strain and consequently the high limiting value of the temperature. Cavitation cannot occur when this limit is exceeded, because it identifies the condition in which the energy of a cavitated particle is never lower than the energy of an intact rubber particle. The limit is identified by imposing  $W_{min} < W_0$ , the necessary condition of the cavitation process. In order to fit the experimental times registered during the isothermal curves a rearrange of *Equation (7.14)* is required in which the height of the energetic barrier is expressed as  $\Delta U$ .

$$\ln(1/\tau) = \ln A + \frac{1}{k_B} \left[ \frac{\Delta U}{T} \right] \quad (7.15)$$

This represents the typical Arrhenius expression used to find the activation energy of a process, knowing the time and the temperature.

Sample A	
Temp (°C)	$\tau$ (sec)
-65	696
-57	1630
-55	1024
-52.5	894
-50	728
-47.5	1313
-45	2388
-42.5	5647

*Figure 7. 6 Values of activation time for the isothermal curves conducted on Sample A*

All the calculations related to the experimental data have been done considering the following properties' values:

- $\beta_m = 1.80E - 04 K^{-1}$
- $\beta_r = 7.60E - 04 K^{-1}$
- $v_m = 0.37$
- $G_r = 0.85 MPa$
- $K_r = 2000 MPa$

- $K_m = 3500 \text{ MPa}$
- $\Gamma = 0.035 \text{ J/m}^2$
- $F(\lambda_f) = 1$
- $T_{g,matrix} = 103^\circ\text{C}$

As first analysis just the experimental data registered for Sample A will be considered and reported in *Figure 7.6*. The best fit of the experimental data is reported in the following plot, in which it can be noted that the model seems to describe well just part of the experimental data obtained for  $\tau$ .

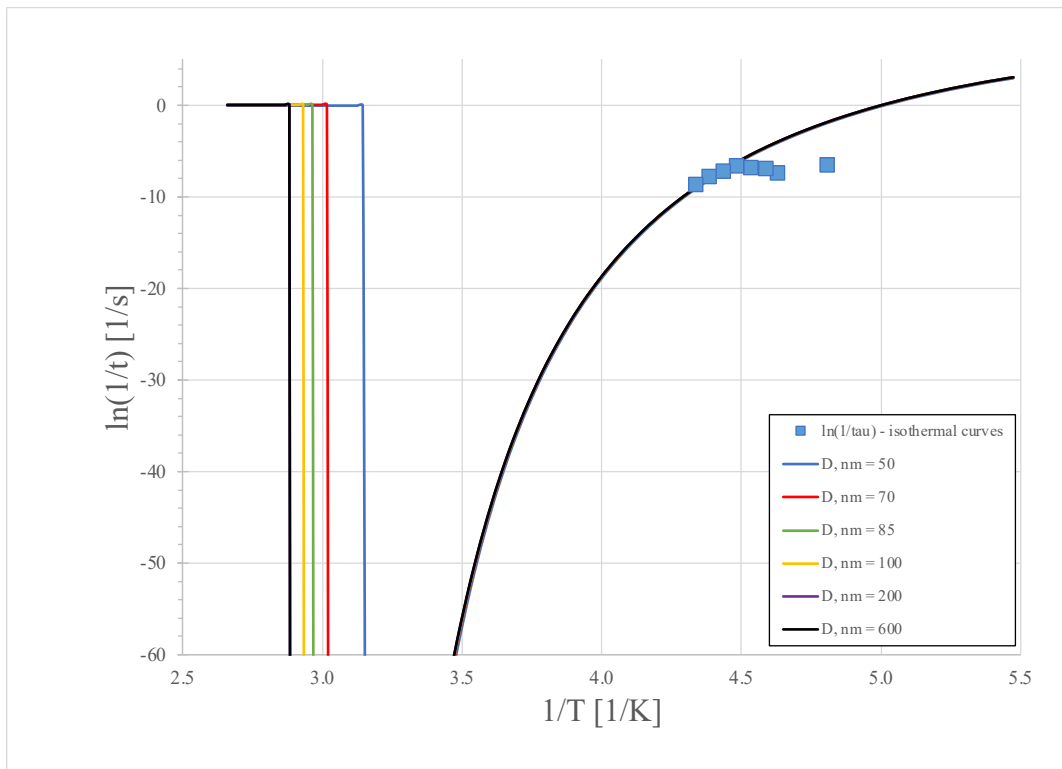


*Figure 7. 7 Arrhenius plot fitting the experimental data of Sample A*

It is particularly evident that the experimental values at lower temperatures show a stronger deviation from the predicted behaviour, reaching a limiting value of about 700 seconds. At the moment, the reliability of these data has not been tested, consequently further and future analysis are necessary to show the goodness of the results obtained. Furthermore, it must be pointed out that the experimental temperatures, at which the cavitation starts, are much lower than the critical values predicted by the energetic model. Consequently, at the experimental conditions all the particles, no matter which diameters, are in the favourable energetic condition in which the energy of the cavitated particles is lower than the initial energy. A possible extension of the

Arrhenius approach, accounting for the particle diameter dependence of the void formation kinetics, could be that of trying an alternative approach: the Eyring equation.

### Eyring equation

The equation of Arrhenius, as shown in the previous paragraph, seems to correctly describe the general dependence of the activation times of Sample A on temperature. However, according to Arrhenius all rubber particles, no matter the dimensions, are equivalent in terms of cavitation kinetics due to the height of the energetic barrier and at small diameters of voids, that does not depend on the particle's diameter  $D$ . Consequently, this approach does not consider the difference in elastic energy present between the cavitating particle and the intact particle that represents the necessary condition for cavitation denoted in *Equation (7.3)*. This energy minimum is strongly dependent on the particle's diameter. Indeed, it is quite intuitive that the elastic energy of a big particle released during cavitation is higher than the energy released by a smaller one. A modification of the kinetic model is required because the limit to cavitation introduced by the height of the energetic barrier is not sufficient. Also, the energy difference between one state and the other must be considered. This is a problem quite similar to the deformation rate in creep experiments that can be studied by using Eyring's model. This model has been described also in *Chapter 1* and can be expressed as:

$$\dot{\epsilon} = \dot{\epsilon}_0 \exp\left(-\frac{\Delta H}{k_B T}\right) \sinh\left(\frac{V\sigma}{k_B T}\right) \quad (7.16)$$

in which  $\dot{\epsilon}$  is the plastic strain rate,  $\dot{\epsilon}_0$  represents a pre-exponential factor,  $V$  is the activation volume and  $\sigma$  is the stress applied. The second term can be approximated at high values of its argument to  $1/2 \exp(x)$ .

All the parameters of the equation must be adjusted in order to consider the cavitation process. Indeed, the activation enthalpy is expressed below.

$$\Delta H = (W_{max} - W(0)) V_p = (W_{max} - W(0)) \frac{\pi}{6} D^3 \quad (7.17)$$

The volume strain, to which the rubber particles are subjected, represents the driving force of the phenomenon and can tentatively be identified with the stress applied, just by multiplying the bulk modulus of the rubber  $K_r$  by the volume strain  $\Delta V_r$ . On the other hand, in order to retrieve the particle diameter dependence, it seems adequate to consider the activation volume proportional to the volume of the rubber particle.

$$V \sigma = \Delta V_r K_r B \frac{\pi}{6} D^3$$

(7. 18)

Where  $B$  represents a proportionality constant. The resulting Eyring equation expressed as cavitation probability is given by:

$$\frac{1}{\tau} = A \exp \left[ \frac{\frac{\pi}{6} D^3 \left( B \Delta V_r K_r - (W_{max} - W(0)) \right)}{k_B T} \right]$$

(7. 19)

The curves will be obtained by calculating  $W_{max}$  considering the first derivative equal to zero but also the critical condition for which its  $W_{min}$  is lower than its initial values.

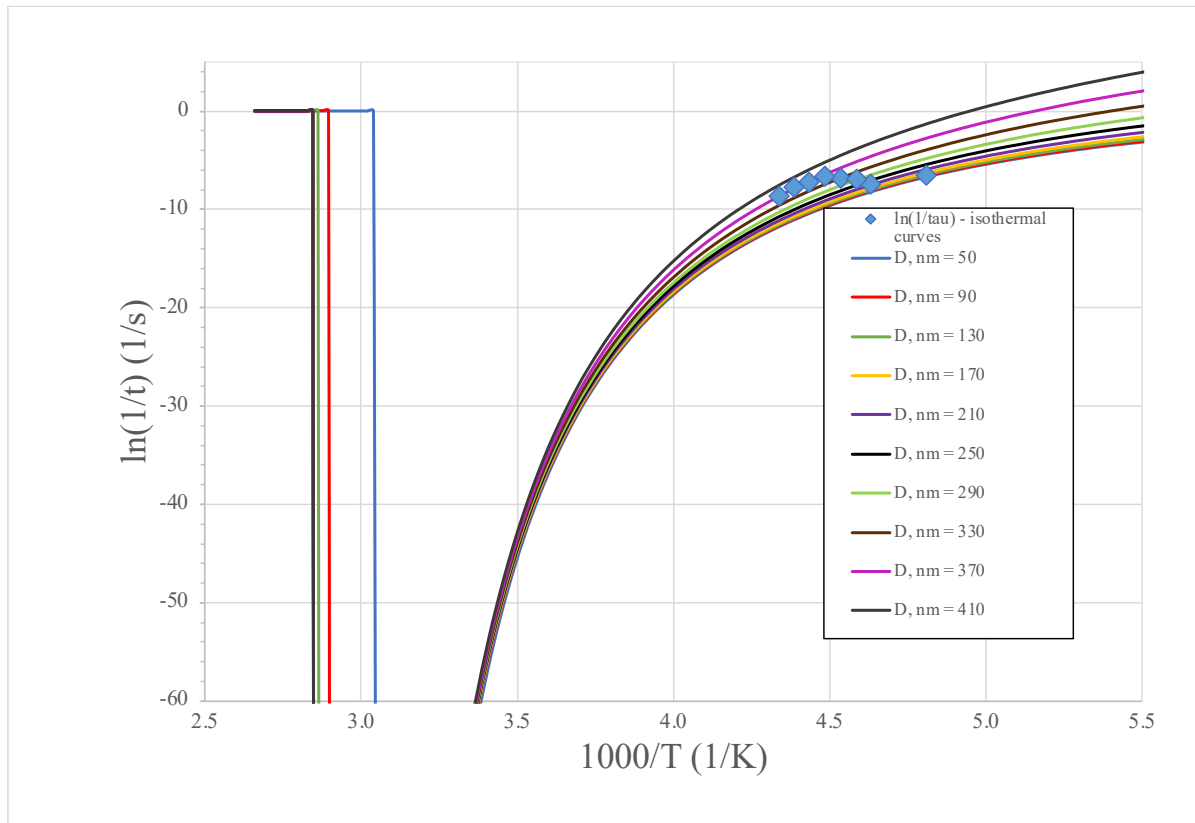
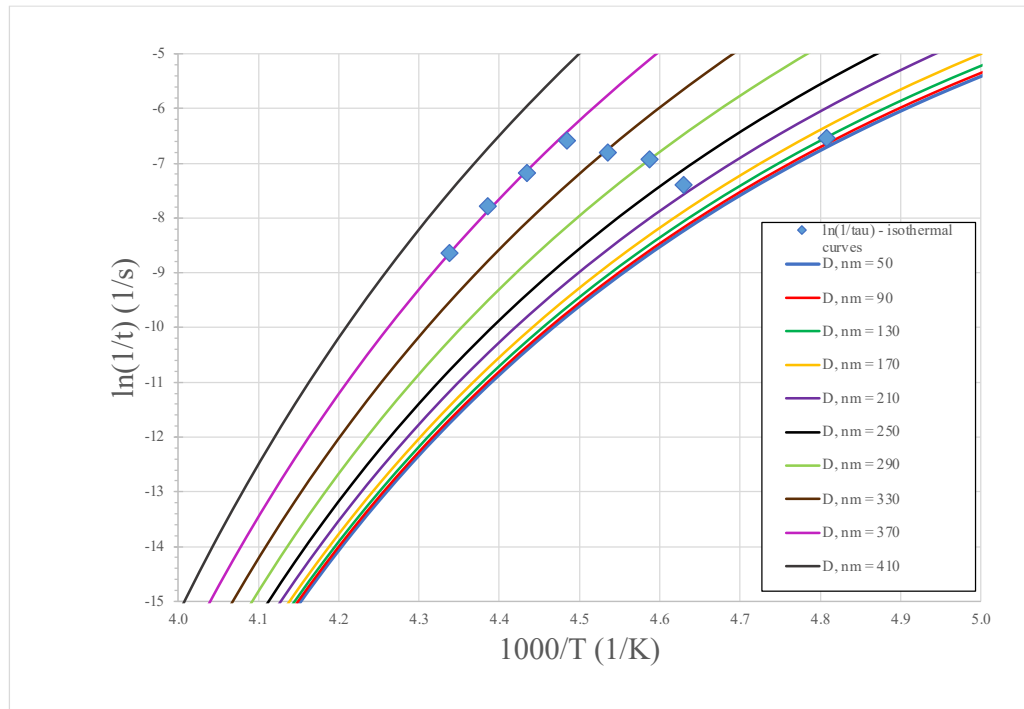


Figure 7. 8 Probability of cavitation versus  $1000/T$  for different rubber particles' diameters

The parameters used are those reported in the Arrhenius model, while the pre-exponential factor  $A$  is taken as  $1E+12$  and  $B$  is equal to  $3E-9$ . Rescaling the zone of the isothermal data *Figure 7.9* is obtained.



*Figure 7.9* Zooming of the isothermal zone in *Figure 7.8*

It is evident that Eyring seems to provide a better description of the experimental data with respect to the Arrhenius equation, and it also retrieves the important influence of the rubber particle diameter.

This tentative approach to describe and inspect the cavitation kinetics is just part of an ongoing research that, in a near future, will surely verify the goodness of the experimental results and assumptions done.

## Conclusions

The cavitation phenomenon in ABS has been studied in detail in this thesis whose goal was inspecting and detecting thermally induced rubber particle cavitation using a rheological approach. The significant experimental work has provided interesting results along with inspirations for future works. A clarification is needed: most of the experimental work has been conducted on tensile geometry and by monitoring the length variation with respect to temperature and time, experiments that can be also carried out with a dilatometer. However, all the instruments used during this thesis were rheometers and tensile experiments were coupled with linear viscoelastic information retrieved with three-point bending and shear geometry. So, it can be concluded that even if the dilatometric curves can be obtained using a dilatometer, this thesis is proof of the remarkable versatility of rheometers that can provide both dilatometric and viscoelastic curves.

Dynamic Mechanical Analysis tests conducted on the investigated samples have shown the already well-known splitting of the damping and loss peak, but further information has been achieved. In particular, a quantitative approach to determine and justify the glass transitions temperature shifting has been found, considering the experimental difference in glass transition temperature between the unconstrained rubber and the intact rubber particle subjected to the negative hydrostatic pressure and the calculated difference retrieved from the formula of the volume strain generated by the thermal expansion coefficient mismatch. Furthermore, this quantitative analysis of the position of the glass transition temperature has also provided the basis of a method for the estimation, knowing the shear modulus of the rubber and considering materials subjected to the cavitation process, of the most reliable value for the rubber bulk modulus and consequently for the Poisson's ratio that till now were not discussed in detail in the literature.

Dilatometric curves have shown the influence of cavitation during cooling experiments, but their elaboration gave rise to a method able to calculate the percentage of cavitated particles at any temperature without using the thermal expansion coefficients but just the data registered for the ABS specimens and the matrix alone. In this way, any problem

related to the necessity of having a complete linear zone before and after cavitation to calculate the percentage of cavitation has been eliminated.

Isothermal experiments can be considered the most original part of this work. Indeed, they represent the first experimental approach that can provide a monitoring of the rate-controlling step of the cavitation phenomenon strictly related to the energetic barrier that must be surmounted in order for void nucleation and growth to occur. The data elaboration has given information about the percentage of cavitated particles achieved during the isothermal experiments, but also the time scale of the cavitation kinetics.

The times calculated during the isothermal curves could represent a direct observation of the thermally and stress activated cavitation step that, as suggested by this thesis could be tentatively described using Eyring. This aspect necessitates in any case of further analysis. Moreover, two original and useful results are the analytical expressions for the maximum and minimum of the model of the energetic balance that, till now, were not available in the literature.

This thesis proposes interesting results for the study of the cavitation phenomenon, using an original and new approach. Not just the thesis' goal has been achieved, but significant starting points for future studies and experiments have been suggested. The picture that emerges from this thesis is that, studying the cavitation phenomenon is complicated and requires very sensitive experimental techniques. However, acquiring all the possible information and taking into consideration new possible experimental approaches and protocols is fundamental to study and understand all the aspects that determine the final properties of rubber toughened plastics.



## *Appendix*

### *Derivation of the formula for the volume strain*

Derivation is provided by Selsing in 1961<sup>29</sup>, the volume strain generated by a difference in thermal expansion coefficient can be retrieved. Assuming a hydrostatic pressure  $P$  present in a spherical cavity of radius  $R$  in an infinite isotropic phase with elastic modulus  $E_1$  and Poisson's ratio  $\nu_1$ , the radial and tangential stresses  $p_r$  and  $p_t$ , at the distance  $r$  from the centre of the cavity can be expressed by the following equation.

$$p_r = -2p_t = -\frac{PR^3}{r^3}$$

(A. 1)

Considering the radial deformation of a radial line element at a distance  $r$  from the centre:

$$ds = dr \left( \frac{p_r}{E_1} + \frac{2\nu_1 p_t}{E_1} \right) = -\frac{PR^3}{r^3} \frac{1 + \nu_1}{E_1}$$

(A. 2)

The integration of this expression from  $R$  to infinite gives rise to the total linear expansion:

$$\Delta R_1 = \int_R^\infty ds = PR \frac{1 + \nu_1}{2E_1}$$

(A. 3)

Similarly for a solid sphere of radius  $R$  subjected to an external hydrostatic pressure  $P$ , the internal radial and tangential stresses will be equal to the negative hydrostatic pressure and the radial deformation will be expressed as:

$$ds = dr \left( \frac{g_r}{E_2} - \frac{2\nu_2 g_t}{E_2} \right) = -P \frac{1 - 2\nu_2}{E_2} dr$$

(A. 4)

In which  $g_t$  and  $g_r$  are the tangential and radial stresses. The total decrease in radius is given integrating the previous formula from zero to  $R$ .

$$\Delta R_2 = - \int_0^R ds = PR \frac{1 - 2\nu_2}{E_2}$$

(A. 5)

Assuming that the spherical cavity is made in an infinite glass phase and a spherical crystal is forced into the cavity despite the misfit in radius  $\Delta R$ , this can be possible just if the sample pressure  $P$  in the cavity and on the crystal is applied allowing the misfit to disappear. This will occur when the pressure satisfies the following equation:

$$\Delta R = \Delta R_1 + \Delta R_2 = P R \left( \frac{1 + \nu_1}{2E_1} + \frac{1 - 2\nu_2}{E_2} \right)$$

(A. 6)

Furthermore, if the misfit was originally zero and then developed by a misfits of thermal expansion the following  $\Delta R$  can be calculated:

$$\Delta R = R \Delta\beta \Delta T$$

(A. 7)

in which  $\Delta T$  is the cooling range and  $\Delta\beta$  is the difference in thermal expansion coefficient. Equating the two expression for  $\Delta R$ , the hydrostatic pressure can be retrieved.

$$P = \frac{\Delta\beta \Delta T}{\left( \frac{1 + \nu_1}{2E_1} + \frac{1 - 2\nu_2}{E_2} \right)}$$

(A. 8)

This hydrostatic pressure can be explicated into volume strain just diving the equation by the bulk modulus of the material.



## ***Bibliography***

1. Echte, A. *Rubber-Toughened Styrene Polymers*. (1989).
2. Bucknall, C. B. *Toughened Plastics*. (1977).
3. C.B Bucknall. Rubber toughening in 'The physics of glassy polymer'. in (1997).
4. Bucknall, C. B. New criterion for craze initiation. *Polymer (Guildf)* **48**, 1030–1041 (2007).
5. Bucknall, C. B. & Smith, R. R. Stress-whitening in high-impact polystyrenes. *Polymer (Guildf)* **6**, 437–446 (1965).
6. Newman S. & Stella S. Stress-strain behavior of rubber-reinforced glassy polymers. *J Appl Polym Sci* **9**, (1965).
7. Breuer, H., Haaf, F. & Stabenow, J. Stress Whitening and Yielding Mechanism of Rubber-Modified PVC. *Journal of Macromolecular Science, Part B* **14**, 387–417 (1977).
8. Lazzeri, A. & Bucknall, C. Dilatational bands in rubber-toughened polymers. *J Mater Sci* **28**, 6799–6808 (1993).
9. Bucknall, C. B., Ayre, D. S. & Dijkstra, D. J. Detection of rubber particle cavitation in toughened plastics using thermal contraction tests. *Polymer* **41** (2000) 5937–5947 (2000).
10. Yang HH. Effect of rubber particle cavitation on the yielding of High Impact PolyStyrene. *thesis Cranfield* (1997).
11. Ramsteiner, F., Heckmann, W., Mckee, G. E. & Breulmann, M. Influence of void formation on impact toughness in rubber modified styrenic-polymers. (2002).

12. Bucknall, C. B. & Paul, D. R. Notched impact behavior of polymer blends: Part 1: New model for particle size dependence. *Polymer (Guildf)* **50**, 5539–5548 (2009).
13. Bubeck, R. A., Buckley, D. J., Kramer, E. J. & Brown, R. *Modes of deformation in rubber-modified thermoplastics during tensile impact. JOURNAL OF MATERIALS SCIENCE* vol. 26 (1991).
14. Lin, C. S., Ayre, D. S. & Bucknall, C. B. A dynamic mechanical technique for detecting rubber particle cavitation in toughened plastics. *Journal of material science* **17**, (1998).
15. Morbitzer, L., Kranz, D., Humme, G. & Ott, K. H. Structure and Properties of ABS Polymers. X. Influence of Particle Size and Graft Structure on Loss Modulus Temperature Dependence and Deformation Behavior\*. *J Appl Polym Sci* **20**, 2691–2704 (1976).
16. Kato, K. Osmium tetroxide fixation of rubber latices. *J Polym Sci B* **4**, 35–38 (1966).
17. Declat-Perez, C., Francis, L. F. & Bates, F. S. Cavitation in block copolymer modified epoxy revealed by in situ small-angle X-ray scattering. *ACS Macro Lett* **2**, 939–943 (2013).
18. W. S. Bahary, D. I. Sapper & J. H. Lane. Structure of Polybutadienes. *Rubber Chemistry and Technology* (1967).
19. H. J. Karam & L. Tien. Analysis of Swelling of Crosslinked Rubber Gel with occlusions. *Journal of Applied Polymer Science* (1985).
20. Dipartimento di Ingegneria Civile e Industriale.  
<https://www.dici.unipi.it/laboratori/formulazione-lavorazione-e-modifica-superficiale-di-materiali-polimerici-e-compositi>

21. Bucknall, C. B., Rizzieri, R. & Moore, D. R. Detection of incipient rubber particle cavitation in toughened PMMA using dynamic mechanical tests. *Polymer* **41**, 4149–4156 (2000).
22. Cailliaux, A., Alba-Simionesco, C., Frick, B., Willner, L. & Goncharenko, I. Local structure and glass transition of polybutadiene up to 4 GPa. *Phys Rev E Stat Phys Plasmas Fluids Relat Interdiscip Topics* **67**, 4 (2003).
23. Huang, D., Colucci, D. M. & McKenna, G. B. Dynamic fragility in polymers: A comparison in isobaric and isochoric conditions. *Journal of Chemical Physics* **116**, 3925–3934 (2002).
24. Ayre, D. S. & Bucknall, C. B. Particle cavitation in rubber-toughened PMMA: experimental testing of the energy-balance criterion. *Elsevier Science Polymer* **39**, 4785–4791 (1998).
25. Lazzeri, A. & Bucknall, C. B. Recent developments in the modeling of dilatational yielding in toughened plastics. *ACS Symposium Series* **759**, 14–35 (2000).
26. Bucknall, C. B., Karpodinis, A. & Zhang, X. C. A model for particle cavitation in rubber-toughened plastics. *JOURNAL OF MATERIALS SCIENCE* **29**, 3377–3383 (1994).
27. Wolfram Alpha. <https://www.wolframalpha.com>
28. Bucknall, C. B., Ayre, D. S. & Dijkstra, D. J. Detection of rubber particle cavitation in toughened plastics using thermal contraction tests. (2000).
29. Selsing Jorgen. Internal Stresses in Ceramics. *Journal of the America Ceramic Society* (1961).

30. Stress strain behavior of polymers. *Polymer Database*  
<https://polymerdatabase.com/polymer%20physics/Stress-Strain%20Behavior.html>
31. TA instruments. *RSA-G2 SOLIDS ANALYZER*. <https://www.tainstruments.com/rsa-g2/>  
(2019).
32. Collyer A. A. *Rubber Toughened Engineering Plastics. Rubber Toughened Engineering Plastics* (Springer Netherlands, 1994).
33. TA Instruments. *DILATOMETRY PUSH-ROD AND OPTICAL*.  
<https://www.tainstruments.com/wp-content/uploads/BROCH-DIL.pdf> (2022).
34. Flory-Fox\_curve. [https://commons.wikimedia.org/wiki/File:Flory-Fox\\_curve.jpg](https://commons.wikimedia.org/wiki/File:Flory-Fox_curve.jpg)